June 28, 2021

Feasibility of Micro Wind Turbines as Power Solution for Future Mars Missions

Luca Lange (2205769)

Bachelor Thesis Advanced Technology

Faculty of Engineering Technology
Engineering Fluid Dynamics Group

Assignment Committee

Chairman: prof.dr.ir. C.H. Venner

Supervisor: dr.ir. A. van Garrel

External Member: dr. R.J.A.M. Stevens

UNIVERSITY OF TWENTE.

Abstract

To meet the increasing energy demands for Mars missions, the feasibility of using micro wind turbines (<500W) as a possible power solution for standalone applications is investigated. The potential of using micro wind turbines lies in providing an alternative or additional power supply for devices such as landers, rovers, or drones, as photovoltaic cells are the only currently used sustainable energy supply. The approach to the study is threefold, consisting of an assessment of the winds on Mars, an analysis and evaluation of the design considerations, and a quantitative aerodynamic design of a possible turbine as power supply for a drone mission.

Assessment of the wind power density on Mars using data from a general circulation model shows that most regions have an annual mean of under $10 W/m^2$, mainly attributed to the low air density of the Martian atmosphere. Mountainous regions receive the highest wind speeds because of the effect of slope winds.

Looking at the factors that drive the design of systems for Mars reveals weight as the main design driver. A power production per mass of around 2.5W/kg is necessary to match the performance of photovoltaic systems. Dense packing of the turbine for transportation while also being autonomously and independently deployable during installation is another challenge, tied closely to the structural and environmental challenges that the Martian environment imposes.

A rotor was designed in QBlade based on the insight acquired from the general analysis, which is suitable to supply a 'Mars Science Helicopter' with power for over 100 operations a year. The 5-bladed design features the NACA4602 airfoil to reach a maximum power coefficient of 0.38. Implications of the ultra-low Reynolds environment ($Re<10^4$) reflect in the selection of the foil. It is noted that stall control is not a viable control solution anymore because of the more gradual decrease in lift-to-drag ratio for increased angle of attacks. The final turbine produces an average of 11.9W at a turbine diameter of 2.2m.

Further research is suggested in terms of the structural analysis and design of the turbine to reach conclusions on the weight efficiency of the system. This allows for direct comparison to competitive systems. Concrete decisions in terms of transport, deployment, and component and material selection are necessary for this. A significant value is seen in CFD and experimental investigation of various airfoil profiles at ultra-low Reynolds numbers over large ranges of angles of attacks as a way to validate the currently employed design methods. Overall, an optimistic outlook on the general feasibility is adopted, given the preliminary results and the overall utility of diversifying power generation methods for Mars missions.

Contents

1 Introduction **4**
- 1.1 Background on Power Generation for Space Missions . . . 4
- 1.2 Past Research on Wind Turbines for Mars . . . 5
- 1.3 Plans for Investigation . . . 6

2 Wind Resource Assessment **7**
- 2.1 Fundamental Comparison of Earth and Mars . . . 7
- 2.2 The Mars Climate Database . . . 8
- 2.3 Winds on Mars . . . 8
  - 2.3.1 Origins of Wind . . . 8
  - 2.3.2 Boundary Layer Effects . . . 12
- 2.4 Assessment of Wind on Mars . . . 14

3 Concept Analysis **17**
- 3.1 Objective Definition and Utility . . . 17
  - 3.1.1 Objective Statement . . . 17
  - 3.1.2 Preliminary Utility Estimation . . . 18
- 3.2 System Drivers . . . 19
  - 3.2.1 Transport . . . 20
  - 3.2.2 Installation . . . 24
  - 3.2.3 Operation . . . 27
- 3.3 General Design Considerations . . . 35

4 Initial Wind Turbine Design **37**
- 4.1 Problem Statement . . . 37
- 4.2 Baseline Design . . . 39
  - 4.2.1 Airfoil Selection . . . 39
  - 4.2.2 Turbine Design . . . 43
  - 4.2.3 Power Control . . . 45
- 4.3 Performance Prediction . . . 48
  - 4.3.1 Design Performance . . . 48
  - 4.3.2 Mission Performance . . . 51
  - 4.3.3 Future Considerations . . . 53

5 Discussion and Conclusions **55**
- 5.1 Discussion . . . 55
- 5.2 Conclusions . . . 56
- 5.3 Looking Ahead . . . 57

Bibliography **58**

Nomenclature

α	Power-law Exponent	$[-]$
λ	Tip Speed Ratio (TSR)	$[-]$
λ_r	Local Speed Ratio	$[-]$
$\dot{m}$	Mass Flow Rate	$[kg/s]$
μ	Dynamic Viscosity	$[Pa \cdot s]$
ω	Angular Velocity	$[1/s]$
ω_w	Angular Velocity of Wake Rotation	$[1/s]$
ρ	Fluid Density	$[kg/m^3]$
ρ_{blade}	Blade Area Density	$[kg/m^2]$
ρ_{tower}	Tower Area Density	$[kg/m^2]$
σ_{max}	Maximum Stress	$[Pa]$
φ	Angle of Relative Wind	$[-]$
φ_{betz}	Betz' Optimal Angle of Twist	$[-]$
a	Axial Induction Factor	$[-]$
a'	Angular Induction Factor	$[-]$
A	Swept Area	$[m^2]$
A_{cross}	Cross-sectional Blade Area	$[m^2]$
A_{foil}	Airfoil Area (Projected)	$[m^2]$
A_{tower}	Cross-sectional Tower Area	$[m^2]$
B	Number of Blades	$[-]$
c	Speed of Sound	$[m/s]$
c	Weibull Scale Factor	$[m/s]$
C_d	Drag Coefficient	$[-]$
C_l	Lift Coefficient	$[-]$
C_m	Pitch Moment Coefficient	$[-]$
C_p	Power Coefficient	$[-]$
c_p	Specific Heat at Constant Pressure	$[-]$
C_t	Thrust Coefficient	$[-]$
c_{betz}	Betz' Optimal Chord Length	$[m]$
c_{blade}	Maximum Distance from Neutral Axis of Blade	$[m]$
$C_{d,tower}$	Tower Drag Coefficient	$[-]$
$C_{l,0}$	Incompressible Flow Lift Coefficient	$[-]$
$C_{p,max}$	Maximum Power (Betz) Coefficient	$[-]$
d	Zero-plane Displacement	$[m]$
E	Energy	$[J]$

F_c	Centrifugal Force	$[N]$
F_d	Drag Force	$[N]$
F_g	Gravitational Force	$[N]$
F_l	Lift Force	$[N]$
F_N	Normal Force	$[N]$
F_t	Thrust Force	$[N]$
g	Gravitational Acceleration	$[m/s^2]$
h	Tower Height	$[m]$
I	Area Moment of Inertia	$[m^4]$
k	Kármán's Constant	$[-]$
k	Weibull Shape Factor	$[-]$
L	Surface Length	$[m]$
l	Airfoil Span	$[m]$
m	Mass	$[kg]$
M	Overturning Moment	$[Nm]$
M	Mach number	$[-]$
M_p	Pitching Moment	$[Nm]$
M_∞	Freestream Mach Number	$[-]$
M_{thrust}	Thrust-induced Moment	$[Nm]$
m_{top}	Mass on Top of Tower	$[kg]$
M_{tower}	Tower-induced Moment	$[Nm]$
p	Pressure	$[Pa]$
$p+$	Pressure before Turbine	$[Pa]$
$p-$	Pressure behind Turbine	$[Pa]$
P	Power	$[W]$
p_∞	Atmospheric Pressure	$[Pa]$
Q	Volume Flow Rate	$[m^3/s]$
Q	Torque	$[Nm]$
R	Turbine Radius	$[m]$
r	Radial Position	$[m]$
Re	Reynolds Number	$[-]$
S	Shear Force	$[N]$
T	Axial Thrust	$[N]$
T	Temperature	$[K]$
u	Wind Speed (also v)	$[m/s]$
u^*	Friction Velocity	$[m/s]$
u_{blade}	Blade Speed	$[m/s]$
v	Wind Speed (also u)	$[m/s]$
v_2	Downstream Wind Speed	$[m/s]$
v_∞	Undisturbed Wind Speed	$[m/s]$
v_{rel}	Relative Wind Speed	$[m/s]$
z	Height	$[m]$
z_0	Surface Roughness Length	$[m]$
z_r	Reference Height	$[m]$

Chapter 1

Introduction

1.1 Background on Power Generation for Space Missions

Through the technological advances of the last decades, the developments in Mars exploration are pushed forward at increasing speeds. With the newest rover 'Perseverance' touching down on the red planet at the beginning of 2021, plans for Mars exploration are ever-expanding. Equipped with better instruments, mobility, and communication, Perseverance can further investigate the possibilities of ancient life and collect samples for a possible return to Earth. Nevertheless, the power supply of the 2021 rover bears remarkable similarity to the power supply of the first successful Mars lander in history, the 1976 'Viking 1'. Both harvest the thermal energy released by the decay of Plutonium-238. Overall, nuclear and solar energy form a monopoly that reigns the power generation for Mars exploration, and space exploration in general, since its beginning [1].

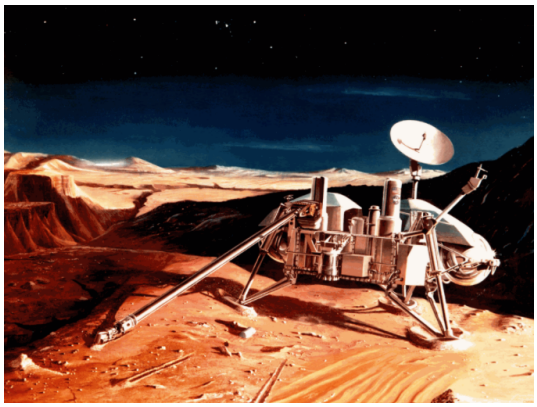

(a)

(b)

Figure 1.1: Illustrations of the (a) first successful Mars lander, Viking 1 and (b) the latest contributor, the Perseverance rover. Source: [2; 3]

The simplest metric to compare energy sources in a space exploration context is through the specific energy. Since one of the biggest economic challenges is to make mass escape the gravitational field of the Earth, having the most energy per unit mass is a good preliminary indicator of the feasibility of the generator. The specific energy of MMRTGs (multi-mission radioisotope thermoelectric generators) and PV (photovoltaic) cells can be found as follows:

$$\text{Specific Energy } [kWh/kg] = \frac{\text{Device Power } [kW] * \text{Device Operation } [h]}{\text{Device Mass } [kg]} \tag{1.1.1}$$

For these two power sources, this gives the following specific energies [1]:

$$\text{MMRTG} : 46kWh/kg \qquad \text{Photovoltaic Cells} : 41kWh/kg$$

The high specific energy of both technologies is what makes them so suitable for space missions. Yet, both sources also have some disadvantages associated with them. Solar panels have the issue of not being able to supply continuous power. The day-night cycle limits the potential operation time periodically, which becomes a more significant issue with increasing latitude. Climate variations can cause non-periodical outages. Dust suspended in the air during storms can decrease the amount of radiation reaching the cells, and the deposition of dust on the panels can disable them for indefinite periods. This leads to overall limited predictability and reliability of the power generation. Nuclear reactors do not have these disadvantages. The power output is not only disjointed from any external environmental effects, but it is also highly predictable and can be calculated very accurately before the mission. The biggest issues with nuclear power are the risk of launching radioactive material and the public opinion associated with it. Some previous missions were prohibited from using nuclear power as a primary energy source because of the safety concerns [4]. Nowadays, systems are in place that limit the risk of radioactive contamination in case of launch failure [5]. These include methods to minimize the possibility of air, water, and soil pollution and try to maximize the contaminant's immobilization in case of failure. However, it is acknowledged that accidents have the potential of causing damage, including land contamination and adverse health effects [6].

Clearly, both solar and nuclear power stood the test of time and proved to be effective solutions. However, finding alternative power sources that might avoid some of the issues that both of the described methods have would aid to further the potential merit of Mars missions. To ensure the possibility of diverse space exploration missions, an equally diverse collection of energy sources will be needed. For this reason, the feasibility of wind turbines as power supply on Mars will be analyzed.

1.2 Past Research on Wind Turbines for Mars

The knowledge base and research conducted regarding possible designs for wind turbines on Mars are minimal. Several articles analyze the feasibility of using wind energy on Mars on large-scale, manned exploration missions [7; 8; 9]. To summarize, the theoretical analysis conducted generally finds mixed results. Vertical turbines are preferred for structural reasons but show lower efficiency and require high winds for start-up. It is argued that these turbines could compete with nuclear power, but the validity of the results is questionable, as the authors raise doubts about their results and suggest wind tunnel testing for validation [7], while another article argues that low-altitude wind turbines are not feasible at all [8]. All of the mentioned research is over 20 years old, as more recent research is much more focused on using wind turbines for smaller-scale unmanned missions, e.g. rover-based missions. This research primarily includes vertical axis wind turbines [10; 11; 12]. Even though the lower efficiency compared to horizontal configurations is acknowledged, the structural and construction complications are regarded to outweigh the higher efficiency. The studies suggest that an application in the martian atmosphere is possible, and even that it could compare to the power generation of solar panels during times of high wind speeds [11]. All of these approaches are still purely theoretical and more methodology-oriented, compared to focusing on a practical application. This is further shown by the fact that no prototype was constructed and that no relevant experiments have been conducted, at least none from which data relevant for this study can be derived [13; 14]. The most recent mention of wind turbines on Mars comes from a Forbes article that describes a proposal for powering weather stations on Mars, specifically in the polar region, using horizontal-axis micro wind turbines [15]. This suggests that this al-

ternative, small-scale or even micro-scale application is a very recent development, for which research is just starting out.

Overall, the absence of recent research findings regarding medium- and large-scale wind turbines for application on Mars suggests the opposite of what the older articles found. The feasibility of such a system is likely severely crippled by the enormous difficulty of construction of heavier turbines on Mars, which can be seen in why the research into classical large-scale wind turbine designs faded into history. Alternative designs that take advantage of buoyancy as a way to reduce structural loads are also considered [16]. Given that these issues apply less to turbine designs for smaller scale, the most potential is seen in scaling down the size of the turbine.

The innovations made in designing airborne devices for the Martian atmosphere is another valuable focus for developing wind turbines. It includes the research on the Ingenuity helicopter [17], possible future developments of airborne systems [18], and especially their aerodynamic design [19]. The developments necessary for flight in the thin atmosphere on Mars likely resemble the aerodynamic challenges faced during the turbine design.

1.3 Plans for Investigation

This report will analyze the feasibility of using micro wind turbines as power supply for future Mars missions. In this context, the term micro refers to turbines with a rated power of under 500W [20]. While both vertical and horizontal axis wind turbines have their advantages, this report focuses mainly on the topology of horizontally oriented turbines. The general superiority of horizontal turbines, mainly related to their higher efficiency, is widely acknowledged for most ranges of applications [21]. The structural advantage of vertical-axis turbines also becomes less relevant when designing turbines in the micro scale.

The report is divided into three components, each focusing on a different type and level of analysis. First, the wind on Mars will be assessed. By defining and understanding the climatic and environmental conditions on Mars, an understanding of how and why winds form on Mars is gained. Using the quantitative data from the Mars Climate Database (MCD) 5.3 [22; 23], conclusions can be drawn on the amount of power that can be harnessed based on regional and temporal variations. Knowing which regions receive high and consistent wind speeds is useful for siting possible missions involving wind power. It also allows contrasting the amount of power that can be generated on Mars to the amount that can be generated on Earth. In the second step, the concept of operating a wind turbine on Mars will be analyzed. After introducing primary and secondary mission objectives, the critical system design drivers are elaborated upon. This type of high-level analysis allows for a general overview of the possible issues that can arise while designing a wind turbine for Mars. The aim is to obtain a complete picture of all factors that have to be considered, which is elemental for designing an entirely novel system. Laying out a wide range of possible problems and determining factors can allow for initial design choices and help identify the main restricting factors. As such, this overview lays a foundation for future wind turbine design approaches.

However, keeping the analysis general does not allow for any concrete, quantitative results. Therefore, the last section will focus on a trial wind turbine design coupled with a specific application. The focus lies on the aerodynamic design, allowing the evaluation of possible blade design approaches and performance. By applying theoretical concepts to a practical design problem, conclusions can be drawn on the feasibility of the design concerning the requirements set out by the mission, which allows for a decision on whether the system is suitable or not. This conclusion can be generalized to answer whether using micro wind turbines on Mars is feasible.

Chapter 2

Wind Resource Assessment

This chapter focuses on the climate on Mars, and the ways in which wind is generated in its atmosphere. The chapter begins with a broad analysis of the key factors determining the Martian climate conditions, and ends in an overview of the available wind power on Mars.

2.1 Fundamental Comparison of Earth and Mars

The general understanding of wind energy is usually seen in the context of the environmental parameters set by the characteristics of the Earth. To understand how the same fundamental principles apply in the Martian atmosphere, a short summary of the key orbital, physical and atmospheric parameters of Earth and Mars is illustrated below:

	Earth	Mars
Distance from Sun [AU]	0.98-1.02	1.38-1.67
Length of Day [h]	24	24.66
Length of Year [d]	365.24	686.98
Obliquity [deg]	23.4	25.2
Equatorial Radius [km]	6378	3396
Surface Gravity [m/s^2]	9.81	3.72
Surface Pressure [atm]	1	0.0063
Surface Density [kg/m^3]	1.2	0.02
Surface Temperature [K]	230-315	140-300
Atmospheric Composition (molar ratio of major components)	N2 (77%) O2 (21%) H2O (1%)	CO2 (95%) N2 (2.7%) Ar (1.6%)

Table 2.1: Major orbital, physical and atmospheric differences between Mars and Earth [24].

Mars orbits the Sun at roughly 1.5 times the radius of Earth's orbit, making the year on Mars around twice as long as on Earth. The diurnal cycle, however, is very similar for the two planets. Mars has a much thinner atmosphere with a density of only 0.02 kg/m^3, which along with the lower gravity, leads to a surface pressure of only around 0.6% of the Earth's atmospheric pressure. This has significant implications on the effect of wind, as a less dense atmosphere carries less power. Having only a third of the gravitational acceleration of Earth, structural limitations of Mars-based infrastructure are decreased. With obliquity, the planet's axial tilt with respect to its orbit, being very similar between Earth and Mars, seasonal varia-

tions are equally similar on the two planets. The temperature on Mars is still relatively similar to the ranges on Earth, but with more significant variations, especially towards very low temperatures. The atmosphere on Earth also includes significant humidity, whereas the Martian atmosphere is almost completely arid.

2.2 The Mars Climate Database

In the following analysis, an overview of the climate on Mars, emphasizing low-altitude winds, will be given. Quantitative results are crucial for resource assessment, which is what the Mars Climate Database (MCD) 5.3 [22; 23] will be used for. The MCD is a database derived from a numerical model of Mars' atmosphere, validated and tuned by various observational data. The model is a general circulation model that considers the Martian atmosphere's various processes, including radiative transfers between gasses, carbon dioxide and water cycles, dust transport mechanisms, and additional chemical processes. As a result, the database allows for the prediction of various meteorological parameters, including temperature, pressure, density and wind speed, among many others. These data are available hourly for the full martian year, as well as for all latitudes, longitudes, and altitudes.

Some limitations have to be taken into account when utilizing the model. The first is the inter-annual variation of the climate. The MCD values default to an 'average' martian year. However, levels of UV radiation vary strongly in an 11-year cycle, and dust suspension in the atmosphere, which has large influences on the climate of Mars, also has a considerable variability over multiple years. It is possible to enable different scenarios in the MCD, e.g. to show the effects of a particularly dusty year. Secondly, because of the relatively low sample frequency of the model, the data is not suitable to find maxima and minima of parameters, e.g. wind gust speeds. More information can be found in the MCD documentation [25]. Finally, since the quantitative results of this assessment are based on values from the MCD, the accuracy is dependent on the reliability of the climate model.

2.3 Winds on Mars

2.3.1 Origins of Wind

In its most basic form, wind is the flow of gas caused by regions of different air pressure. If a pressure difference forms between two regions, the air in the high-pressure region will diffuse into the low-pressure region, causing a flow. The origin of these pressure differences are temperature variations caused by incoming solar radiation, partly balanced with the cooling caused by the spontaneous emission of infrared radiation. In many ways, the meteorological conditions on Mars represent a simplified version of the climate on Earth. This is thanks to similar key parameters like similar rotational speed and obliquity, which are the main reason for seasonal differences. The lack of humidity in the air, along with the absence of significant water bodies [26] leads to a climate that can be compared to the polar deserts on Earth. By looking at how temperature varies, a good understanding of the winds on Mars can be reached.

The first difference is that Mars has a much lower thermal inertia compared to Earth. A large amount of Earth's surface is covered by bodies of water, while Mars is almost exclusively covered by igneous rock. Water has a specific heat capacity of around 4184 J/kgK, while the crust of Mars only has an average heat capacity of 741 J/kgK [27]. This difference leads to much more significant seasonal differences in temperature and overall climate, as differences in radiation are not damped by a bulk storage of heat. Practically, this leads to a very stable

atmosphere (low wind speeds) in summer and an unstable atmosphere (high wind speeds) in winter [26]. To validate this, the monthly mean wind speed at 10m above the surface of Mars was calculated. Then, the wind speeds were averaged for the northern and the southern hemispheres, which is illustrated in Figure 2.1. The climate model indeed reflects the described behavior. For the first half of the year, the northern hemisphere experiences summer and the southern hemisphere winter. It is apparent that the summer/northern hemisphere has an overall lower-than-average wind speed. The roles reverse at one point, roughly when winter and summer switch during the equinox.

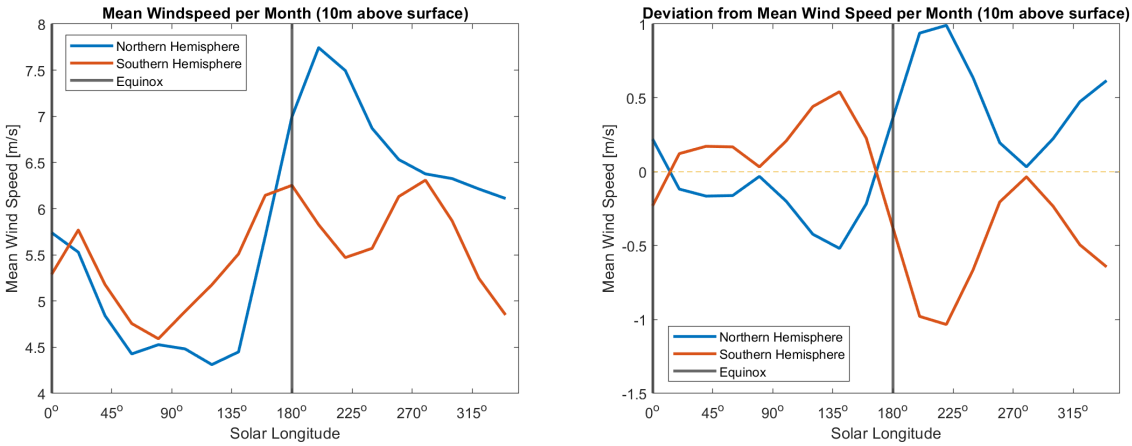

(a) (b)

Figure 2.1: Mean wind speed and deviation from mean for northern and southern hemispheres of Mars, derived from the MCD.

Diurnal wind speed variations are based on the shift in the area exposed to the sun during the rotation of Mars around its axis. The diurnal cycle on Mars is similar to the one in deserts on Earth. However, the temperature differences between day and night are much larger and can regularly reach up to $\Delta T = 100K$ [26]. This results in so-called thermal tides, which lead to predictable cyclic variations of temperature and wind speeds. The amount of suspended dust has a considerable influence on this. With more dust, heat is diffused more in the atmosphere, and the atmosphere has a greater heat capacity [28], therefore decreasing the temperature variations and thus the amount of wind.

Temperature also decreases with latitude. Close to the equator, incoming solar radiation is perpendicular to the surface, while close to the poles, the angle of the incoming radiation is much smaller, which leads to a lower radiation density per area. As a result, as the angle of incoming radiation decreases towards the poles, so does the average surface temperature. Lower temperatures and temperature variations towards the poles lead to reduced wind speeds. Additionally, the southern hemisphere of Mars is 5km higher than the northern atmosphere, which is the main reason for the differences in the climate of the two hemispheres. This is also apparent in Figure 2.1. Practically, this means that the southern hemisphere is generally warmer than the northern hemisphere, which results in much more frequent storms in the South [26].

Temperature also generally decreases with altitude, with a rate defined as the lapse rate. From thermodynamic relations, it follows that the lapse rate can be defined as [21]:

$$\left(\frac{\mathrm{d}T}{\mathrm{d}z}\right)_{\text{adiabatic}} = g\frac{1}{c_p} \tag{2.3.1}$$

For Mars, assuming a constant specific heat c_p = 860 [29] and the afore defined gravity of 3.72m/s^2, this gives a lapse rate of 4.3K/km, which is around half of the lapse rate of Earth's

atmosphere [29]. This, however, is the theoretical lapse rate. On Mars, mostly because of the dust suspended in the atmosphere, the real lapse rate is about half of the theoretical one [30]. Temperature profiles from the MCD were averaged to obtain a general relation between altitude and temperature. By fitting a linear function to the plot and taking the inverse of the slope, a lapse rate of 2K/km was obtained. Studies show an average lapse rate of 2.5K/km [29], which deviates from the value obtained through the MCD. A reason for this deviation can be the high variability in atmospheric dust concentration.

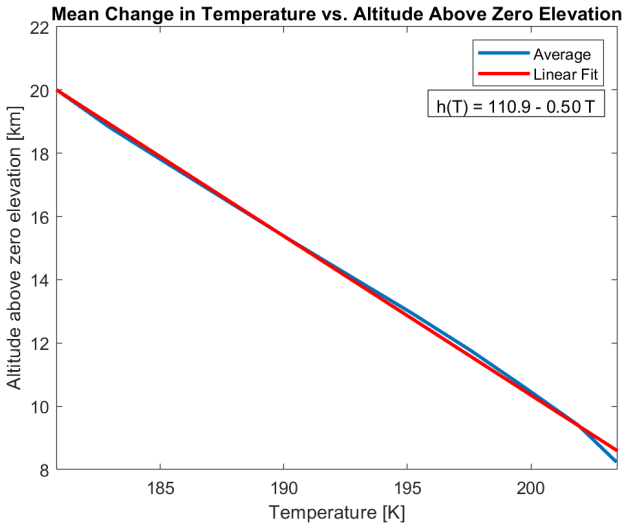

Figure 2.2: Average vertical wind speed profile between 8km and 20km of altitude above zero elevation. Lower elevations are omitted to avoid clipping the surface.

Slope wind are created through the change of temperature depending on altitude and time of day, together with varying topography. This effect is far more important on Mars than on Earth, as the differences in elevation are roughly amplified by a factor of 3 on Mars. During the day, the air close to a surface warms up quicker than the air of a similar altitude that is not in near contact with the surface. This creates pressure differences for regions of uneven terrain, causing an airflow up the slope of a mountain [31]. At night, higher situated regions cool off quicker than lower regions because of their lower density, resulting in an inverse pressure difference, leading to an airflow down the slope [32]. As mentioned earlier, variations in temperature are much larger on Mars because of the lower thermal inertia, which also strongly amplifies slope wind effects. The impact of this effect can be clearly recognized when comparing the average wind speed on the Mars surface with its topography. The average wind speed on Mars was calculated from the MCD, at an altitude of 10m above the surface, by averaging hourly data over the period of 1 year, illustrated in Figure 2.3a. Comparing this to the topographic map of Mars in Figure 2.3b, a correlation between the slope of the terrain and the wind speed is visible. The Tharsis rise, the large mountainous region in the West, has the highest average wind speed on Mars, and the edges of the Hellas basin at roughly 45^{o}S, 70^{o}E also demonstrate increased wind speeds at its slopes. For reference, a map of Mars can be found in Appendix A.

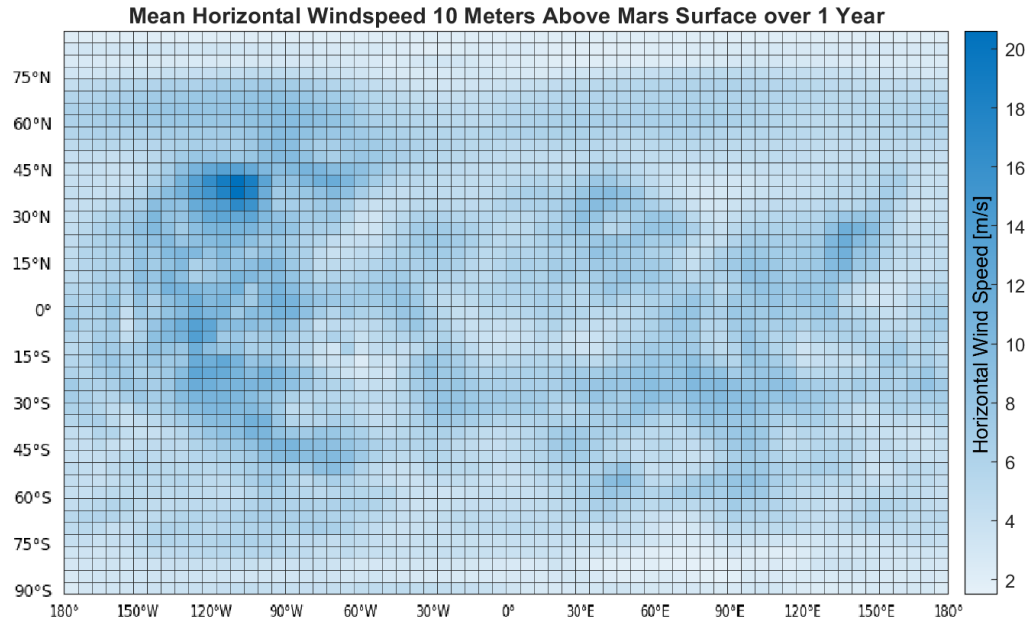

(a)

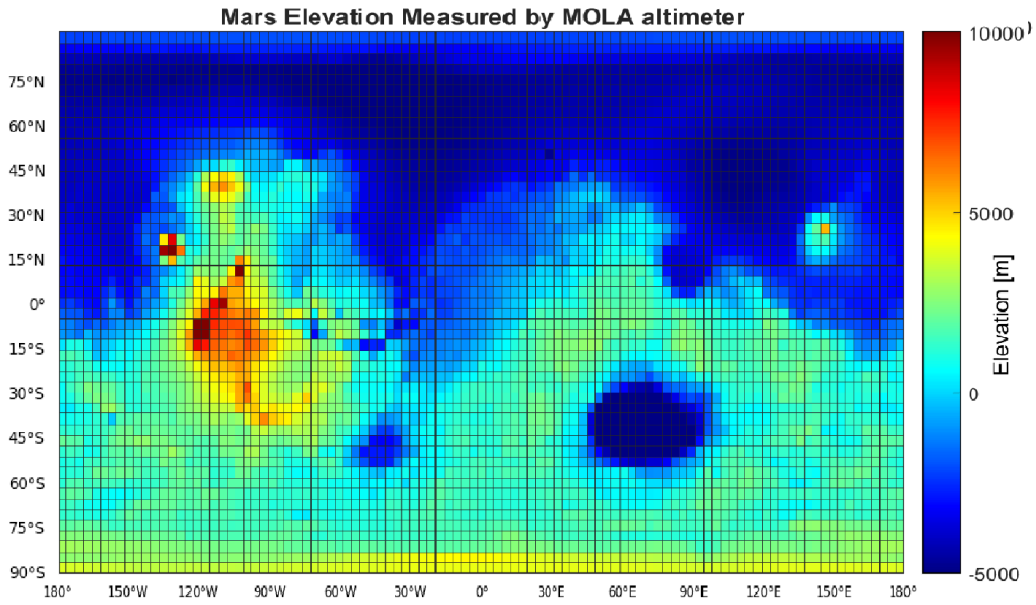

(b)

Figure 2.3: Comparison between (a) mean horizontal wind speed map derived from the MCD (b) measured Mars surface elevation illustrated by the MOLA topographic map [33].

The dust devil is an additional meteorological phenomenon that is important to mention when describing winds on Mars. These vortices, ranging from a few to over 100m in diameter, are created from local temperature hot spots caused by uneven surface heating. As hot air is more buoyant than cold air, local temperature maxima cause a small patch of air to rise, with the surrounding air following. The initial rotation can be induced by a variety of factors, including slight shear through wind, topography, or even planetary rotation, which is then amplified when the whirlwind compacts to conserve angular momentum [26]. Dust devils

appear mainly in spring and summer, and most frequently around noon, most likely related to the fact that it is the time of maximum solar radiation. The spawn of dust devils also varies regionally. The highest frequency of encounters is in latitudes between 30^oS and 30^oN, which can be explained again with the larger differences in solar radiation at lower latitudes. Wind speeds of up 100m/s were inferred from measurement results, with significant amounts of fine dust being lifted into the air through the upwards-directed airflow.

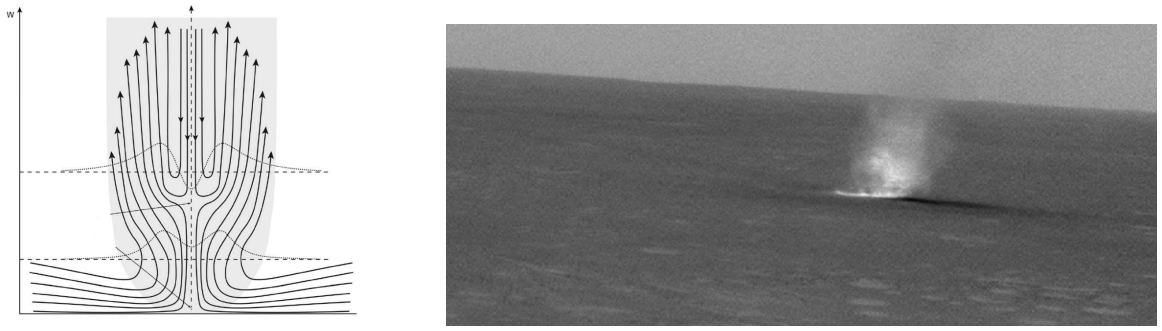

(a) (b)

Figure 2.4: (a) Schematic of possible air flow inside a dust devil (b) Dust devil photograph captured by the Spirit rover in the Gusev crater. Source: [34; 35]

2.3.2 Boundary Layer Effects

Until now, wind speeds were analyzed based on their generation, and as such, mainly based on the pressure difference. This alone does not accurately describe the wind speeds at very low altitudes. Boundary effects play a major role close to the planet's surface, which is where most wind turbines operate. Assuming no slip between surface and fluid, which means that the outermost layer of particles adheres to the surface, leads to the conclusion that the flow velocity is zero at the surface. This leads to a transition region between the surface and the undisturbed flow, known as the surface boundary layer. There are two main ways in which this behavior can be modeled, namely the power law and the log law [21]. The power law is given as:

$$\frac{u(z)}{u(z_r)} = \left(\frac{z}{z_r}\right)^{\alpha} \tag{2.3.2}$$

Alternatively, rewritten to find the wind speed as a function of altitude:

$$u(z) = u(z_r)\left(\frac{z}{z_r}\right)^{\alpha} \tag{2.3.3}$$

with u being the wind speed, z the height, z_r a known reference height, and α being the power-law exponent. Alternatively, the lower boundary layer can also be described by the log law:

$$u(z) = \frac{u^*}{k}\ln\left(\frac{z}{z_0}\right) \tag{2.3.4}$$

with u^* being the friction velocity, k being Kármán's constant, and z_0 being the surface roughness coefficient. For the application of finding the vertical profile from a reference, this can be expressed as:

$$u(z) = u(z_r)\frac{\ln((z-d)/z_0)}{\ln((z_r-d)/z_0)} \tag{2.3.5}$$

which only requires the surface roughness, which has been mapped for the surface of Mars [36]. The variable d represents the zero-plane displacement, which describes the shift in surface, and therefore the zero-wind boundary condition. On Mars, without vegetation or structures, this is usually zero. Practically, this also means that the boundary layer is much more developed, as no significant ground obstructions interfere and push the layer towards larger heights. Overall, both equations can describe the boundary layer fairly well, as long as correct coefficients are found beforehand. In direct comparison, both the power law and the log law fit the climate model reasonably well. Figure 2.5a shows the difference between the models for a sample location and time. The reference height needed for the two laws was chosen at an altitude of 800m, as low altitudes 0-100m led to much more inaccurate approximations. The still visible deviations could be caused by the fact that the MCD does not describe a single uniform flow over a surface, but other winds and turbulence at different altitudes can also play a role, skewing the boundary layer. Additionally, the MCD result shows linear segments in the wind profiles. There is no apparent physical background to this, and as such, likely an artifact of data interpolation. In Figure 2.5b, multiple vertical wind profiles were extracted

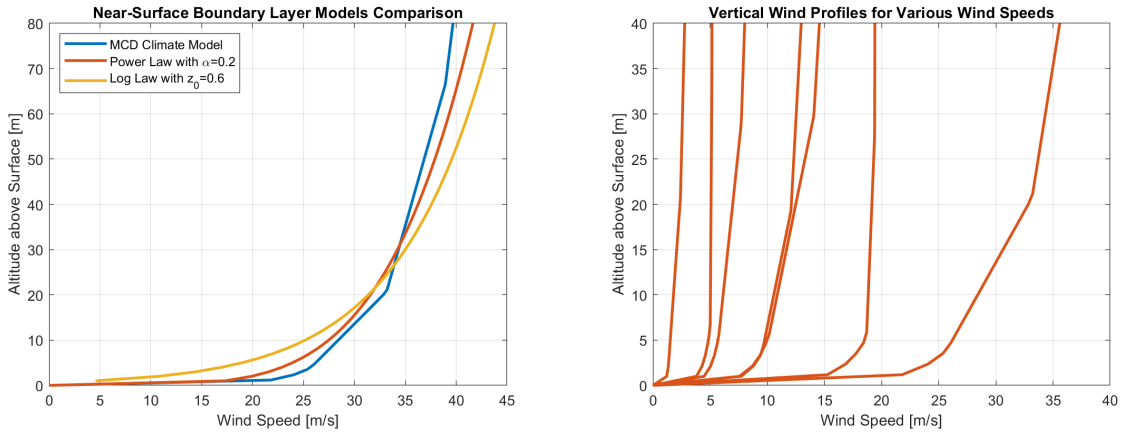

(a) (b)

Figure 2.5: (a) Comparison of modeling the surface boundary layer using the Mars Climate Database, the log law and the power law. (b) Comparison of the surface boundary layer at various wind speeds, derived from the MCD.

from the MCD to illustrate how low altitudes are affected, which is relevant for the placement and design of the wind turbine. It can be seen that the size of the boundary layer increases significantly with wind speed. For speeds under 10m/s, 5m of altitude is sufficient to reach an almost unaffected flow, while wind speeds that exceed 35m/s are still reduced considerably at 20m of altitude.

2.4 Assessment of Wind on Mars

In order to determine the potential of wind turbine power generation on Mars, a measure of suitability has to be determined, which also enables the comparison of regional variations. This can be done using wind power density. The mass flow rate is defined as:

$$\dot{m} = \iint_A \rho \mathbf{v} \cdot \mathrm{d}\mathbf{A} \tag{2.4.1}$$

Assuming a uniform (wind) velocity field normal to the (rotor) surface, the equation becomes:

$$\dot{m} = \rho v A \tag{2.4.2}$$

Power of a flow can be written as:

$$P = \frac{1}{2}\dot{m}v^2 \tag{2.4.3}$$

Plugging in the mass flow rate and rewriting the equation to represent the power as a surface density gives:

$$P/A = \frac{1}{2}\rho v^3 \tag{2.4.4}$$

This represents the wind power per unit area, which indicates the energy that can potentially be harvested. The actual power generated will always be significantly lower because of fundamental efficiency limits and other losses, which will be described later on. The assumption that the velocity field is uniform is also only approximate, as the surface boundary layer effect will always lead to a wind profile along the height. In this simple metric, the power is only a function of density and wind speed. Power prediction maps can be created with this metric. First, air density and wind speed values were extracted from the MCD for the full Mars surface, at heights of 2m and 10m above the surface. From the hourly wind speed data, the corresponding power densities were calculated using Equation 2.4.4. The resulting values were averaged over time and classified into 6 magnitude evaluations, illustrated in Figure 2.6.

The maps clearly indicate that topography plays a major role in the wind power potential of a region. There is a large bias towards the western mountain ranges, especially for winds at very low altitudes. Next to this, a decrease in winds towards the polar regions can be noted. This is most likely caused by the fact that solar radiation is much more consistent in these regions, as diurnal variations in radiation drop out more and more the further the latitude increases. Increasing the altitude increases the overall power density consistently, which is related to the described boundary layer effect. All in all, a general increase in power density of 60% can be noted when increasing the altitude from 2m to 10m. The strong increase is because velocity is cubed in relation to power, and therefore small increases in wind speed have strongly amplified effects on the power. Quantitatively speaking, no region has the potential of generating power in a similar way to Earth. The terms 'very poor' to 'excellent' were chosen relative to the distribution of power on Mars. On Earth it is common to classify everything below $100\mathrm{W/m^2}$ or even $200\mathrm{W/m^2}$ as poor for wind energy generation [21]. Therefore, it is likely that the overall power production for a similar-sized turbine will be much lower on Mars compared to Earth.

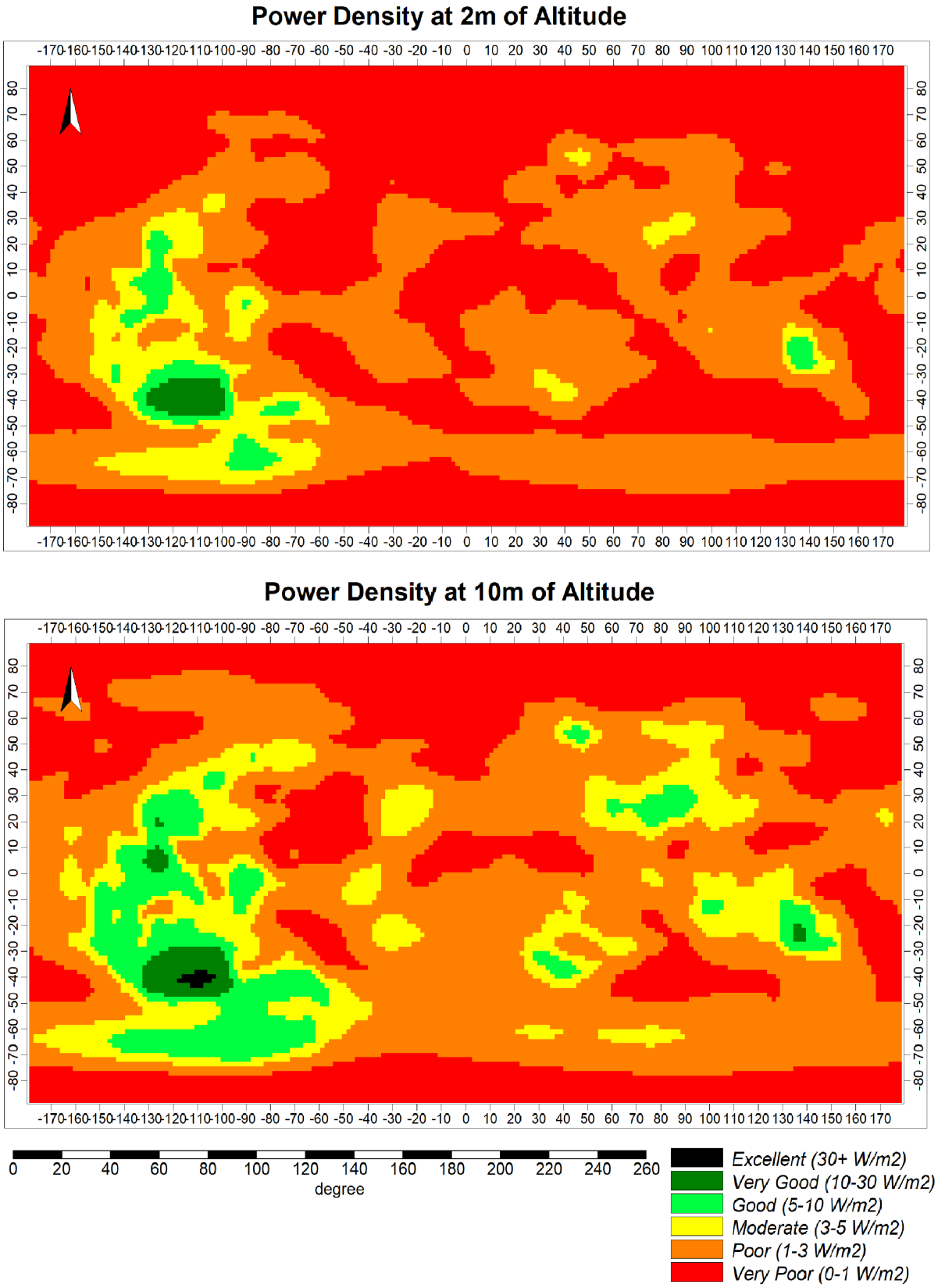

Figure 2.6: Available wind power on Mars at altitudes of 2m and 10m.

The variability in wind speed is another important consideration. Even if a site features an exceptionally high mean wind speed, it might still not be a suitable location if the variability is too high. Especially for stand-alone applications, having a consistent supply of power is essential as storage capabilities will be limited. High variability can also indicate frequent extreme wind speeds, which usually cannot be harnessed fully by the turbine. On the other hand, for the same average wind speed, regions with higher variability also have a higher power density, as wind speed is cubed in relation to power.

A common way to look at wind variability is using a Weibull distribution, as it was found to accurately fit the distribution of wind speeds. Also on Mars, it was found that the wind speed distribution fits the curve well. It is a two-parameter approximation based on a shape factor k and a scale factor c, defined as [21]:

$$f(v) = \frac{k}{c}\left(\frac{v}{c}\right)^{k-1} \exp\left\{-\left(\frac{v}{c}\right)^{k}\right\} \tag{2.4.5}$$

The shape factor k is the determining factor for variability. Higher k values designate narrower distributions and less wind speed variability. For comparison, values between 1 and 3 are common in the Netherlands, with variability being increased at lower heights [37]. Using the hourly wind speed data from the MCD, a map was created illustrating the regional differences in wind variability on Mars through the Weibull shape factor k, which was determined in Matlab using the `wblfit` function. The 95% confidence intervals associated with the fit rarely exceed ± 0.2, which speaks for the accuracy of the distribution fit.

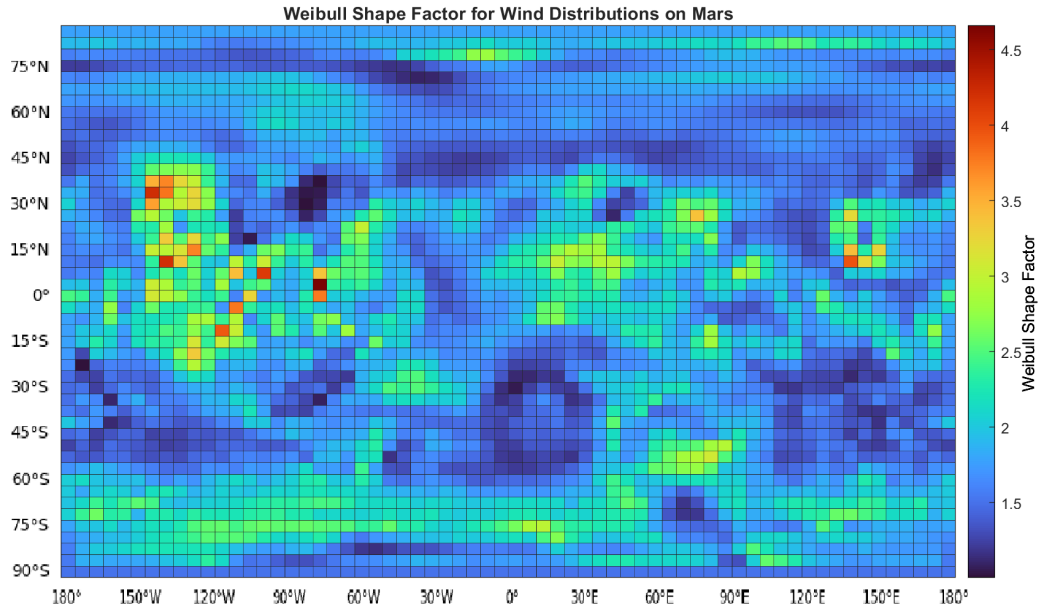

Figure 2.7: Weibull shape factor showing the variability of Martian winds based on hourly wind speed data from the MCD.

Looking at the map in Figure 2.7, it can be seen that the range of k values are similar to the ones expected on Earth. The Tharsis Rise in the West, which was the region with the highest average wind power density, also shows the most consistency. Large differences in k values can be noted, with some regions being much more variable than others. Considering the variability is therefore very important when determining possible potential sites.

Chapter 3

Concept Analysis

This chapter aims to lay a foundation for the potential merits of using wind turbines on Mars and establish functional and operational requirements and constraints to enable the design of initial working systems. The framework and definitions used to structure this analysis are partially based on the work done by Larson and Wertz [38] but adjusted to fit the goals and approach taken in this report.

3.1 Objective Definition and Utility

3.1.1 Objective Statement

As introduced in Chapter 1, the sources of power generation for space missions have remained stable throughout the last 50 years, with nuclear-based thermoelectric generators and photovoltaic cells as exclusive solutions for Mars missions. The *primary objective* of this analysis is to explore the potential in harnessing wind energy on Mars, which in turn can be used to supply electricity to the ever more energy-demanding endeavors on the Martian surface. The frequency and complexity of measurements by rovers and landers is mainly bottle-necked by the supplied energy, forcing power-intensive experiments to operate in intervals, giving time to recharge the batteries acting as an energy buffer. The solar-powered InSight lander, for example, has to switch to lower sample rates for its measurement devices during winter because of the lower radiation levels and increased heating requirements [39]. Similar issues apply to the mobility of rovers, which, when powered by solar radiation, is generally limited to a window of 4 hours around noon [40]. Diversifying energy supply becomes increasingly relevant with the chances of airborne systems being employed soon, given the initial success of the flight tests of the Ingenuity helicopter. Generating enough lift to overcome Martian gravity, albeit considerably lower than on Earth, requires a significant amount of power.

Contrary to the primary objective, *secondary objectives* are not crucial for determining the operation's success, but are additional benefits resulting from the chosen approach. First off, wind turbines can have a dual purpose in simultaneously generating power and measuring wind speeds, therefore functioning as a basic anemometer. With large regions of Mars' climate still unexplored, having the possibility to gather additional information without an additional measurement device can be advantageous. As shown previously, dust storms on Mars can be a significant risk for Mars missions. In order to better understand the underlying fundamental principles, as well as setting up an accurate forecast system, much more wind data is required [26]. Overall, the atmosphere of Mars is a topic that has and will be thoroughly investigated, from climate and weather forecasting to the possibilities of the airborne system, with the pilot

project being the Ingenuity helicopter. The design and implementation of a wind turbine can help understand the aerodynamic implications of the Martian atmosphere. This includes uncovering possible complications or unknown phenomena, next to being a great opportunity to validate computational models and wind tunnel experiments conducted on Earth.

Additionally, creating an increased variety of power sources can prolong Mars missions through the increased redundancy in power supplies. Out of the 10 main lander and rover missions to Mars that successfully relayed information to Earth over a prolonged time, 5 ceased operation because of a drop in solar power, 3 because of energy storage issues, and 2 because of communication issues [1]. The usage of solar power in conjunction with wind power decreases the risk of a drained power supply, as the drops in solar power during nighttime, winter, and dust storms can be at least partially rectified by wind turbine power. Even if wind turbines are not able to supply enough energy to fully supply a system with power, generating just enough for emergency thermal control and communication can allow for far prolonged missions and provide a strong safety feature for more advanced missions.

Especially in recent years, sustainability has become a crucial design factor in virtually all technological endeavors on Earth because of the growing environmental issues that are being faced. Therefore, it becomes increasingly important to promote a sustainable approach to space exploration and scientific research in general. Convincing the general public that measures are taken to design interplanetary missions as sustainably as possible can positively impact the support of such missions.

A more compact overview of the described objectives is displayed in the table below.

	Objective Statement
Primary Objective	To harness winds on Mars to generate electricity suitable to supply rovers or other surface-based devices with power.
Secondary Objectives	To collect measurement data from the wind turbines to gain insight into the martian climate. To better understand the aerodynamic implications within the lower Martian atmosphere. To increase redundancy for advanced Mars missions, decreasing the risk of fatal power drains. To display the importance and value of sustainable energy technology for and beyond space exploration to the general public.

3.1.2 Preliminary Utility Estimation

Before diving into the various factors, constraints, and requirements that have to be considered for a working system, a fundamental definition of what performance constitutes a successful design is necessary. For terrestrial applications, the cost is usually the factor that is minimized. Oversimplified, the most power produced at the lowest cost makes for the best solution. In the end, this is also true for space exploration. However, the big difference lies in the distribution of costs, which can be seen by looking at the budget breakdowns of comparable past missions [41]. Even an extremely capable load is only a small fraction of any mission and usually under 10% of the total cost. For Mars missions budgeted at around 2B$, more than half is spent on the flight system and launch vehicle, while the actual lander/rover only accounts for around 300M$. Since the cost of launch scales dramatically with increased weight, a better initial metric for the power supply is power generated per mass, similar to the specific energy derived in Chapter 1. From the values used to derive specific energies of MMRTG and PV power

supplies [1], Figure 3.1 illustrates a simple scheme of the initial utility estimation.

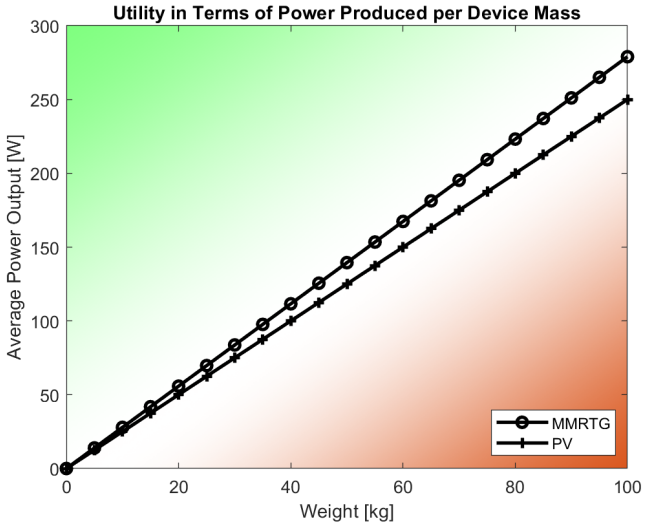

Figure 3.1: Simple quantitative illustration of the utility of a designed system.

With space exploration being a fast accelerating field, it is important to validate whether this data on PV and MMRTG technology is still accurate. This can be done by looking at the latest uses, the Perseverance rover using MMRTGs, and the InSight lander powered by PV cells. The MMRTG powering Perseverance weighs 45kg while producing a declining rate of power, peaking at 110W [42]. Looking at the plot, this still fits well into the expected performance for nuclear systems. The same can be said about solar power since InSight uses the same UltraFlex panels used on the older 2007 Phoenix lander [43], which shows that no disruptive innovation took place between those missions.

For an initial design, it is not crucial that the produced power supersedes the standards set by MMRTG and PV technologies. Even a worse system can still be regarded as a proof of concept and, thanks to the secondary objectives, be deemed a worthy consideration. Technology demonstrators can lead the way for future, more sophisticated versions that are more practical and provide higher utility. A working system has to operate within the performance requirements set out here, but also has to comply with all additional practical constraints and requirements, which will be addressed next.

3.2 System Drivers

The system drivers are the key controllable parameters that determine the feasibility and success of the designed system. These drivers generally limit and are limited by other factors, and therefore lay a groundwork for the decisions, constraints, and trade-offs that have to be dealt with during the design process. Therefore, defining an exhaustive list of these drivers is crucial to minimize the chances of unforeseen complications hindering the achievement of the primary objective. For this analysis, these drivers are split up into three main steps, the *transport* from Earth to the desired installation site on Mars, the *installation* of the setup, and the *operation* of the system. All design decisions have to be suitable choices for the drivers in all three steps to ensure a working design.

3.2.1 Transport

The logistics of bringing equipment to the surface of Mars have been relatively consistent in terms of approach over the last years, while the associated scientific value increased through larger payloads and decreased component weight. The main approach of Mars missions can be broadly separated into three steps. The first step is based on the launch vehicle, which brings the payload into orbit around Earth. These vehicles are commonly classified depending on their payload [44]:

- Small-lift launch vehicle (SLLV): Under 2000kg
- Medium-lift launch vehicle (MLLV): 2000kg to 20.000kg
- Heavy-lift launch vehicle (HLLV): 20.000kg to 50.000kg
- Super heavy-lift launch vehicle (SHLLV): Over 50.000kg

The following step is the cruise stage, which is used to transport the desired item from Earth to Mars and initiate entry into the atmosphere. This stage also requires propulsion for course corrections and maneuvers while also being powered to ensure stable communication with Earth throughout the cruise. The weight of this stage also has to be taken into account when determining launch vehicle payload. The final step is entry, descent, and landing (EDL), which decelerates the item to the surface of Mars. This is generally regarded as the most challenging aspect of the payload transport, which is also the reason for it being dubbed the 'Seven Minutes of Terror'. An aeroshell is used for this, which encapsulates the object entirely, and shields it from high temperatures. The object has to be decelerated enough to survive the impact on the surface. Unlike Earth, on which parachutes are generally used for similar tasks, the low density on Mars makes it inefficient to fully slow down the object this way for a soft landing. For this reason, additional methods have to be employed for the last moments of descent. The three main methods used include the usage of rockets attached to the lander, using airbags to absorb the impact, or using a skycrane system to lower the object to the surface.

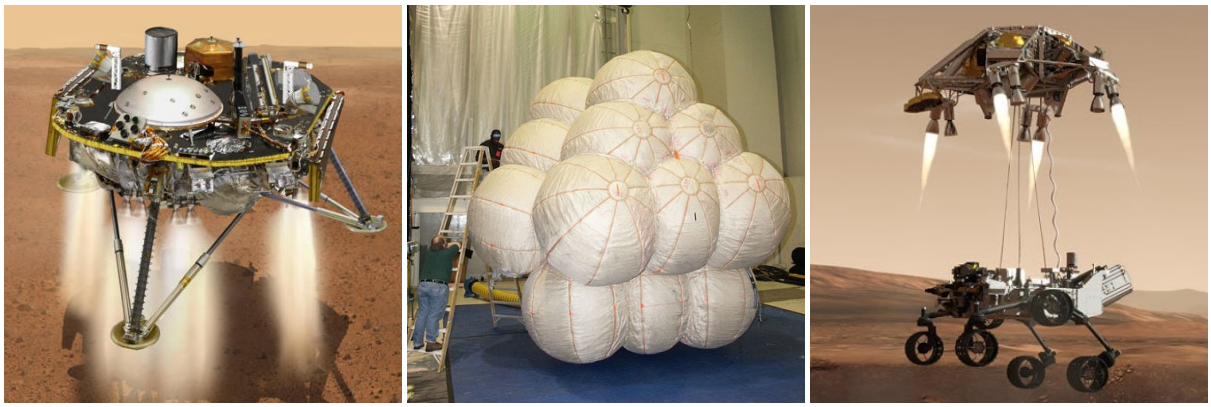

(a) (b) (c)

Figure 3.2: Landing mechanisms employed for Mars missions: (a) rocket-assisted landing, (b) airbag system, (c) skycrane system. Source: [45; 46; 47]

Size and Weight

Size and weight are critical factors in any space exploration mission. A wind turbine designed for a small-scale application does not approach any weight limitations, considering the latest landing of the Perseverance rover having an EDL stage weighing over 2 tons. The weight, however, is the major determining factor of utility. Even though it is technically feasible to

land a 1-ton heavy turbine on Mars, in order for it to compete with existing energy sources, it would need a power output of around 2.5kW, which is unrealistic to achieve. Hence, the weight has to be limited to keep the technology competitive and efficient to use. This also limits the options in terms of landing, as using a rocket-powered lander or even a skycrane system adds significant weight to the entry vehicle that has to be taken into account when determining the utility. Overall, limiting the weight has a major impact on the design value, and therefore is crucial to account for in all aspects of the design process.

A larger concern is the dimensioning of the turbine for transport. The maximum dimensions are mainly limited by the EDL procedure, and therefore by the dimensions of the aeroshell. The aeroshell is designed to provide a balance in lift and drag that keeps temperatures of the bottom heatshield at allowable levels while also slowing down the descent as much as possible. This is especially important for Mars, as the thin atmosphere requires significant deceleration of the aeroshell before parachutes can be deployed, which is only possible through an optimal shell design. Figure 3.3 shows the dimensions of the largest aeroshell used for a Mars EDL. The requirements for an optimal entry lead to a conical construction with a relatively large radius compared to its height. This aspect ratio is not ideal for containing an erect wind turbine, putting severe constraints on the tower height and diameter of the turbine. In order to optimize the design of the mission, the shell should be packed as densely as possible to limit excess weight and size. Designing a system that fits into the shell while also maximizing tower height and turbine diameter requires careful management of necessary deployment mechanisms. These mechanisms will likely become necessary, as a fully assembled turbine has too severe dimensional constraints for efficient transport. Using a large aeroshell for a lightweight turbine is not resource efficient. It is likely that the turbine will have to fit into a very small shell, or share the shell with the device being powered by the turbine. Since most recent missions and the overall trend are heading towards heavier missions, the latter option might be the more likely scenario.

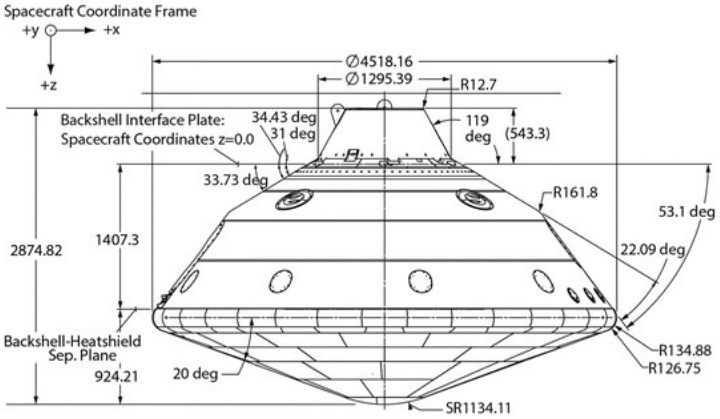

Figure 3.3: Lockheed Martin aeroshell dimensions [48].

Structural Requirements

Structural requirements not only apply in the installed state in reaction to the forces by the wind, but also in the compacted layout of the system in the transport stage. The cargo starts experiencing structural loads during launch and ascent. During this first stage of the mission, these are mainly induced through the operation of the propulsion system of the launch vehicle. The following list illustrates the main events to consider for load analysis as part of the NASA load analyses guidelines [49]:

- Engine Ignition
- Launch Pad Release
- Lift-off
- Maximum Dynamic Pressure
- Transsonic Buffet (shocks and oscillations at high subsonic speeds)
- Maximum Acceleration
- Stage Separations and Engine Shutdowns
- Thrust Oscillations and Combustion Vibrations

For the Atlas V MLLV, which was used for both the Curiosity and Perseverance missions, the encountered loads during these events are documented [50]. During launch, relatively mild axial accelerations of $1.2 \pm 0.5g$ are noted. At the booster-engine cut-off point, the maximum accelerations are noted, with axial accelerations of $5 \pm 1g$ and lateral accelerations of up to $3 \pm 1g$. Additionally, large shocks peaking at $4500g$ are generated at the payload adapters during the pyrotechnic stage separations. More so than during launch, structural loads are critical in the EDL phase. EDL reports can be found for both the Phoenix lander and Curiosity rover, which can help give an idea of the loads during descent [51; 52]. The Phoenix lander experienced a peak deceleration of 8.5g, which is lower than the 12.2g peak of Curiosity. These peaks generally occur as the parachute inflates. Vibrations are common during the approach, not only because of the turbulence associated with the fall but also because of the breathing effect of the parachute moments after deployment. At last, touchdown velocities of past missions are below 1m/s for landing on wheels, around 2.5m/s when using crushable legs, and 5 to 12.5m/s when using airbags [53].

Overall, strict guidelines are imposed on the requirements and their validation for the sake of a successful mission, especially for the ascent, to limit safety concerns during launch. Making sure that the wind turbine design is well suited to handle the forces during transport with high certainty is necessary, as the possibilities of system repairs are extremely limited to non-existent after launch. From the past EDL reports, it is visible that deviations from the calculated procedure and expected loads are common because of the high uncertainties in the execution in the various mission steps, which makes it even more important to overestimate the various design requirements.

Thermal Requirements

Traveling from the surface of Earth to the surface of Mars, the turbine system is confronted with a variety of temperatures. These can influence the integrity of the design, both from a structural and an electronic standpoint, especially for integrated power storage. The design of the components has to happen in close relation to the thermal control possibilities of the transport. During launch, the peak heat flux radiated can reach 550W/m2 for the inner surface of the hull, while temperatures stay below 100^{o}C [50]. Considering the large range of required operating temperatures on Mars, which will be discussed as part of the environmental considerations, these temperature ranges should not pose any issue on the design, especially considering that the aeroshell provides a second layer of insulation.

During cruise, large temperature differences occur between the sun-facing side, which is heated through the sun's radiation, and the sun-trailing side, on which large amounts of radiation dissipates. Regulation happens through using passive (insulation, coatings, shades) or active (heaters, thermoelectric coolers) thermal control systems [54]. To avoid large temperature differences, it is also common for the cruise stage to rotate around its axis to get even levels of solar radiation throughout the surface.

At last, the temperatures during EDL on Mars have to be considered. For this, the thermal

events documented for the EDL of the Curiosity rover can be used for reference [55]. The thermal shielding that the aeroshell provides is highly effective, and even though the bottom heatshield of the shell can reach temperatures up to 1400^{o}C during peak aeroheating, this heat was barely detected inside the shell. The biggest detectable change was after heatshield jettison when the rover was exposed directly to the Martian atmosphere. Even though the air temperature was around -27^{o}C, this process even warmed the rover up in some cases due to the generated friction.

Overall, thermal management of the payload is a crucial aspect to transport to Mars. Still, because of the stringent requirements of various sensitive measurement devices used in space missions, active and passive temperature control generally ensure no damage occurs. Practically, this means that the payload design dictates the thermal control system, more so than the other way round.

Target Site

The limited landing accuracy is the last driver to consider. As the lag in communication between Earth and Mars is larger than the time between crucial decisions that need to be made during the EDL, the descent vehicle has to be fully capable of an automated procedure. This is much more challenging on Mars compared to Earth because of the much lower atmospheric density. The density is too thin to allow deceleration to subsonic speed as quickly as on Earth but still has enough density to generate high amounts of heat due to drag. Coupled with a limited understanding of the air variability within the Martian atmosphere, careful planning is required to ensure a successful procedure [56].

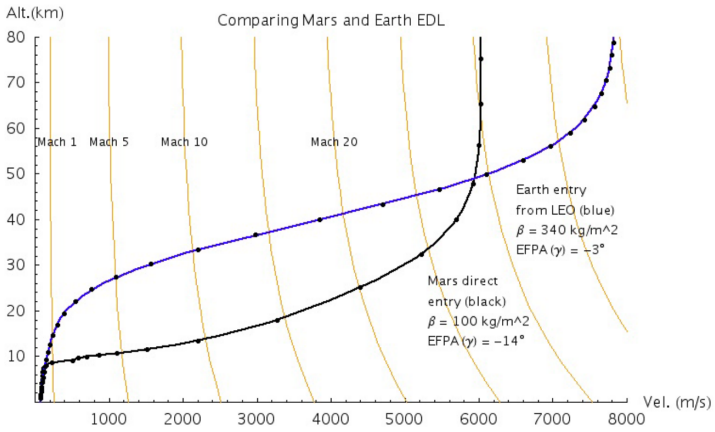

Figure 3.4: Comparison of altitude and velocity for a ballistic EDL on Earth and Mars [53].

These complications are reflected in the execution of past successful EDL designs. Missions were always limited to landing sites below zero-level elevation, to enable maximum deceleration through the thicker lower atmosphere. This leads to all lander/rover missions being limited to the equatorial and northern regions, excluding the southern highlands and mountainous regions. Accuracy in landing is also limited because of these challenges. The recent Curiosity and Perseverance rovers were the first to use hypersonic guidance to increase the accuracy of their descent, still leading to a limited accuracy of 5km radius. The problem of deceleration is largely coupled to weight limitations. An all-propulsive EDL system would solve landing accuracy limitations, but would also require a 20:1 weigth ratio of EDL system to payload. However, if the atmosphere is used for deceleration, this can be reduced to around 5:1 [57].

During landing, complications arise through the rocks scattered on the surface. While

legged landers have a clearance of roughly 30cm, propulsion systems have to be extremely accurate in their cut-off timing, as firing them too close to the ground leads them to dig into the ground and launch debris back in the air, while also destabilizing the lander. This means that the thrusters have to cut-off earlier, leading to a higher impact speed and to an increased risk of tipping over on sloped surfaces [53]. The more recent used alternative is the skycrane, which avoids the risk of firing thrusters close to the surface by lowering the payload from the air, as was shown in Figure 3.2c.

For the case of transporting a wind turbine system, EDL is the most important consideration. When analyzing the winds on Mars in Chapter 2, it was established that the higher situated, mountainous regions receive more wind, especially because of the effect of slope winds. Landing in these regions is the most challenging because of their elevated altitude and limited air density, the large number of surface rocks, and the sloped terrain. High-accuracy systems, lightweight enough to be practical while also providing sufficient accuracy to avoid dangerous terrain, will be necessary for a successful design.

3.2.2 Installation

After arrival, the system must be installed and deployed to reach an operational state. The challenges that apply when transporting a payload impose constraints on the design, especially regarding dimensioning and weight management, which will require a setup procedure once landed. For wind turbines on Earth, this is a complex operation involving building a foundation, assembling and erecting the tower, and attaching the nacelle and the blades. On Mars, a similar procedure is next to impossible because of the complete lack of installation-supporting infrastructure. Hence, all auxiliary equipment has to be contained within the same landing shell. Human interference might become a possibility in the future, but to ensure universal applicability of the design steps, the focus will lie on a human-independent approach, since otherwise, a resulting design cannot be regarded as a current solution.

Anchoring

The first step is the process of making sure the turbine stands stably. A variety of forces act on the turbine during operation, which requires a firm connection to the ground to avoid tipping and to maintain structural integrity. In theory, a system that does not rely on any ground anchoring is a possibility, but only if sufficient weight is allocated at the foot of the turbine. By extending the base, tipping can be avoided. However, such a system can become a less effective solution in terms of power-to-weight ratio, as all the force has to come from the mass of the turbine itself, and no benefit is drawn from friction or shear forces in the ground. This cost in weight is amplified through the fact that gravity on Mars is only around one-third compared to Earth. The trade-off between a simple system requiring more mass and less installation and a more lightweight and more complex anchored system will have to be considered. On the other hand, a significant mass will always be allocated to the aeroshell and heatshield, which never had a purpose post-landing in current mission designs. By including the landed shell as part of the turbine's foundation, the additional weight can be used to provide additional security while already providing a platform for erecting the turbine.

The surface characteristics of Mars are elementary to any design that involves ground anchoring. Depending on geographical location, different surfaces are encountered on Mars. Martian rock can be both sedimentary and igneous. Sandstone or even clay formed from the compression of smaller particles leads to a layered rock formation, often covered by larger amounts of sand. Igneous rock, which forms directly through the solidification of magma and lava can also be found throughout the surface. Overall, fine-grained dust drifts throughout the

surface of Mars, covering a majority of the surface, and leading to the formation of large sand dunes [58].

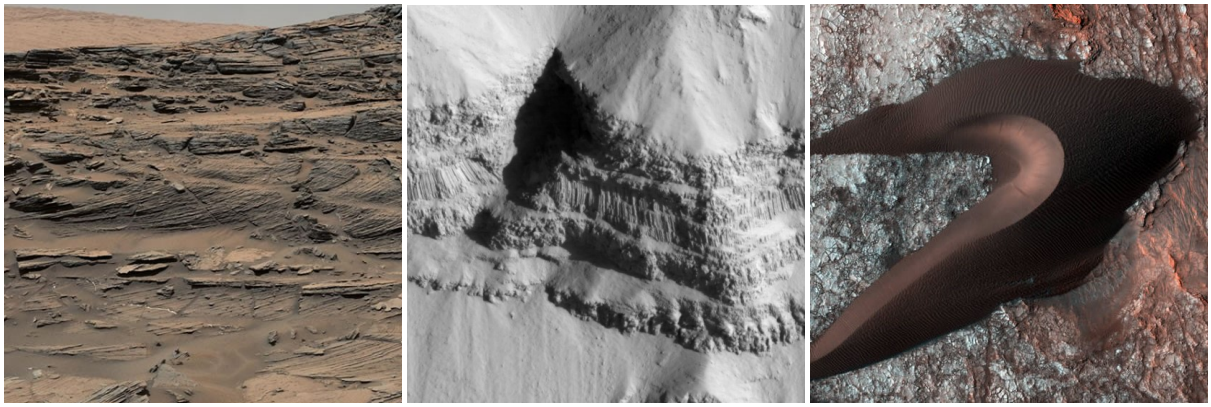

(a) (b) (c)

Figure 3.5: Types of common Martian surface features: (a) sedimentary sandstone, (b) basalt rock pillars, (c) sand dune. Source: [59; 60; 61]

The extent of dust-covered regions can be analyzed by looking at the thermal inertia of the surface. Areas with low thermal inertia generally suggest an abundance of dust, while high inertia relates to exposed rocks and an overall more coarse surface. The northern and southern extremes are an exception to this, as in these regions the larger thermal inertia is caused by the higher heat capacity of the polar caps [58]. Figure 3.6 shows values of thermal inertia of the Martian surface, which shows which regions are most covered by dust compared to higher exposed rock.

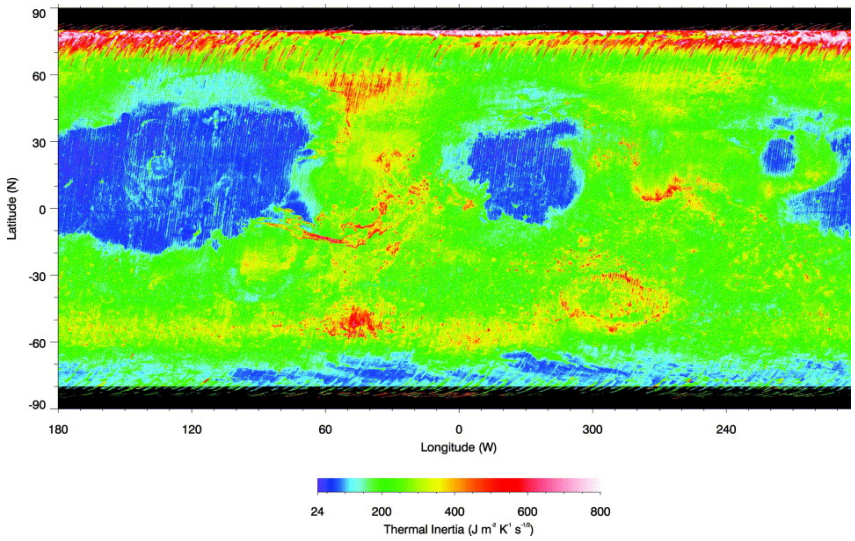

Figure 3.6: Global Thermal Inertia of Mars derived from the MGS mapping mission [62], higher values represent a higher degree of exposed rock.

Detailed knowledge and planning of the landing site's surface characteristics are crucial to determine the necessary ground clearance and possible landing complications. However, it is also vital for the stability of the design and, therefore, for the design life. In regions that are complete covered by deep-reaching dust, the installation would be extremely challenging due to the dynamic nature of deserts. The fine dust is easily picked up and transported by winds, leading to regions of traveling sand dunes. Exposed bedrock or sedimentary and igneous rock formations can provide sound structural integrity to the design, providing a rigid floor

or even opportunities for additional security through drilling. Still, scattered rocks and steep slopes can also make anchoring more challenging.

Deployment

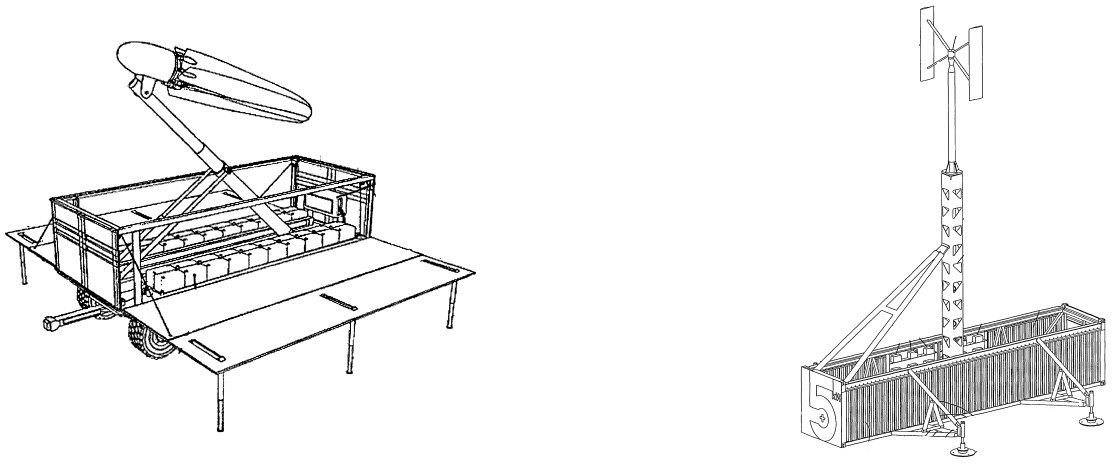

(a) (b)

Figure 3.7: Terrestrial deployable wind turbine designs (a) Rapid Energy Mission Module by NPC Energy [63], (b) ATOPIA Research VAWT [64].

Current aeroshell designs do not feature a layout suitable for the transport of an erect wind turbine. This is why it is important to look at the deploy mechanisms that can be used to allow for a compact transport layout of the system while erecting once the surface of Mars is reached. These mechanisms should allow for a change in geometry, from a compact, stowed configuration to a final, functional version. The denser the design can be packaged, the more cost-efficient the whole system will be. When looking at horizontal axis wind turbines, the dimensions are mainly based on the turbine radius and the tower height.

Aside from the required hinging and orientation mechanisms, a compact way of compressing tower and blade dimensions while still constituting a single deployable component is the main design problem. No similar system has yet been proposed for wind turbine application on Mars, and terrestrial solutions typically follow less strict packaging constraints, as can be seen by the solutions shown in Figure 3.7. The closest reference design elements are found in deployment methods used in spacecraft, which require similar dimensions, albeit the parts are generally confronted with lower loads because of the lack of gravitational acceleration and air resistance.

In a review of deployable booms for space-borne observatories [65], the main design options are listed and compared. From there, the most suitable to be used for a load-bearing part, for example in the application as a turbine tower, are truss structures, telescopic booms, and articulated booms. These options feature the highest stiffness while also allowing for tighter packaging. In designing a suitable mechanism, tight packing will always be a trade-off compared to the system's rigidity. The deployment of the turbine blades is more complicated, given the small tolerances needed for optimal aerodynamic performance. Full-sized rigid blades will most likely have improved performance over any deployable system. However, the power output is then limited by the swept area that fits inside the aeroshell. In principle, telescopic or articulating mechanisms are still possible design options if the increased power output through the larger swept area outweighs the aerodynamic losses caused by the increased surface roughness at the connection points and the decreased structural integrity.

Alternatively, more complex mechanisms can be considered for this critical component. Inflatable structures allow for very compact packing but can lack in bending stiffness [65]. Next to this, there is always a risk of leakage, which would render the whole system nonoperational. Recently, the potential of shape memory polymers for aerospace applications has been investigated more and more [66; 67]. These structures carry information about their shape through a hibernated stage, in which the structure is rolled up or folded. Once activated through heat, radiation, or electric stimulus, they return to their original shape. The mechanical simplicity, large packing density, and low weight are the main advantages, with the biggest challenge being the limited strength of the final component.

Next to the packing of the biggest components, the actual deployment mechanism also has to be considered. Likely, the main required steps are going to be the vertical orientation through the ground anchoring, the expansion of the tower, and the unfolding and extension of the blades. Since the system will likely feature power storage for reliable operation, this battery can be considered as auxiliary power for actuators, or compressors in the case of inflatable components. Storage of potential energy in springs or the usage of shape-memory can be considered as alternatives to limit the required power.

Overall, the deployment is strongly coupled to the structural integrity required for the operation of the design. Trade-offs between weight, packing density, mechanical simplicity, and rigidity require careful design evaluation to determine the optimal solution.

Power Distribution

An additional consideration is the power distribution. Once the turbine is set up in an operational mode, the way power is distributed still must be considered. The main options include a fixed connection, plug-in systems, or inductive systems. Fixed connections are only an option for stationary landers. For applications requiring larger mobility, such as rovers or drones, detachable solutions are necessary. Plug-in systems have minimal losses but require mechanisms to ensure a working connection. Inductive charging can alleviate some of the complexity, as long as losses can be minimized to avoid losing significant power compared to direct connections. The point of distribution also has to be considered. Especially for more complex systems which have a higher chance of failure, such as drones, a power distribution at a reasonable distance from the turbine can minimize the chance of collateral damage in case of one system failing. Deploying a cable during the last stages of descent can be considered a simple mechanism to increase the distance between the turbine and distribution point.

3.2.3 Operation

While transport and installation are one-off steps, the operation is a continuous process. Design choices for the first two steps have to be considered in terms of failure probabilities, but the choices made in terms of operation influence the design life of the turbine. For surface-based missions on Mars, the life expectancies of Curiosity and Perseverance were set out as 1 Martian year. The actual operation has the potential of far exceeding this time span, with Curiosity being active for over 5 times the design life already. However, the understatement of the potential of these missions could be attributed to aid public appearance. The design life required for a wind turbine largely depends on the desired application, which influences the choices made for the various drivers.

The operational design drivers for wind turbines on Mars are relatively similar to the drivers on Earth, only with acoustical and visual considerations largely insignificant for Mars. However, a big disadvantage is the lack of serviceability of the turbine. Regular maintenance

check-ups, testing, repairs, and cleaning are essential considerations for turbine designs for Earth [21]. On Mars, even single maintenance operations are not feasible, as the required infrastructure is far too costly considering the limited power generated by the turbine.

Aerodynamic Efficiency

The aerodynamics of the turbine blades are the core operational aspect of the power generation. As shown at the end of Chapter 2, a power density based on wind speed and air density can be computed. However, this power does not render any help if the rotor does not harness it. The design of the rotor system has a significant impact on the power that can be extracted and requires an understanding of the underlying aerodynamic principles for a sound design. To keep this section balanced and as concise as possible, the focus lies more on the practical design choices instead of a theoretically built analysis. For an understanding of the underlying aerodynamics, along with the derivation of relevant equations, Appendix B can be referred to. Additionally, a detailed quantitative analysis will follow in the aerodynamic design procedure in Chapter 4.

First, the desired power rating has to be found based on the desired application. However, all wind turbine systems have significant losses associated with them. This includes the aerodynamic limits or the mechanical conversion step. Through a rough indication of the power expected, a required swept area based on the available wind power density can be determined. The first parameter relevant for any wind turbine design is the power coefficient C_p, which describes the ratio of extracted power:

$$C_p = \frac{\text{Generated Power}}{\text{Available Power}} \tag{3.2.1}$$

The highest power coefficient leads to the most efficient design. The fundamental limit is given by the Betz coefficient, derived in Appendix B, which gives $C_{p,max} = \frac{16}{27}$. The amount of power extracted is based on the rotational speed of the rotor. A slowly rotating turbine will let more wind pass through undisturbed, while a faster turning turbine will stop more of the incoming wind. The speed at which the turbine rotates with respect to the wind speed is defined as the tip speed ratio (TSR) λ:

$$\lambda = \frac{\text{Speed of Rotor Tip}}{\text{Wind Speed}} \tag{3.2.2}$$

A maximum power coefficient can be found at a certain TSR, marking the optimal rotational speed for the turbine. Keeping the turbine rotating at that ratio to the incoming wind will lead to the highest possible power output. Sometimes, lower TSRs are chosen, sacrificing efficiency to gain a more stable, less complex system, as higher speeds lead to higher loads on the system. For the application on Mars, this also has to be considered carefully. In the end, efficiency is not the key factor to optimize, but reliably getting the most power output at the lowest weight. The optimal TSR also depends on the number of turbine blades. Lower blade numbers lead to less even load distributions and can impose structural constraints. Especially if anchoring the turbine is a large challenge, the design might have to opt for a higher blade count to keep the turbine stable. Lower-bladed turbines have their optimal performance at higher TSR, making them rotate at higher rpm, which can be favorable for efficient generator design. On the other hand, the increased swept area of higher-bladed propellers leads to lower start-up wind speeds, which can extend the operating range of the turbine [68]. Figure 3.8 shows sample power coefficients for various blade numbers at different TSR values. In order to alter the TSR of a working turbine, the pitch of the blades can be controlled by changing the angle of the blade with respect to the wind. The way the turbine defines a relation between TSR and power coefficient can be separated into two distinct approaches, constant speed turbines

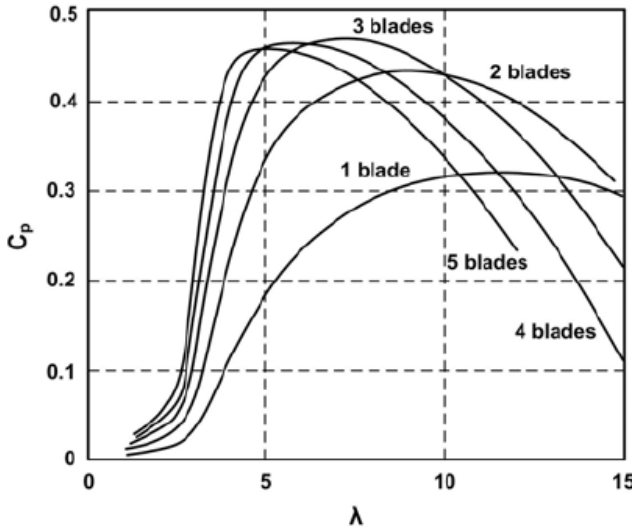

Figure 3.8: Sample power coefficient versus tip speed ratio for different numbers of blades [69].

and variable speed turbines. For maximum efficiency, it would be ideal to have the turbine operate at the most efficient TSR. This would lead to a variable turbine speed, as increased wind speeds would lead to increased rotor speeds. The main issue with the variable speed or constant TSR approach is the power conversion. Additional complications in the power conversion can arise, depending on the transmission and generator. For this reason, constant speed turbines could even be the preferred option, because of the higher simplicity of the power system.

The airfoil design is another core design process necessary for an effective system. While a large variety of airfoil designs exist, the design for Mars imposes some challenges. This is because airfoils behave differently depending on the Reynolds number, defined as:

$$Re = \frac{\rho v L}{\mu} \tag{3.2.3}$$

For low Reynolds numbers, viscous forces play an increased role, which affects the lift generated by the airfoil. Comparing the environmental parameters density and dynamic viscosity in the Reynolds number, leads to the conclusion that for the same wind speed and turbine, the Reynolds number is 40 times smaller.

$$\frac{\rho_{mars}}{\mu_{mars}} \frac{\mu_{earth}}{\rho_{earth}} = \frac{0.02 kg/m^3}{1.2\text{e}{-5} Pa \cdot s} \frac{1.79\text{e}{-5} Pa \cdot s}{1.22 kg/m^3} = 0.025$$

As such, finding airfoils that maximize lift against drag at these low Reynolds numbers is important, and might require novel designs, as current profiles often fall short at these lower limits [70]. Higher drag works against the torque generated by the lift, and therefore lower ratios limit the efficiency of the foil severely. To maintain better lift-to-drag ratios, the thickness of the blade can be reduced to limit the drag. However, this also increases the blade loads, especially at the root [71]. In Chapter 4, this issue will be picked up again in greater detail.

Another non-dimensional parameter that influences the behavior of airfoils is the Mach number, defined as the ratio between the velocity of the flow and the speed of sound:

$$M = \frac{v}{c} \tag{3.2.4}$$

Related to its lower density, the speed of sound in the Martian atmosphere is lower being around 250m/s compared to the 340m/s on Earth, varying mainly based on temperature [72].

This means that at comparable flow velocities, the Mach number will be larger on Mars, and therefore the flow will be more compressible.

With the matching airfoil design, blade element momentum (BEM) analysis can be used to determine the optimal chord length and angle of twist of the blade. Both of these factors vary throughout the length of the blade, as the relative velocity of the blade section increases with radius, demanding a different geometry and orientation for optimal operation. In BEM theory, the rotor blade is segmented, and for each element, the aerodynamic forces are calculated separately. In Appendix B, the Betz optimal twist angle and chord length are derived. In practice, this design step is integrated with software such as QBlade [73; 74], which also allows for performance prediction of the final turbine.

Power Conversion

Through the interaction of the turbine blades with the flow, torque is generated that has to be converted into current for storage or distribution to appliances. This is done with the means of a generator. Three main types of generators can be distinguished, direct current (DC) generators, synchronous alternating current (AC) generators, and asynchronous AC generators [21]. Contrary to application on Earth, in which turbines are mainly intended to be connected to a power grid, the application on Mars will be standalone. This also means that a DC output is desired, since energy will have to be stored in a battery for reliable supply. As with many other components, a lightweight design will generally be preferred over a cost-efficient design. This is not only because of the transport costs, but also because of the deployment, as HAWTs generally feature the generator in the nacelle, and therefore the deployed tower has to bear its load. Given the limited dimensions of the turbine, combined with the lower wind power density, the generated power will also be much smaller compared to traditional turbines.

In its most simple form, a generator consists of a rotating and stationary part. One of these parts generates an electric excitation field, while the other contains a coil. Through the change in the magnetic field caused by the rotation, an induction current is generated in the coil, which then can be used to store electrical energy in a battery, or to supply power to an appliance. For small-scale turbines, the most used generator is the permanent magnet synchronous generator (PMSG) [71; 75]. In this generator, the excitation field is generated by a permanent magnet. Compared to systems that use electromagnets, a permanent magnet does not require any current to operate, which simplifies the system. Still, losses are imminent for any conversion system. In the case of generators, the most power is lost through the resistance of the wiring, friction generated in the change of magnetic field as well as the mechanical friction for rotating parts.

Depending on the number of poles of the generator, and the rotational speed of the rotor, gear reduction can be used to optimize the angular velocity for the generator. This leads to a distinction between direct-drive (no gear reduction), medium speed, and high-speed generators. The usage of transmission introduces further mechanical losses but can allow for a more compact design and even better overall efficiency [76]. As an additional note, as permanent magnets are used, depolarization can be an issue during transport, mainly through mechanical shocks or high temperatures. The actual efficiency of the generator will largely depend on the variation in rotational speed of the rotor, the rated power, as well as the design of the generator, e.g. type and reduction of the transmission system, number of magnets, or whether a variable or constant speed turbine is used. Comparable PMSG designs for wind turbines reach efficiencies around 85%, with slight decreases in efficiency above the optimal load, and drastic reductions at very low loads [77].

An additional consideration is the overall power management of the turbine. Wind speeds

are highly variable, and with the turbine having to supply power to the application, but also to control systems or heaters, a reliable energy supply is necessary. Especially for standalone applications without secondary power generators, discrepancies between availability and consumption need to be addressed. In case of excess generation, the power should be stored, so that energy is still available during generation deficits. Figure 3.9 shows that power production is reduced at both exceptionally low and high wind speeds.. Such a buffer has to be carefully optimized to have enough capacity to avoid system failure, but should also not be overestimated to limit the weight of the system, as battery weight scales linearly with battery capacity. Lithium-ion batteries have been the most used solution for Martian exploration missions lately, and continue to be promising from both an economic and specific energy standpoint [78]. As will be further addressed when discussing the environmental influences, active temperature control through heaters will be necessary for any battery operation, and possibly even for other turbine components. A reliable energy buffer to keep the battery from freezing is elemental to a long-lasting system, that does not fail in times of exceptionally low wind speeds.

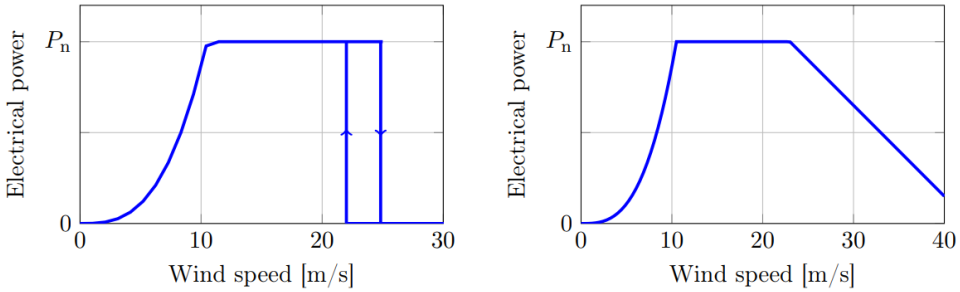

Figure 3.9: Ways of handling turbines at large wind speeds, through sharp cut-out (left) and soft cut-out (right) [79].

Structural Loads

Another very noteworthy driver are the structural loads that the turbine experiences during operation. Not only are the loads tightly woven to material choices and component design, but they also determine what power output can be achieved through the turbine, as blade dimensions and geometry, tower height, or even parameters such as cut-out speed are based on the forces that apply. Loads on turbines arise for multiple reasons, the most significant being aerodynamic and gravitational loads. The lift and drag forces generated by the turbine blades cause loads on the design, and for small turbines, considerable gravitational loads are mainly due to the weight of the rotor and nacelle on top of the tower. Other forces include the ones introduced by motion, e.g. centrifugal forces, the yaw orientation of the turbine to face the wind, or control systems such as pitch regulation or cut-in and cut-out procedures [21].

The two load-bearing components that have the most impact on the design choices are the rotor and the tower. The main forces on the rotor are caused by the thrust, for which a formula is derived in Appendix B:

$$T = \frac{1}{2}\rho v_\infty^2 A C_t \tag{3.2.5}$$

(Duplicate of Equation B.27)

Even though flapwise, edgewise and torsional moments occur on turbine blades during operation, in smaller lightweight designs, flapwise deflection is dominant. By integrating the thrust over the rotor radius in rings of width dr, with swept area $dA = 2\pi r dr$, the flapwise

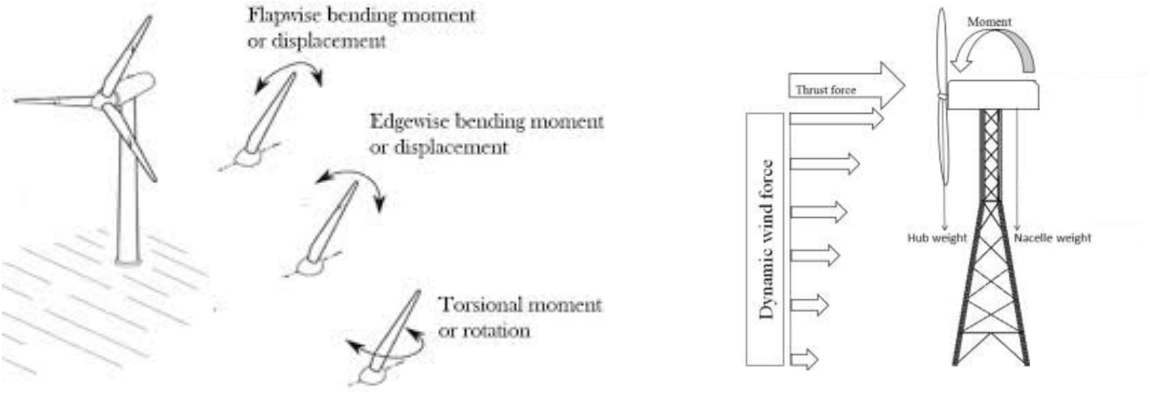

(a) (b)

Figure 3.10: Main load considerations in terms of (a) main blade moment modes under operation [80] and (b) main tower loads (cite).

bending moment at the root can be calculated [21]:

$$M = \frac{2}{B}\int_0^R \frac{1}{2}\rho v_\infty^2 \pi r^2 C_t dr = \frac{\rho \pi C_t v_\infty^2}{3B} R^3 \tag{3.2.6}$$

Which can be rewritten in terms of the thrust:

$$M = \frac{2T}{3B}R \tag{3.2.7}$$

From the moment, the maximum stress as well as the shear force per blade can be defined:

$$\sigma_{max} = \frac{c_{max} M}{I} = \frac{2 c_{max} T R}{3BI} \tag{3.2.8}$$

$$S = \frac{T}{B} \tag{3.2.9}$$

with I the area moment of inertia at the root. The stress increases with distance from the neutral axis in the middle of the blade, being highest at the position with furthest distance c_{max}.

With the blades rotating, centrifugal forces also have to be considered. The definition of the centrifugal force is [68]:

$$F_c = m\omega^2 r \tag{3.2.10}$$

Since instead of a point mass at distance r, a rotor has a distributed mass that is a function of radius from 0 to R, the centrifugal force has to be calculated through integration:

$$F_c = \int_0^R \omega^2 \rho_{blade} A_{cross} r dr \tag{3.2.11}$$

The structural properties of the turbine also limit the power output of the turbine at high wind speeds by limiting the rated power and determining the cut-out speed. It can be seen that the derived flapwise bending moment in Equation 3.2.7, as well as the centrifugal force in Equation 3.2.11, are magnified at higher wind speeds. The flapwise bending moment is proportional to the square of the wind speed, while the centrifugal force is proportional to the turbine's rotational speed. Therefore, at some point, if the wind speed is high enough, the structural limits of the blade will be exceeded. Accounting for exceptionally high wind speeds is not usually feasible, as that would limit the overall efficiency of the turbine at most other wind speeds or greatly increase the structural requirements. Forces can be limited by active and passive control mechanisms, which will be compared in the turbine design in Chapter 4.

The second component experiencing the bulk of the loads is the tower. These loads can be separated into three main components, the dead load, the thrust load on the hub, and the thrust load on the tower. The dead load consists of the gravitational force caused by the tower's self-load and the weight on top of it (blades, hub, generator, nacelle). This constant downwards pointing force is:

$$F_g = g\left(m_{top} + \int_0^h \rho_{tower} A_{tower} dz\right) \tag{3.2.12}$$

with m_{top} being the mass on top of the tower, h the tower height, ρ the area density of the tower, and A_{tower} the cross-sectional area of the tower. The thrust loads on the hub and tower contribute to an overturning moment, aiming to topple the tower. The component of the overturning moment caused by the thrust is:

$$M_{thrust} = Th \tag{3.2.13}$$

While the moment produced by the tower can be described as:

$$M_{tower} = \frac{1}{2}\int_0^h \rho D_{tower} C_{d,tower} v(z)^2 z dz \tag{3.2.14}$$

which essentially describes the drag on the tower for a velocity field varying with height, leading to a total overturning moment of:

$$M = M_{thrust} + M_{tower} = Th + \frac{1}{2}\int_0^h \rho D_{tower} C_{d,tower} v(z)^2 z dz \tag{3.2.15}$$

Anchoring the turbine so that a reaction moment equal to the overturning moment can be generated is essential to ensure the stable orientation of the turbine. Similarly, this moment can also induce bending on the tower, which has to be avoided. Next to the described loads, transient loads caused by the tower shadow effect when a blade passes the front of the tower or stochastic loads caused by turbulence in the wind also have to be considered. This dynamic loading, including effects such as resonance, can cause fatigue failure if not considered in the structural design.

Overall, the main difference in structural design compared to small wind turbines on Earth are the reduced loads, both by gravity and forces by the wind. The stresses in the blades can be a major design factor, considering that very thin blades are required to minimize drag. Similarly, the requirement of designing a deployable system can cause stress concentrations at hinges or connectors, always leading to less structural integrity compared to a solid counterpart. Finally, finding an optimum trade-off between a lightweight structure and maintaining enough structural integrity for reliable operation is a crucial design step. Material choice is critical for that, and because of the extreme environment and high development costs, this could include innovative solutions that might be regarded as too expensive for commercial production, such as carbon nanotubes [81]. The structural design plays an equally important role, including additional measures such as supports or internal structures for the blades, which can be important for an efficient and long-lasting system.

Environmental Resistance

During their lifetime, all wind turbines are constantly exposed to the elements, which requires measures to ensure reliable operation for prolonged periods of time. Operating temperature is a crucial consideration for the design of turbines on Earth, making it even more critical for application on Mars, given the amplified temperature variations. Temperature changes affect various turbine components in different ways, so careful design choices have to be made. In

cold temperatures, lubricants can increase in viscosity, leading to higher frictional forces that can lower the mechanical efficiency of the system. Material properties of solids also change. The structural components generally have a lower fracture strength and are more brittle at lower temperatures, and seals gain rigidity which can cause functional problems. [21]. Additionally, low temperatures also pose issues on the power storage, which is a significant concern for all Mars missions. Rovers such as Perseverance and Curiosity use the thermal energy released from their nuclear thermoelectric generators to warm up their batteries, while other missions have to rely on active thermal control systems to keep their batteries operational during low temperatures. For example, the Mars helicopter Ingenuity uses around half of its battery capacity every night to keep the battery temperature from dropping below -15^{o}C [17]. A similar system would be necessary for any power storage associated with the wind turbine. At last, icing is a major concern for cold climate applications on Earth. However, because of the very low air humidity on Mars, this is not a concern. The polar regions form an exception, in which temperatures drop enough to cause the solidification of carbon dioxide, leading to the formation of dry ice [26].

On the other hand, elevated temperatures can cause degradation of electronic components as well, and in the case of the usage of permanent magnet generators, the field generated by these magnets drops at higher temperatures, which can influence the power generation. At last, the fluctuation in diurnal temperatures of up to 100K [26] can influence the integrity of the design. Tolerances might change, and mechanical components such as transmissions can suffer from increased friction and wear if the thermal properties of the materials are not carefully adapted to the encountered conditions.

The second environmental aspect to consider is the frequently encountered phenomena of the dust storm and the spawn of dust devils. High wind speeds have less impact on Mars because of the low atmospheric density, but still have to be considered when designing the turbine control to avoid sudden failures. Dust devils can generate extremely high wind speeds locally and are very hard to predict. Thus, both the probability of encountering a dust devil and the associated safety mechanisms are important considerations. Apart from the exceptional wind speeds that can occur, the dust itself is likely the primary concern. Dust on Mars is highly ferromagnetic because of considerable magnetite concentrations [58]. Additionally, because of the lack of moisture in the air, these particles do not aggregate as quickly as they would on Earth, leaving very fine-grained particles suspended in the air for extended periods of time. This can, for example, result in the deposition of particles on the airfoils. If particles stick to the surfaces of the foils, drastic reductions in the lift coefficient can be noted, depending on the roughness height [82]. Dust removal is a major challenge on Mars, as even solar panels

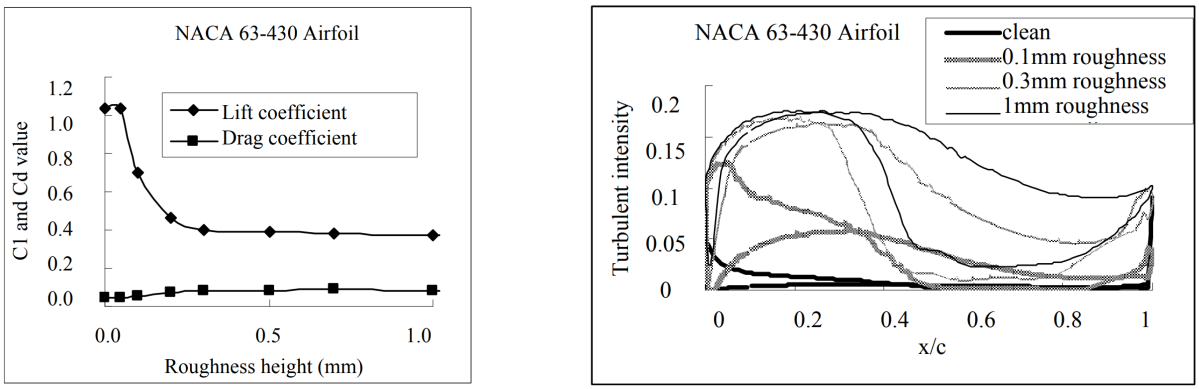

(a) (b)

Figure 3.11: Impact of surface roughness on airfoil performance [82].

suffer from dust deposition that cannot be removed actively at this point. They rely on so-called cleaning events, which are gusts of high wind speeds relieving the surface of the cells from dust. The cleaning of wind turbines is standard procedure on Earth but unrealistic to achieve on smaller-scale Mars missions. Additionally, natural cleaning through precipitation is possible on Earth, while no precipitation occurs on Mars. Therefore, the susceptibility of blade materials and designs to dust deposition has to be considered carefully, as well as the effect rough blades have on the lift to drag ratio.

The ferromagnetic properties of the dust also require careful design of the power system. Especially components such as the generator, which generates electromagnetic fields during operation, are most likely required to be sealed off from the environment completely, to avoid the attraction of dust particles into the machinery of the turbine, and e.g. causing clogging of the moving parts or even short circuits. Similar challenges are already prevalent on Earth, especially for offshore wind farms, to avoid the accelerated decay of parts through a salty and humid environment.

3.3 General Design Considerations

Overall, the design for space missions differs significantly from the commercially oriented design on Earth. First off, space mission design is much more value-driven than cost-driven product design on Earth. The focus lies on providing scientific value at a reasonable expense based on the proposed gain in knowledge or capabilities. The value of having a wind turbine on Mars should be related to the increased possibilities of scientific research through increased power generation and the knowledge gained through operating such an advanced system in a foreign environment. Since expenses are amplified either way because of the high associated costs in research and transport, factors such as material or component costs do not play a significant role.

Because of the large costs associated with any technological application on Mars, the longevity and thus reliability of the system has a much higher priority than on Earth. A simple, reliable design is preferred over a more complex, less reliable, albeit more efficient system. Limiting possible points of failure and putting even more emphasis on safety mechanisms is extremely important. For a design to be deemed feasible, it should also be implementable in the near future and consider the current budgets to wage the value of the implementation against the costs. An incrementally complex system can spin-off from an initial working design and allow for systems with lower technology readiness levels (TRL) for future implementation. TRL describes a scale illustrating the maturity of new technology, ranging from 1 (basic principles observed) to 9 (actual system proven in operational environment) [83]. For initial designs confirming the feasibility of the approach, components of similarly high TRL provide the most compelling argument as they are fully implementable in a short time span. Through future sustained investments, lower TRL solutions can be considered to, for example, improve the efficiency of the design, leading to an incrementally more capable technology.

Even though research and development for space missions continue to expand with a variety of new possibilities emerging, some issues in the approach taken can be noted. One commonly referred to issue is the management of development time versus the level of improvement gained. Past missions have often extended their development time significantly to venture into improved designs and technologies while not waging the gained advantages against the time and money spent during research. This leads to better technology, but at a cost that is disproportional to the level of improvement that was gained. Secondly, a lack of flexibility is often noted in design procedures. Approaches tend to be relatively rigid regarding initial choices and premises of the solution. Keeping options open while watching out for alternative

solutions has the benefit of allowing to explore ideas that might lead to a more valuable end result [38]. Only through an open-minded and diverse approach to research, the best solution can be found that avoids the danger of getting stuck in a local optimum solution.

At last, an unaddressed but essential point for space mission design is that research and development of new technologies live within the context of law, policies, and politics. The support of the entities that invest in research and development is crucial to exploring new possibilities. Associated with this could come further requirements and constraints, such as having to include certain facilities or regions for development, adjusting the research goals to apply for funds and grants, or altering the approach based on the availability of specific technologies. Larson and Wertz [38] argue that modern space exploration is more dependent on these factors than on technological limitations, leading to new technologies emerging from what is chosen to be affordable or beneficial instead of what is possible. The intelligent development and use of space missions become more important due to environmental problems on Earth and are also what Larson and Wertz describe as the main challenge for space exploration in the early 21st century.

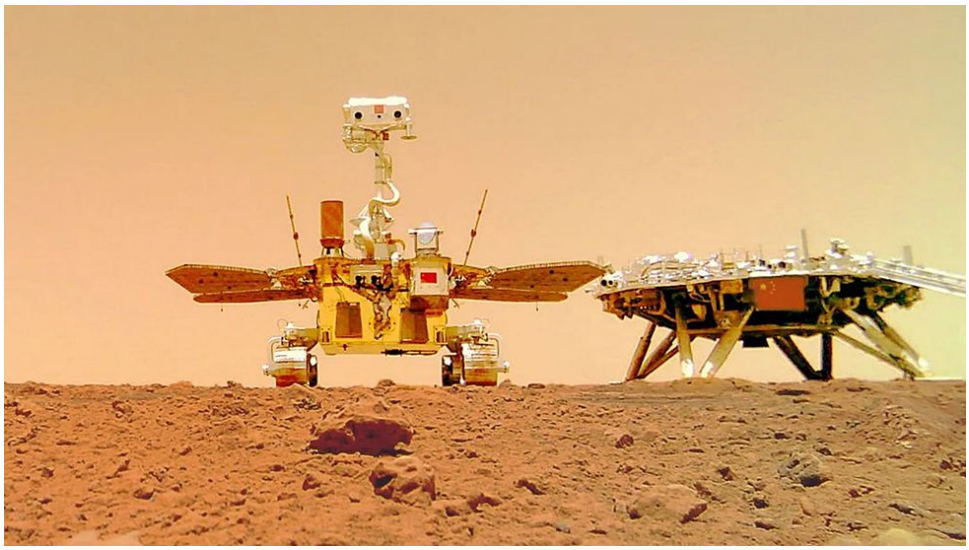

Figure 3.12: Image of the first Chinese Mars mission, the Zhurong rover, taken in June 2021. Source: [84]

Chapter 4

Initial Wind Turbine Design

In this chapter, a turbine will be designed to reach preliminary quantitative results on the actual feasibility of wind turbines when coupled to a specific application. While each major component of the turbine deserves a detailed design for a complete proof of concept, this analysis will primarily focus on reaching an aerodynamically feasible design. Auxiliary design choices required for a coherent result, such as power system or structural components, will be made using reference designs or reasonable assumptions but will not be analyzed in equal detail. Therefore, concrete designs will result for components such as the blades but not for the generator or tower. First, the application of the turbine will be defined, ending in an overview of the critical requirements. Through the design of a turbine, along with the final analysis, conclusions can be drawn on the feasibility of the system and potential of the application in general.

4.1 Problem Statement

With the first airborne device 'Ingenuity' successfully mastering its first flight attempt on the Martian surface, the future development of other helicopter-like systems is a logical progression. Possible applications include high-definition surface mapping, or even payload transport, both of which are enhanced by the possibility of navigating over terrain that is too steep or too rough for traditional rover designs. Power generation plays a crucial factor in this, as it is the main limiting factor in terms of flight duration and payload capabilities. Ingenuity charges its batteries through an attached solar panel, from which roughly half is used to keep the battery warm overnight. This simple solution is sufficient for a technology demonstrator with a drone that carries no additional scientific instruments. Airborne systems require large amounts of power while having to be as lightweight as possible, making external power systems most valuable. Drone capabilities can improve by outsourcing power generation and storage for thermal management.

The design will thus be focused on designing a wind turbine to power an exploratory drone mission. It was found that the highest wind speeds being in the mountainous areas of Mars, which coincides with the region where the mobility of drones is most advantageous. The design will be based on the 'Mars Science Helicopter', a mission designed by the Jet Propulsion Laboratory as the second generation helicopter mission [18]. The following helicopter design will be regarded as the appliance which the turbine will power:

Hexacopter Design Base	
Gross Weight	17.7kg
Scientific Payload	2.02kg
Range	2km
Hover Time	4min
Battery Capacity	500Wh

Table 4.1: Reference specifications for the Mars Science Helicopter.

In reality, the battery requirements would diminish in choosing an external power supply over the attached PV cells, as the weight of the panels can be subtracted from the gross weight. The fraction of the battery needed for thermal heaters during the night can be outsourced to a ground-based battery. For the sake of simplicity, this will be neglected for the initial requirements and might as well be regarded as an additional energy buffer or range/payload boost.

The dimensioning depends on the amount of power that has to be generated. The required power to charge the drone in 24 and 72 hours is given as an initial estimator in Table 4.2. The competitive weight is derived from the specific energy of photovoltaic cells operating on Mars.. It is unlikely that the turbine will reach this weight efficiency. It is therefore not a design constraint, but can be regarded as a benchmark to evaluate against. This is also the ideal scenario in which all energy can be used to power the drone. Similar to Ingenuity, a significant amount of power will be necessary to heat the internal components during nighttime.

Wind Turbine Design Base	24h between Operation	72h between Operation
Power Output	20.8W	6.9W
Competitive Weight	8.32kg	2.76kg

Table 4.2: Requirements for the wind turbine design.

Selection of a landing site is also necessary to judge the wind speeds that the turbine will be confronted with. Low wind variability is preferred as it minimizes the required battery buffer. High consistent winds are most common in mountainous areas, where slope winds are more pronounced. On the other hand, too mountainous regions lead to issues with EDL and installation. By looking at results from Chapter 2, along with data from the MCD, the site 30^{o}S, 126^{o}W was chosen, located in the mountainous region of the Tharsis Rise. The selection was made by taking into account the power density and its variability and the altitude and slope of the area. This region has a high wind power density of over $10\mathrm{W/m^2}$, having a moderate wind variability with a standard deviation $\sigma = 6.7\mathrm{m/s}$, at an average wind speed of $10.2\mathrm{m/s}$. These values were again derived using the MCD. This corresponds to a Weibull distribution with a scale factor c of $11.45\mathrm{m/s}$ and shape factor k of 1.86. As described in Chapter 2, wind speed is largely influenced the height above surface. For this design, a tower height of 3m will be assumed. As such, all parameters derived from the MCD will be taken at 3m of height to approximate the differences between the lower and upper points of the area swept by the turbine.

It is important to note that the results of the database are interpolated, leading to a limited accuracy of of the model at the exact location. It was found that in the region of interest, the values in wind speed vary less than $1\mathrm{m/s}$ per 59km (1 degree of latitude).

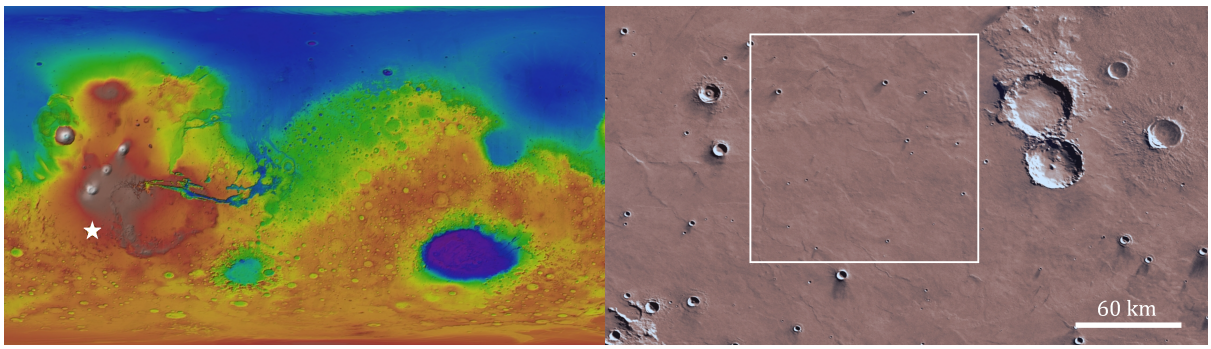

(a) (b)

Figure 4.1: Location choice, (a) marked position on an altitude chart (b) a range of roughly 2.2 degrees at the target location with reasonably even surface.

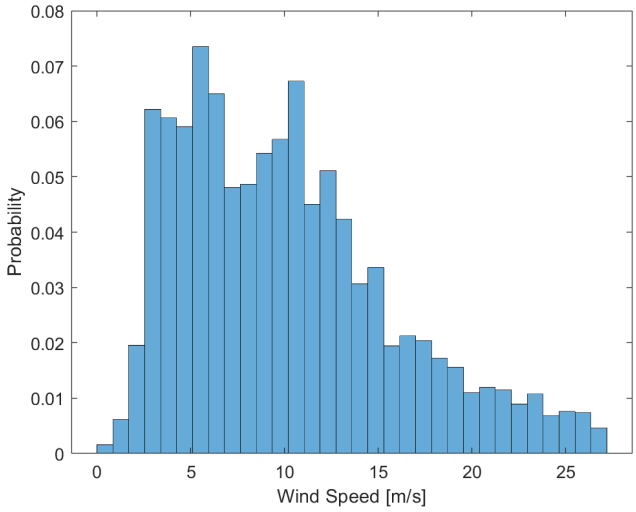

Figure 4.2: Distribution of wind speeds at the chosen location, 3m above ground.

4.2 Baseline Design

4.2.1 Airfoil Selection

The overall design process will be conducted in QBlade, an open-source software used to design and evaluate wind turbines. It integrates multiple components, containing XFoil for airfoil analysis, BEM for blade optimization and performance prediction, and various other simulation approaches to simulate the operation of the turbine.

The shape of the airfoil is crucial for good turbine performance, as even an otherwise perfect system will not generate power if the profile cannot generate lift. Any foil performance is largely dependent on the Reynolds number it encounters on its surface. The Reynolds number, as defined earlier in Equation 3.2.3, is a function of density, dynamic viscosity, free stream velocity, and chord length. Density and viscosity can be regarded as environmental constants, but chord length and free stream velocity are parameters that depend on the final wind turbine design. Using the Betz optimal chord length derived in Appendix B, a Reynolds number of 7500 was found as an initial estimation. Iterating through the design process in QBlade, it was found that for wind speeds of 5-20m/s, the Reynolds number will generally vary between 500 and 11.000 throughout the blade, confirming the trial value. An illustration of the variation in Reynolds numbers for the final turbine design can be found later on in Figure 4.16. This

means that the foil designed for the wind turbine will mostly operate in the ultra-low ($< 10^4$) Reynolds range. This regime is rarely encountered, as it only comes into play for very thin atmospheres, as is the case with Mars, or in very small scale aerodynamics, such as the flight of insects.

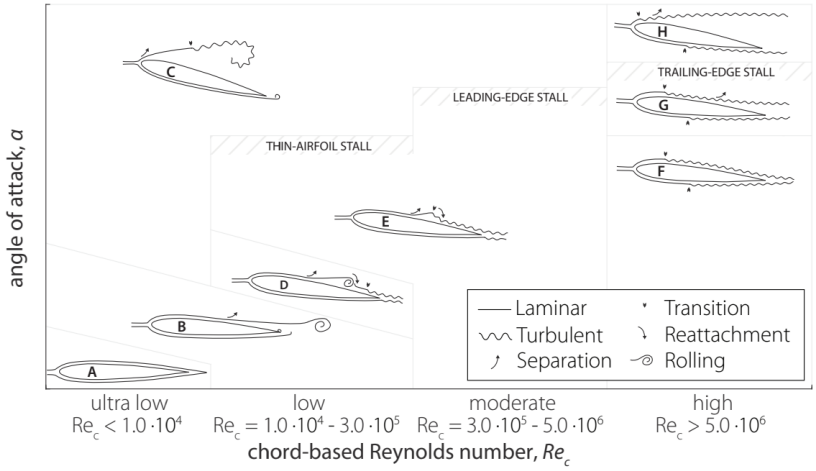

Figure 4.3: Schematic of airfoil behavior in the different Reynolds regimes.

Lower Reynolds numbers describe the increased influence of viscous forces over inertial forces, leading to increased laminar behavior at boundaries. This can be seen in Figure 4.3 by looking at the flow separation at the upper surface. While at high Reynolds numbers, the flow turns turbulent very soon after the negative pressure on top of the foil is encountered (F), the transition is larger for moderate Reynolds numbers. There, a separation bubble forms between the laminar and turbulent section (E). Lowering the Reynolds number further, this bubble increases in size, and the turbulent boundary layer gets thicker (D), increasing the drag on the foil more and more. At some point, the reattachment point moves over the trailing edge so that no reattachment takes place (B) [70]. Finally, in the region of ultra-low Reynolds numbers, even the separation point moves over the trailing edge of the foil, leading to a fully laminar flow over the surface of the foil (A). How these effects influence the behavior at higher angles of attack, i.e. at stall, will be discussed when looking at wind turbine stall control.

This change in flow behavior towards lower Reynolds numbers has major implications on the design and performance of the foil. The first difference is the increased influence of viscous drag. Somewhat similar to the lower atmospheric boundary layer discussed in Chapter 2, the fully laminar flow over the airfoil will also have a transition region between the zero velocity at the surface and the region of undisturbed flow at a certain distance above the foil. This causes shear stress, which is pronounced because of the dominance of viscous effects at low Reynolds numbers, which in turn causes the drag. The lift decreases on the other hand, which is why lowering the Reynolds number takes a significant toll on the lift-to-drag ratio, causing lower airfoil efficiency [85].

In order to find a suitable foil for the ultra-low Reynolds application, the 4-digit NACA profile designation is used as a way to accurately designate the variations in geometry, which is defined as:

1st Digit: Maximum camber (in % of chord length)

2nd Digit: Position of maximum camber (in tenths of chord length)

3rd and 4th Digit: Maximum thickness of the foil (in % of chord length)

For example, NACA2412 would designate an airfoil with a maximum thickness of 12% and the maximum camber of 2% positioned at 40% of the length.

To evaluate the performance of various foils, XFoil will be used. The two non-dimensional parameters that have to be set for the evaluation are the Reynolds number and the Mach number. A Reynolds number of 7500 was chosen since it lies relatively centered within the range of Reynolds numbers that the turbine blades most commonly encounter. The Mach number can be determined by looking at the relative flow velocity over the foil during operation. For the final design of this section, the relative velocity on the foil reaches 73m/s, and given the speed of sound of 250m/s, this leads to a maximum Mach number of 0.3. It should be noted that this value is only reached shortly before cut-off and only at the tip of the blade. In all other circumstances and positions, the Mach number will be lower. The natural choice would be to choose a value that lies within this range for the XFoil simulations. However, XFoil struggles with nonzero Mach numbers in the analysis of low-Reynolds foils, leading to issues in convergence or even complete termination of calculation '*CpCalc: Local speed too large, Compressibility Corrections Invalid*', which is an acknowledged issue within XFoil. Given that the Mach numbers encountered are still at low subsonic speeds, compressibility will be neglected by setting the Mach number to zero. The Prandtl-Glauert transformation provides a way to approximate compressible flow from incompressible flows. It states that the pressure coefficient, and therefore also the lift coefficient, scales based on the Mach number:

$$c_l = \frac{1}{\sqrt{1 - M_\infty^2}} c_{l,0} \tag{4.2.1}$$

Which for the maximum Mach number encountered in this case leads to:

$$c_l = 1.048 c_{l,0} \tag{4.2.2}$$

This means that the deviation in lift coefficient introduced by the zero Mach approximation will not exceed 4.8%.

The thickness of the foil has a large influence on the foil performance, with thinner foils being generally superior to thicker ones [70]. This was confirmed to be the case using an XFoil analysis of foils of varying thickness shown in Figure 4.4. Adverse effects of thickness on both

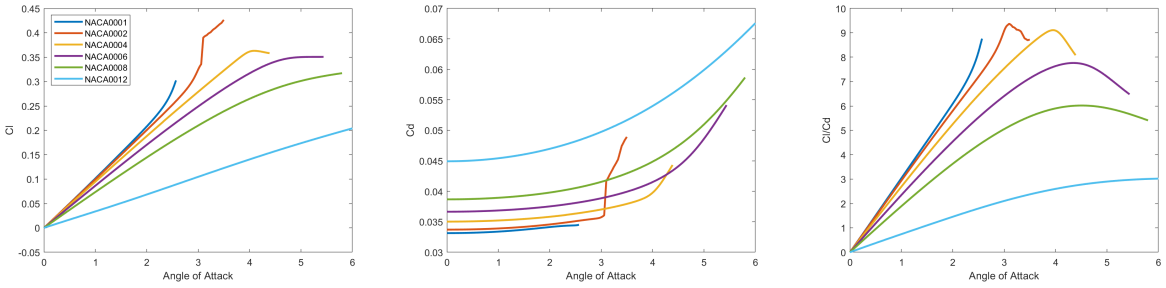

(a) (b) (c)

Figure 4.4: XFoil analysis of symmetrical foils of varying thickness at 7500 Re, showing (a) lift coefficient, (b) drag coefficient, and (c) lift-to-drag ratio. The simulation was terminated once a value failed to converge.

lift and drag can be noted for low angles of attack. The increased drag for thicker foils is related to the higher pressure gradients caused by the larger vertical displacement of the flow. This creates an increased pressure drag [70], as laminar flow has a harder time to deal with pressure gradients compared to turbulent flow. The quasi-linear region of lift has a higher slope for thinner foils, while the drop in lift at higher angles of attack is more severe. Similarly, the drag increases more significantly at higher angles of attack as well, as the laminar boundary layer

struggles to stay attached to the foil. Since the aim is to operate the blade at the optimal angle of attack to maximize the lift-to-drag ratio, the maximum of Figure 4.4c is most important to judge the efficiency of the foil.

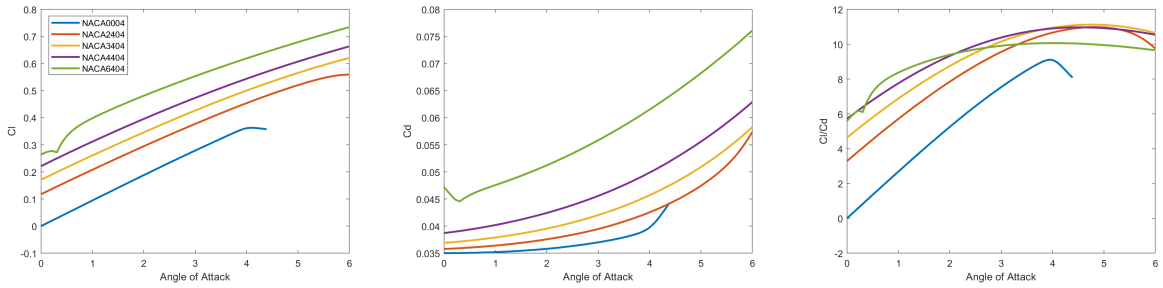

(a) (b) (c)

Figure 4.5: XFoil analysis of airfoils of varying camber at 7500 Re, showing (a) lift coefficient, (b) drag coefficient and (c) lift-to-drag ratio.

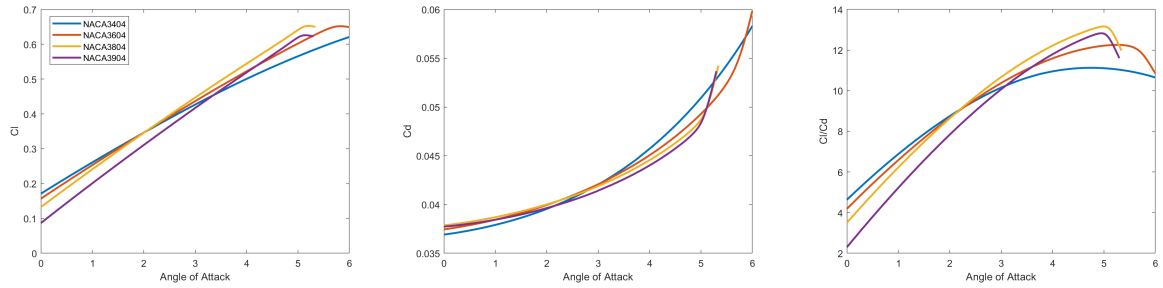

(a) (b) (c)

Figure 4.6: XFoil analysis of airfoils of varying camber position at 7500 Re, showing (a) lift coefficient, (b) drag coefficient, and (c) lift-to-drag ratio.

Introducing camber has the potential of further improving the foil performance. Even though the drag increases with added camber, the lift also does. Because the drag scales increasingly rapidly for higher cambers, an optimum can be found that maximizes the lift-to-drag ratio. An optimum can also be found for the camber position. Increasing the camber leads to larger pressure differences around the foil, which is why lift coefficients increase. On the other hand, flow separation is more severe towards the end of the region because of the dropping geometry. This causes an increased separation behind the foil, introducing more drag [70]. It can be seen that moving the camber further back has a positive effect on the airfoil performance, as it reduces the onset of flow separation, limiting the added drag, but also has positive effects on lift.

Scale and position of camber are not independent variables, so both have to be optimized together. A foil thickness of 2% was chosen because of the convergence issues that XFoil faces for even lower thickness airfoils. Structural complications increase as foils get this thin, which will have to be accounted for during the structural design. The optimal camber was found by computing the maximum lift-to-drag ratio for a grid of foils of different cambers and camber positions in XFoil. The highest ratio was found for the NACA4602 foil, which is illustrated in Figure 4.7, with a maximum lift-to-drag ratio of 15.6 reached at an angle of attack of 4.7^o. As a final step, the polar plots of lift and drag have to be extrapolated to a full 360 degrees of angle of attack, which is a requirement set out by QBlade to allow the analysis of the turbine in all circumstances. As indicated earlier, it is impossible to simulate the full range of AoA in XFoil, as the solutions stop converging relatively soon. Even before convergence problems,

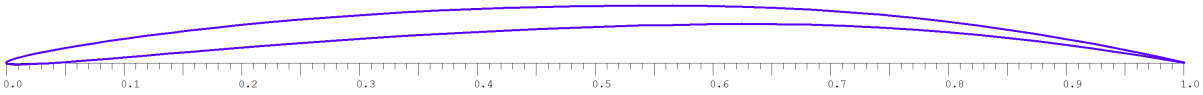

Figure 4.7: Geometry of the NACA4602 airfoil.

the resulting values often start to oscillate or spike, which requires early termination of the calculation. For the NACA4602 foil, it was found that reasonable values could be retrieved from XFoil only between -6^o and +12^o.

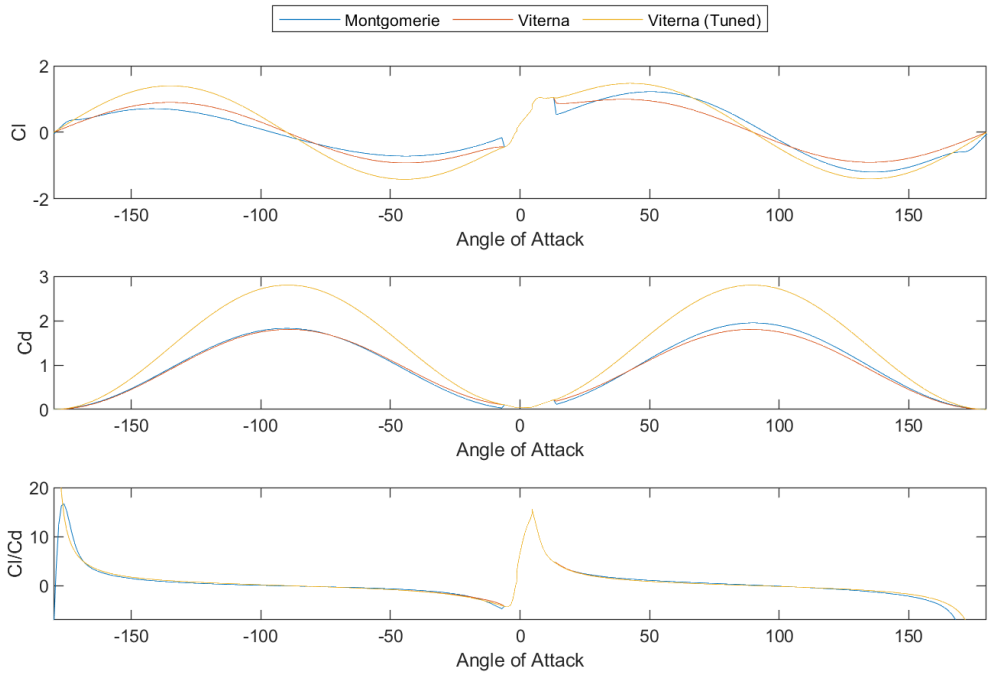

Figure 4.8: QBlade 360^o polar extrapolation results.

The two different extrapolation methods that are implemented are the Montgomerie and the Viterna method. Figure 4.8 shows the result from these two methods, along with a third variant which is a version of the Viterna method with a manually tuned CD90 value to remove the discontinuities that occur otherwise at the transition from XFoil data to interpolated data. While the tuning caused large effects on the lift and drag coefficient, the impact of these changes cancels out in the ratio between the two. Overall, the Viterna method appears slightly better than the Montgomerie method, which has larger discontinuities. The tuned Viterna polar extrapolation will be used for the rest of the analysis, as QBlade also emphasizes the importance of avoiding discontinuities and kinks. The only discontinuity that has to be considered is the asymptotic behavior at 180^o, but that is not an AoA that HAWTs encounter during usual operation. The polar of the foil created in this step will be used to build the blade geometry and perform simulations that indicate the turbine's performance. Overall, a maximum lift-to-drag ratio of 15.6 is low compared to the performance of foil geometries on Earth, which can easily have ratios above 50-100 [86].

4.2.2 Turbine Design

From the selected airfoil, the geometry of the turbine can be defined. For this, the primary design choice is the number of blades, which will determine the solidity and ideal TSR of the

turbine. For this initial design, a 5-bladed construction was chosen. Structurally it is more beneficial to choose an uneven number of blades, as it reduces the amount of resonance, as fewer harmonic frequencies are encountered. On Earth, wind turbines usually default to 3 blades. Using more blades lowers the optimal TSR for operation, which leads to lower rpm. 3-Bladed turbines usually operate at a TSR of around 6, while it was found that the 5-bladed turbine is most efficient at a TSR of 3. Higher rpm are usually easier to convert by the generator so that transmission systems become necessary for slow rotating turbines. However, the smaller the turbine, the larger the rpm at given TSR, which can negate this effect. Lower blade counts can also be more efficient, as the spacing between the blades lowers the amount of turbulence that the next blade will encounter. Higher blade counts have the advantage of having increased torque, leading them to operate at lower wind speeds. The higher torque makes them suitable for actions such as water pumping, which is their main application on Earth.

When considering the application on Mars, a couple of additional points have to be considered, which speak for the usage of 5-bladed turbines. Using more blades leads to lower forces on the construction, as the induced moments are smaller, and rotationally induced forces such as centrifugal forces are lower at a lower TSR. This allows for a more lightweight design, as overall decreases in loads ease the structural requirements. Additionally, higher bladed turbines can achieve the same rated power at a smaller swept area, leading to shorter blades. Since transport and deployment are a major difficulty in operating wind turbines on Mars, having a denser packing ratio can be beneficial and reduce added complexity of unfolding or extending the turbine blades during deployment. Lastly, through comparing an optimized 3-bladed construction at TSR 6 and a 5-bladed construction at TSR 3 in QBlade, an increase in power coefficient of over 20% was noted. Going from 5 to 7 blades did not yield a similar significant improvement, with the power coefficient only increasing by less than 3%. While on Earth more blades can lower the power coefficient because of the turbulence caused by each passing blade, this effect likely plays a smaller role on Mars because of the fully laminar flow over the foils.

The turbine was designed in QBlade, with the following parameters required as input:

Parameter	Design Choice
Number of Blades	5
Tip Speed Ratio	3
Turbine Radius	1.1m
Hub Diameter	0.1m
Number of Elements	15

Table 4.3: Wind turbine design parameters.

From the earlier defined power requirements shown in Table 4.2, it was found through simple power prediction in QBlade that a turbine with 1.5m would be required to reach the upper limit of producing over 20.8W at average wind speed. In order to simplify transport and deployment, a trial radius of around 1.1m was chosen instead, which is more manageable. An output of around 12W for the mean wind speed can be expected for this radius, using preliminary performance analysis. The hub dimension was chosen so that the blade elements would not interfere with each other, while also being as small as possible to reduce additional size and weight. This leads to a hub diameter of 0.1m. Finally, the number of elements is a parameter set out by the Blade Element Momentum theory, which determines for how many sections the optimal geometry is calculated. In between those elements, interpolation is used to define the geometry. QBlade suggests at least 10 elements, so 15 elements were chosen for this design. The spacing of elements was decreased towards the root and tip of the blade as more considerable changes in geometry occur there. After setting the design parameters,

optimizations are used to determine the optimal geometry. In Appendix B, the derivation of optimal angle of twist and chord length according to the Betz method was derived using Blade Element Momentum theory. While this is a good first approximation, the relation for the chord length developed by Schmitz leads to more accurate results, as wake rotation is accounted for. The formula used for the chord length calculations can be found in the QBlade documentation [74]. QBlade gives the option to optimize the angle of twist to achieve a maximum lift-to-drag ratio for all blade elements at the designated TSR. Using the Schmitz chord approximation and lift-to-drag optimized twist, the rotor shown in Figure 4.9 was designed.

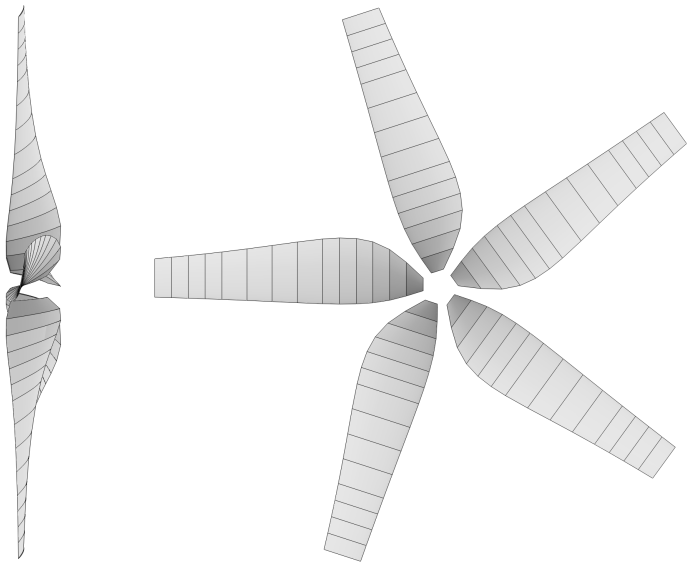

Figure 4.9: QBlade Final 5-bladed Wind Turbine Design.

4.2.3 Power Control

There are multiple ways in which a turbine can control the generated power. For most designs, structural loads become too large at high wind speeds to keep the turbine operating, requiring a reduction of the aerodynamic efficiency of the turbine. Because of the rare occurrence of these high wind speeds, accounting for them in the structural design is inefficient, as the increase in obtained power is negligible. The primary way this regulation can be achieved in conventional turbines is through stall or pitch control. In stall-controlled turbines, the rotational speed of the blades is roughly constant over wind speed, and the blades have a fixed pitch. Therefore, as wind speed increases, the angle of attack increases as the relative wind shifts more in line with the axis of rotation. Depending on the fixed pitch angle, this leads to stalling at a specific wind speed, as the angle of attack becomes too large for the foil to still generate lift. In pitch control, the turbine actively limits the generated lift by altering the pitch of the blades through a control mechanism by decreasing the angle of attack. Similarly, the blade can also be stalled by increasing the pitch of the blades, in which case the control is referred to as active stall control. While such systems are more mechanically complex, they also allow the turbine to keep the produced power at its maximum structural allowance beyond the rated wind speed [87]. In Figure 4.10, the power curve for stall and pitch control is illustrated. A caveat to active control comes into play considering the rated power of the turbine that will be designed. Overall, wind turbine research is focused on larger scale turbines for commercial grid application, which leads to technology from these systems being transferred to smaller scales [89]. In the application on Mars, the designed wind turbine will only have an average

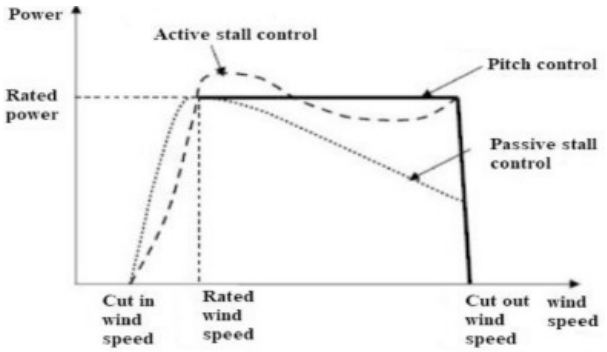

Figure 4.10: Comparison in power curves for pitch and active/passive stall controlled turbines [88].

power output of 10-20W, as defined in the problem statement. At this power, any other control system or actuator can toll the output significantly, which speaks for the usage of a passive system. In the conclusion of the concept analysis, it was also stated that simplicity has value in providing reliability, given the lack of maintenance possibilities.

An alternative passive control method is furling. A tail vane is often used in smaller wind turbines to keep the turbine facing upwind, eliminating the need for an active control yaw mechanism. Offsetting the pivot of the vane and turbine creates a furling system that turns the turbine out of the wind as it strengthens. The main issue with furling systems apart from the

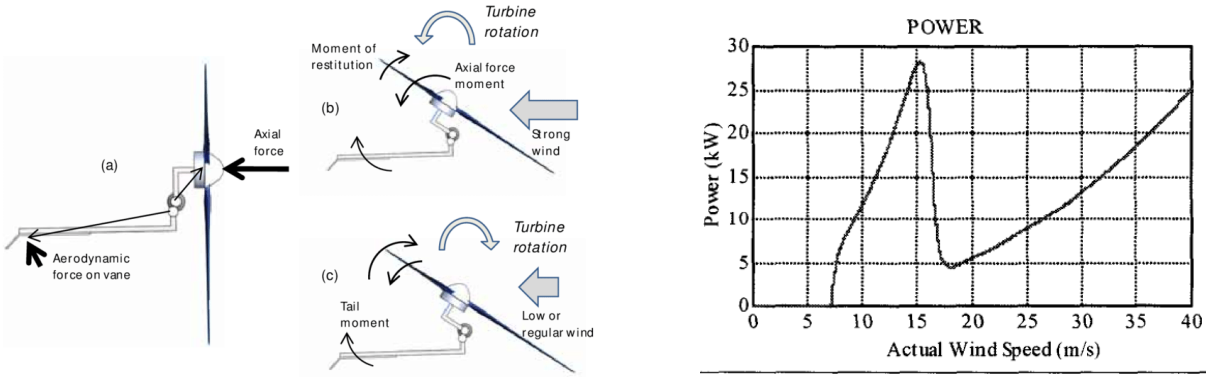

(a) (b)

Figure 4.11: Furling of wind turbines (a) Forces and moments on a furl-controlled wind turbine [90] (b) power curve for an undamped furling system [91].

sharp drop in power in the furled state is the uneven loading and fatigue the turbine experiences. The whole system resolves into a dynamics problem, with dampers that can be used to limit the oscillations at the cost of performance and springs to alter the restoring moment. Hysteresis also has to be accounted for, as generally a considerable drop in wind speed is needed to unfurl the turbine, which can further limit the efficiency of the system.

By comparing passive control through furling and stalling, it can be reasoned that stall control is the superior system, given the higher efficiency and the fact that the turbine does not experience any considerable additional loads. However, it is worth looking at the stalling behavior of airfoils in the ultra-low Reynolds regime before defining the operation of the control system. For this, the lift-to-drag ratio of the chosen NACA4602 at ultra-low Reynolds was compared to a typical small wind turbine application Earth, namely the NACA6405 in the moderate Reynolds regime. The comparison was made using XFoil computations, with the NACA4602 results taken from the results of the previous section. As airfoils are much less efficient at lower Reynolds numbers, Figure 4.12 also shows the results but scaled between 0

and 1 (maximum) lift-to-drag ratio for easier comparison. A third line shows the NACA4602 at an even lower Reynolds number. Looking at the XFoil results, it can be seen that for the

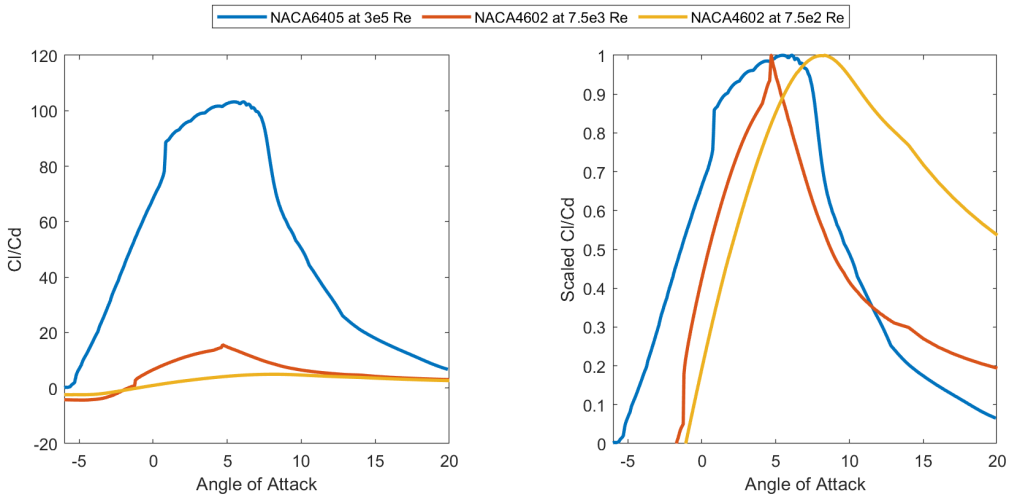

Figure 4.12: Comparison of lift-to-drag ratio for a wind turbine airfoil operated on Mars and Earth.

NACA4602 operating at 7500 *Re*, there is a significant drop in the lift-to-drag ratio after the optimal angle of attack, indicating stalling of the foil. This suggests that stall control might still be a possibility to regulate the turbine at high wind speeds. However, the slope is less steep and does not drop as low as the higher Reynolds counterpart, which could mean a reduction in the effectiveness of the regulation. For high Reynolds numbers, increasing the angle of attack leads to flow separation at the trailing edge, proceeding more and more up the foil if the angle of attack increases further. The lift drops suddenly while drag increases, causing stall [70]. This is illustrated in Figure 4.3 from (G) to (H). At low Reynolds numbers, the laminar flow separates, without reattachment, leading to a similar low lift and high drag situation, with the difference that this occurs much earlier, resulting in stall-like behavior for most angle of attacks. For even lower Reynolds number the separation of the flow is delayed and much more gradual because of the laminar flow, leading to a reduction in stall behavior [85].

From Figure 4.12 it seems as if the designed airfoil can still stall at 7500 *Re*, suggesting that enough flow separation occurs to generate enough drag and limit the lift enough for a considerable drop in efficiency, which is comparable in slope to the stalling of the moderate Reynolds foil. For comparison, operating the foil at a Reynolds number that is a magnitude smaller, stalling is replaced by a gradual decrease in lift, as flow separation is not as sudden anymore.

Usually, stall controlled turbines operate under constant speed, i.e. variable TSR [21]. However, comparing the lift-to-drag curve of the Martian foil to the one on Earth, it can be seen that the maximum efficiency is only reached at a particular angle of attack, with much sharper drop-offs on either side. This means that it is very beneficial to operate the turbine at variable speed to avoid significant losses when wind speed deviates from the rated wind speed, at which the correct TSR and angle of attack is obtained. In order to still stall the turbine when operating under variable speed, the turbine has to be slowed down at a critical wind speed to force an increased angle of attack, leading the turbine into stall. This can be achieved using generator torque control. By altering the load on the generator, the torque can be adjusted to decrease the rotational speed of the turbine. A higher load causes the torque to increase, slowing down the rotation of the turbine. Given the very narrow range of angle of attack at which high power coefficients can be achieved, the generator torque control also has to ensure that the TSR is always kept close to 3, which means that maximum power point tracking will

have to be employed in the control system. This control system responds to variations in wind speed and adjusts the load on the generator accordingly to fine-tune the turbine's rotational speed. At last, exceptionally high wind speeds may require the turbine to shut down completely, which generally requires a mechanical braking system. Spring or hydraulic activated friction disks are most commonly used for this [21].

4.3 Performance Prediction

4.3.1 Design Performance

The BEM simulation integrated into QBlade provides a way to predict the power that the turbine can generate. Necessary simulation and environmental parameters, along with the multiple correction factors integrated in the model, are displayed in Figure 4.13.

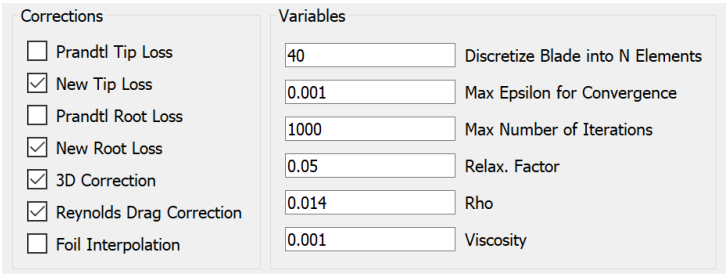

Figure 4.13: Parameters and Corrections in the QBlade BEM Simulation Module.

The number of blade elements determines for how many independent sections the BEM algorithm is executed. Generally, $N = 40$ is the recommended value to get an accurate result. Since the blade geometry is relatively simple, without any sudden changes, this value was kept at its default. Similarly, the max epsilon for convergence and the max number of iterations remained at default values since no improvement in the results was noticed through their alteration. The relaxation factor dampens oscillating values in calculating the axial induction factor, with lower values leading to higher damping. For the default of 0.35, multiple spikes and overall fluctuations were found in the results. Lowering the factor to 0.05 helped in achieving smoother results while not skewing the overall curve.

The two required environmental parameters are density and kinematic viscosity. The density at the desired location was found to be $0.014 \mathrm{kg/m^3}$ using the Mars Climate Database, while the kinematic viscosity was found from literature [92].

Multiple correction factors can be activated to improve the accuracy of the model. The root and tip losses that BEM does not consider, as it treats all blade elements in 2D without edge effects, are most accurately accounted for using the 'new' tip and root losses by Shen [93]. These factors build on the Prandtl losses while implementing additional improvements, especially regarding the axial induction and loads at the blade's tip.

QBlade uses the polars computed in Section 4.2.1 for the BEM simulation. These, however, were only generated at a single Reynolds number, and as such, are really only valid for that value. Since the Reynolds number is a function of both chord length and relative wind velocity, it is bound to change over the length of the blade, depending on the turbine's rotational speed and the wind speed. The Reynolds drag correction factor by Hernandez and Crespo [94] alters the drag coefficient to account for these differences. However, this is a very simplified way to deal with changes in Reynolds numbers, especially when dealing with the more complex ultra-low Reynolds regime.

The foil interpolation is a solution to issues in the discretization of the blade elements when using different airfoil sections within one blade. Since this is not the case in the chosen design, this can be left unchecked as it will not influence the results.

The last correction factor is the 3D correction, which accounts for the influence of the Himmelskamp effect. This effect describes the increase in lift coefficient under the rotationally-induced centrifugal and Coriolis forces. While the exact effects are not fully characterized yet, the increase in lift is related to the thinning of the boundary layer as it is accelerated outwards by centrifugal forces. Additionally, radial airflow creates a Coriolis force against the direction of rotation of the turbine, decreasing the suction pressure. It was found that enabling this correction carries significant implications on the behavior of the turbine. Usually, the Himmelskamp effect causes stall to shift towards higher angles of attack, which is why it is also referred to as the stall delay effect. Figure 4.14 shows the first results for the BEM simulation,

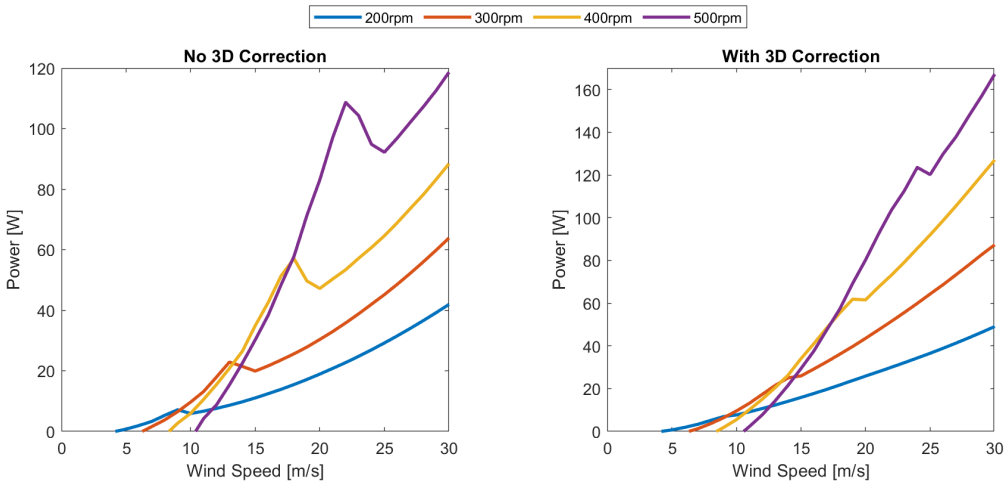

Figure 4.14: Comparison of power prediction and stall behavior with and without the Himmelskamp effect.

both with and without the Himmelskamp effect. For this initial evaluation, the turbine is kept at a constant speed while varying the wind speed to better illustrate the stall behavior. Already without the 3D correction applied, the stalling behavior is minimal. While it is possible to limit the turbine's output for a selected range of wind speeds, the decrease in power coefficient cannot counteract the increased power density in the wind for a considerable range and is soon overpowered. With 3D correction, only a small kink can be related to a remnant of stalling, but effectively no regulation through stalling is possible. When discussing the stall behavior in the ultra-low Reynolds regime, it was concluded that for the situation at hand, stall control may still be a possibility, while the effectiveness will likely already be reduced, as illustrated in Figure 4.12. No evidence for loss of validity of the 3D correction at lower Reynolds numbers was found, leading to the decision to regard the results with the correction enabled as more accurate. This leads to the conclusion that stall control is not a possibility.

With furling limiting the efficiency and imposing structural constraints, pitch control is chosen to limit the output at high wind speeds. While pitch control usually involves an active system, which can thus be prone to failure, efforts are also made to develop passive pitch control systems, for example, using centrifugal forces to drive the change in angle [95]. QBlade allows for a pitch-controlled turbine simulation, for which some relevant parameters are illustrated below, along with the simulated power curve. The generator capacity determines at which point pitch control limits power, while the cut-in and cut-out speeds cause the turbine to halt completely. Selecting an optimal transmission means that the turbine can operate at variable rotational speeds, which in this configuration range from 80rpm to 650rpm. Setting the

fixed pitch to 0 ensures that the turbine operates at maximum power coefficient when possible.

Generator Capacity	30W
Cut-in	4 m/s
Cut-out	25 m/s
Transmission Type	optimal
Fixed pitch	0^o

Table 4.4: QBlade performance prediction turbine control parameters.

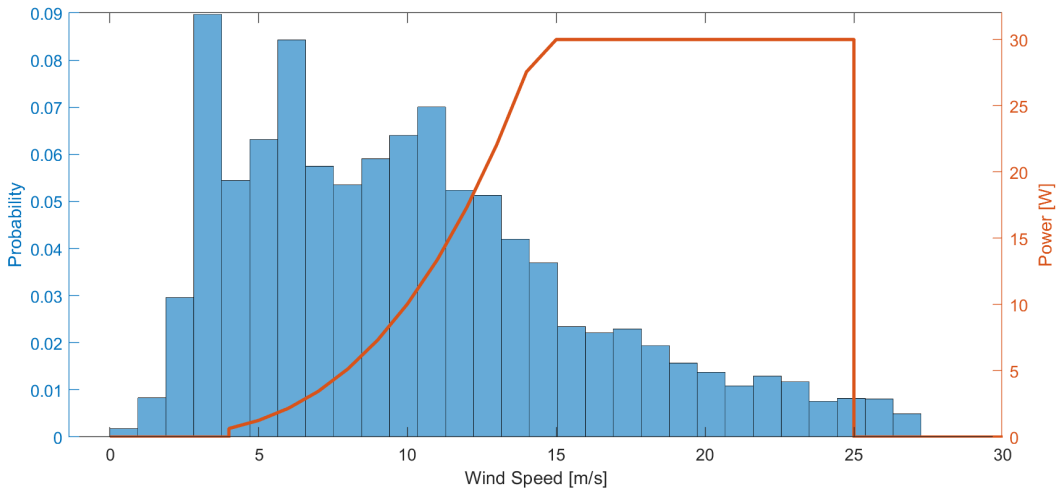

Figure 4.15: Power curve for the turbine design and wind speed distribution.

In order to find the best operational points for the turbine, the cost of supporting a larger range of wind speeds has to be waged against the increased structural requirements, requiring thorough knowledge of the structural properties of the design. Since this level of detail is not reached yet, the operational points were determined by looking at the distribution of wind speeds. If a certain wind speed is not reached frequently, it is most likely not feasible to alter the full design of the turbine to make it most efficient at that point. The cut-in was chosen at 4 m/s, at which the turbine already only generates under 1W. At even lower speeds, it is unlikely that there is significant power production possible. The cut-out speed was chosen at 25m/s. Higher speeds occur less than 2% of the time and will not significantly impact the power output. The generator capacity value determines the point at which the pitch angle is progressively decreased to limit the total power. This happens at 30W, which represents a wind speed of 15m/s. Additionally, the wind turbine was set to operate with an optimal transmission, meaning that the turbine operates at variable speed, generator losses are not considered. From Figure 4.15, it can be seen that statistically, the turbine will not be operational around 16% of the time, mostly due to too low wind speeds. In 67% of time, the turbine can operate at maximum power coefficient, while it is limited to its rated power 17% of the time.

As mentioned earlier, QBlade uses the airfoil performance at a single Reynolds number for all simulations. Therefore, having extrapolated the lift and drag coefficients for a Reynolds number that is very far off from the actual values found during operation can introduce large inaccuracies. It can be seen from Figure 4.16 that the estimation of 7500 Re is acceptable. Naturally, the Reynolds number will increase with wind speed because of the increased stream velocity and decrease towards the blade's root because of the larger chord length and decreased relative velocity.

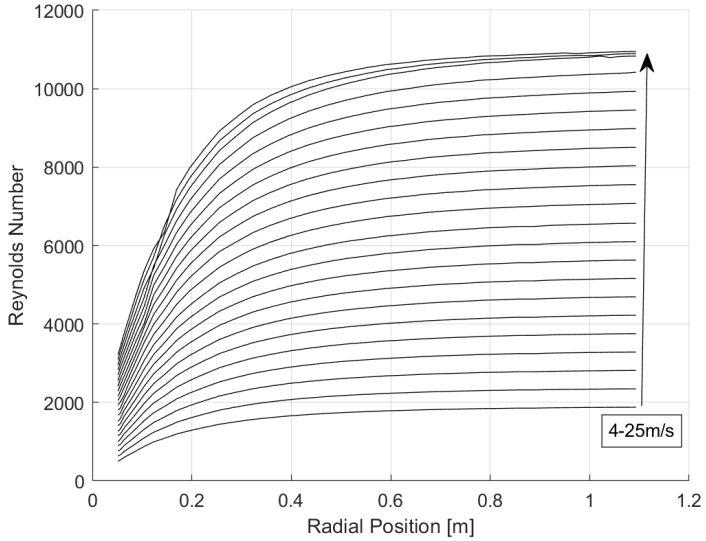

Figure 4.16: Reynolds number distribution over the turbine blade for wind speeds between 4m/s and 25m/s.

4.3.2 Mission Performance

For now, only the performance of the aerodynamic design was evaluated, but not the performance of the complete power supply system. This is an important step, as up until now, the variability of wind speed was not taken into account. Even if the power curve matches the expectations for a yearly average wind speed, large issues can arise if extraordinarily high or extremely low wind speeds occur for prolonged periods. In order to determine this mission feasibility, a simple operational model was created, consisting of three components: the wind turbine, a battery, and the drone. The wind speed data at 3m of altitude from the MCD is used to determine the power generated by the turbine using the derived power curve, which charges the battery based on the power conversion efficiency. This battery consists of a fixed component as part of the turbine and the battery integrated into the drone. The battery discharges at a steady rate every night as part of the heating requirements necessary to keep the battery above -15^{o}C. Whenever a certain charge threshold is reached, the drone can operate, depleting its energy storage.

Up until now, the power that was predicted was the power related to the mechanical motion of the turbine. However, not all the torque that is generated by the aerodynamic forces by the blades can be converted into electricity and stored in the battery. The implementation requires assumptions on the variable losses through limited generator efficiency and the fixed losses through the battery heater. While the generator's efficiency depends on the power point tracking using the generator torque and the efficiency of mechanical components such as bearings or transmission, a fixed efficiency rating of 85% is assumed for this initial estimation. For the heating losses, the values from the Ingenuity helicopter can be used as a reference again [17]. The Ingenuity helicopter uses 21Wh per night to heat a 42.1Wh battery, meaning that roughly half of its energy is used to maintain acceptable temperatures. With this drone battery holding 500Wh and using an additional buffer of 200Wh, the total battery system is 19 times the size of the one from Ingenuity. It is assumed that more elaborate and thus more efficient heating can be used, also considering the increased heat capacity of the battery. Therefore, 25% or 175Wh will be assumed as fixed heating power consumption per night. An overview of the power system parameters is shown in Table 4.5. The drone operation is scheduled only to take place during the daytime if the drone is fully charged and the buffer is 50% charged, so the total

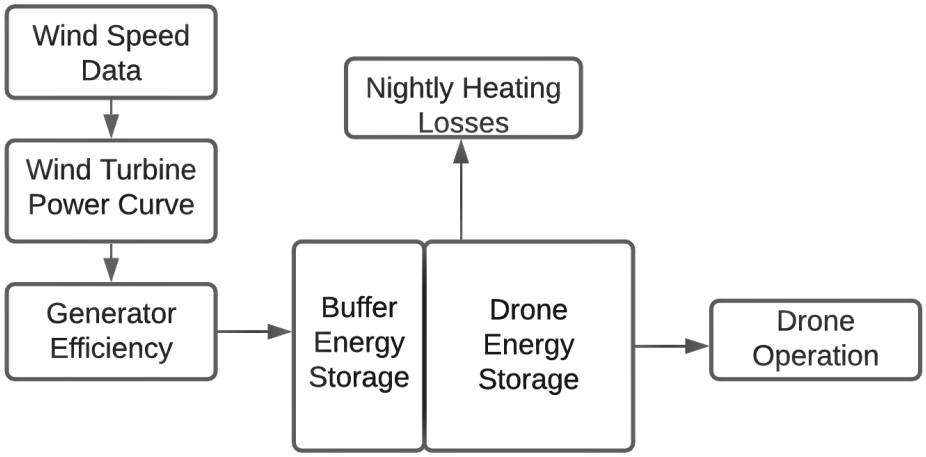

Figure 4.17: Model Overview.

Drone Battery	500Wh
Buffer Battery	200Wh
Drone Operation	400Wh
Heater Consumption	175Wh/night
Electrical Losses	0.15

Table 4.5: Power system parameters for the mission model.

charge exceeds 600Wh. This ensures that not too much energy is drawn too early to make sure that there is still enough energy left for the heating requirements in case of low wind speeds. The drone's flight is also limited to times when the wind speed is below 15m/s to account for most power being generated in unfavorable conditions for airborne operations. Additionally, a drone flight is set out to consume 400Wh out of the 500Wh battery to allow room for possible complications. From this mission design, it is possible to operate the drone a total of 115 times in a Martian year, with a maximum of 14 times a month and a minimum of 6 times a month. The wind speed is consistent enough that the 200Wh buffer is enough to support the operation, with the available power never dropping below 75Wh. Occasionally, maximum capacity is reached because of excessive wind speeds, but increasing the capacity to allow for further accumulation of charge was found to not increase the efficiency because of the increased heating requirements. Also, from the hourly data from the MCD, the annual yield and the average generated power can be found. For the final design, a yield of 166.7kWh/year at an average production of 11.9W can be found. When comparing the yield to systems on Earth, it is important to note that a year on Mars consists of 687 days. The variability throughout the year is very low, and no trend throughout the year is noted, with the lowest monthly average being 10.7W and the highest being 13.5W. The design can power the drone, but compared to the problem statement, the heating requirements increase the charging times considerably, and as such, a larger turbine or smaller drone would be more appropriate.

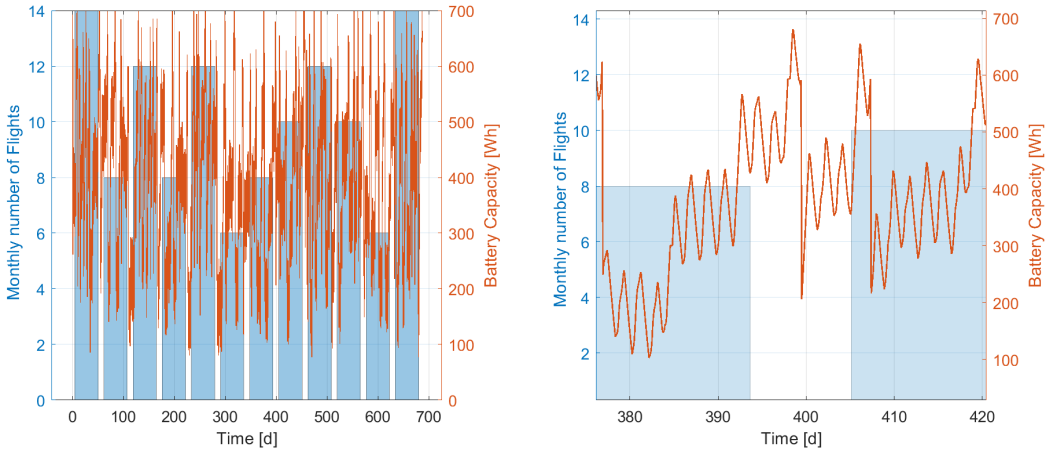

Figure 4.18: Mission model results for a year of operation.

4.3.3 Future Considerations

The structural aspects of the wind turbine have to be considered carefully to ensure successful operation. While this design procedure focused on the aerodynamic considerations, an equivalent methodology for the construction design and material selection will be essential to allow for a more detailed understanding of wind turbines' potential compared to other systems. The loads on the turbine give an initial idea of the weight required to support the structure of the turbine. As part of the BEM simulation, the main components of forces on the blades were already calculated. The maximum values of these are shown in Table 4.6. These values can be

Component	Maximum Value
Thrust Force [N]	3.9
Root Bending Moment [Nm]	0.56
Normal Blade Loading [N]	0.11
Axial Blade Loading [N]	0.05

Table 4.6: Maximum forces and moments encountered during turbine operation.

interpreted as unusually low when considering a relatively high solidity turbine with a swept area of nearly $4m^2$. On the other hand, it has to be considered that the turbine is subject to weak, low-density flows, in fact only producing up to 30W of power. With the power being almost two magnitudes smaller than comparable turbines on Earth and power coefficients being in the same order, the forces on the turbine have to be equally low. With an average power production of 11.9W it can be deduced that a total weight of 4.76kg would make the turbine as weight-efficient as photovoltaic cells, from the utility estimation shown in Figure 3.1. The main factors that drive the weight of the turbine are the weight of the blades, nacelle, and tower, along with mechanisms that might be required for anchoring and deployment. Given the low forces, it is likely that components such as the tower and blades can be designed to be very lightweight to lower the system's mass. Similarly, anchoring the turbine is also a reduced concern, as the overturning moment will be equally low in magnitude.

Figure 4.19 shows an impression of a possible system design. The turbine fits into the Opportunity rover aeroshell, having a diameter of 2.65m and a mass of 840kg [18]. The turbine is fixed to the aeroshell, which through its weight, keeps the turbine from overturning. A telescopic boom for a tower is illustrated for deployment, while the blades are rigid parts. Hinging the nacelle, vane and hub is necessary to fit the dimensional constraints of the aeroshell.

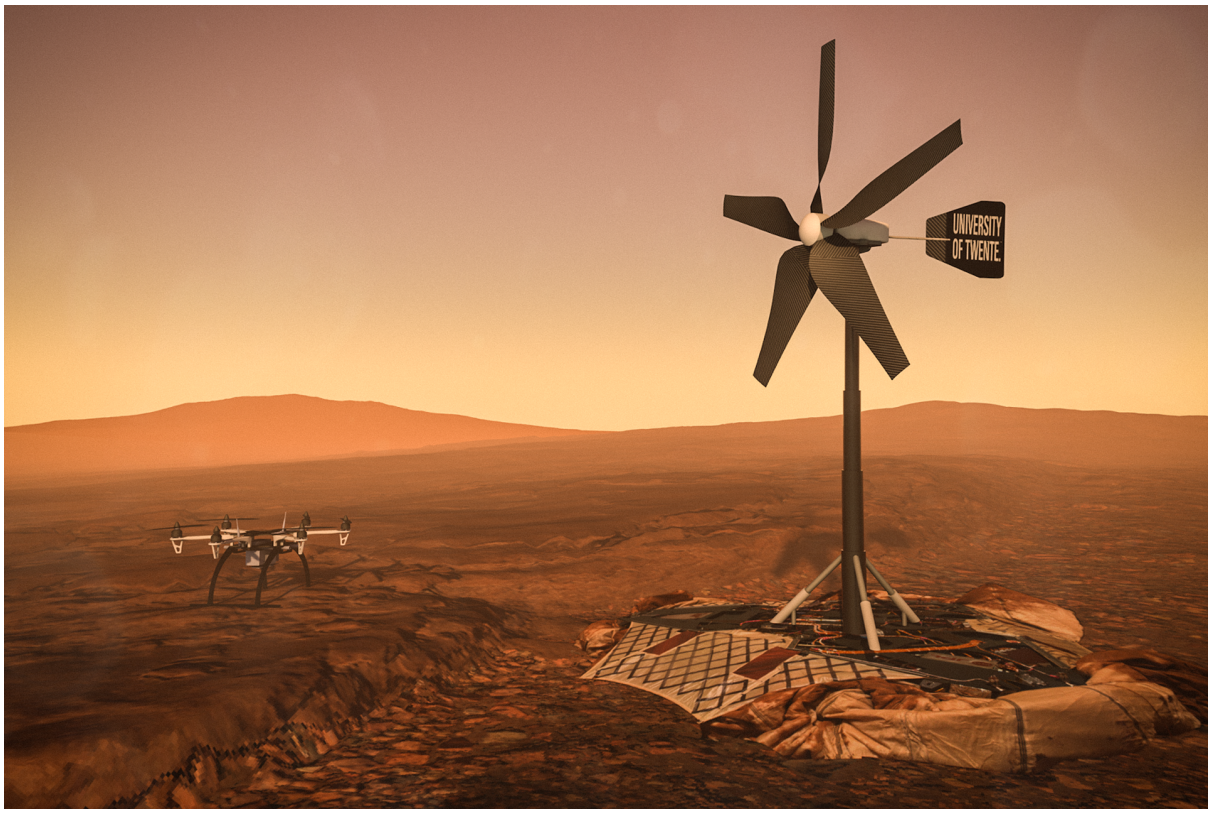

Figure 4.19: Illustration of a possible wind turbine based on the current design

Chapter 5

Discussion and Conclusions

5.1 Discussion

This report aimed to determine the feasibility of using micro wind turbines on Mars to supply power to possible future missions, such as landers, rovers, or airborne devices. Since it constitutes the first look at a novel concept, the extent to which each aspect of the study can be analyzed is limited by virtue of the groundwork that has to be done as the basis for more detailed future designs. Some points of discussion arise from each of the three main chapters of the report that has to be taken into account when looking at the presented results.

For the wind resource assessment, the main limitation is the disregard of inter-annual variability in the used climate model. The Mars Climate Database bases its values on an average Martian year. However, levels of UV radiation vary strongly in an 11-year cycle, and dust suspension in the atmosphere, which has significant influences on the climate of Mars, also has a considerable variability over multiple years. Expanding the wind resource assessment for scenarios with extreme UV radiation and depending on atmospheric dust concentrations would allow for insights into the variability of wind depending on these factors. Overall, quantitative results of this assessment are based on the values from the MCD, the accuracy of the results is therefore dependent on the reliability of the climate model, and skewed meteorological predictions could skew the power prediction results.

When determining the key design drivers, it was mentioned that an exhaustive list of factors influencing the design of the turbine is necessary to ensure the high applicability of future developments. The possibility remains that the key factors highlighted in this report do not fully represent the issues faced in future designs. Revision of these drivers in future developments ensures that reasonable decisions will be made in possible designs to come.

In the aerodynamic design of a possible wind turbine rotor, some limitations apply to the accuracy of the final results. XFoil was used to simulate lift and drag, and to come to conclusions on the optimal foil for the application. However, XFoil struggled in converging over larger ranges of angles of attacks, especially for more extreme shapes, such as very thin foils or foils with aggressive cambers. XFoil likely has issues with these very unsteady laminar flows, which could be a reason why most research on foils in the ultra-low Reynolds regime defaults to CFD simulations instead. This limited the number of foils that could be investigated, such that foils under 2% thickness and alternative shapes like corrugated foils had to be excluded from the analysis. With XFoil results being limited to an AoA range of under 20^o, extrapolation of the rest of the angles was necessary. This extrapolation only has limited accuracy, and manual tuning was necessary to reach continuous plots. Only a single polar of lift and drag is used for the performance analysis in QBlade, while the turbine encounters a range of Reynolds

numbers during operation. The lift is not corrected for the varying Reynolds environment, and the correction applied for the drag is said to only have limited validity for very low Reynolds numbers, making slight deviations possible. Additionally, some minor inaccuracies can be introduced by assuming incompressible flow by setting the Mach number to zero.

5.2 Conclusions

Three steps, each with a different focus, were used to draw conclusions on the feasibility of the concept. Through the wind resource assessment, the distribution and amount of wind that can be harnessed were found. While both diurnal and seasonal differences play a role, regional differences make some regions much more suitable than others. Slope winds play a significant factor because of the low thermal inertia of the surface and the associated large diurnal variations in temperature. Therefore, regions such as the Tharsis Rise, being the most mountainous region of Mars, are very favorable for the siting of wind turbines. Regions with little temperature fluctuations experience reduced wind speeds, which makes the polar regions less suitable. Finding the wind power density leads to the conclusion that overall potential in wind power is reduced by the very low density of the Martian atmosphere, which is not rectified by the comparably high annual mean wind speeds, which can commonly exceed 10m/s. This limits the amount of power that can be generated, with the yearly average wind power only rarely exceeding $10 W/m^2$. The amount of power that can be generated is fundamentally limited by this low power density.

The concept analysis provided a way to look at the general considerations that have to be taken into account for future design approaches. The key objective of wind turbines on Mars is the supply of power to various scientific missions while also increasing redundancy, therefore minimizing the risk of power drains. The possibility of collecting wind measurement data and gaining further insight into the aerodynamic implications of such a foreign environment are additional benefits, next to the displayed importance of sustainable space exploration. The utility of wind turbines was quantified by comparing it to photovoltaic and nuclear solutions. A power generation per mass of around 2.5W/kg would be necessary to match these competitors. The main factors that drive the design of the system in terms of transport, installation, and operation were found. Weight drives the design of space missions, with heavier systems being much more expensive in terms of transport, imposing limits on the structural design. However, the biggest difference in design is the lack of human interaction with the system after launch. This requires deployment mechanisms to reach high packing densities during transport while requiring enough reliability to make the system work reliably and maintenance-free. Focusing on a system design that is easy to transport, lightweight, efficient, and also completely autonomous in terms of installation and operation, while also mainly disregarding the production cost of the system, is very different from the design of commercial turbines on Earth.

A rotor was designed for a wind turbine aimed to provide energy to the possible future Mars Science Helicopter. Because of the ultra-low Reynolds environment ($Re<10^4$) that the turbine will operate in, it was found that thin, cambered foils provide the highest lift-to-drag ratio, with the NACA4602 being the optimal choice. Using a 5-bladed turbine allows for lower start-up speeds, a more compact design, and lower forces, while also improving the efficiency compared to a 3-bladed design, reaching a power coefficient of 0.38. Attributed to the fully laminar flow over the foil, no sufficient stall behavior is noted that can slow down the turbine at high wind speeds. Therefore, pitch control was chosen instead. The optimized turbine design has a tower height of 3m and a rotor diameter of 2.2m, which results in an average power of 11.9W over a Martian year. The system can power over 100 flights of the Mars Science

Helicopter over a year while also having enough power to heat the power storage sufficiently throughout the night. The feasibility of such a design largely depends on how lightweight the construction can be.

Overall potential is seen for the feasibility of using small-scale wind turbines on Mars. While the wind power density is much lower than on Earth, wind turbines still can produce energy in the Martian environment. It was found that regional differences in wind speed are significant, which is why wind turbines can only be a solution for specific regions of Mars. Nuclear power sources are unbeaten in terms of reliability and specific energy, and will likely be superior to possible wind turbine designs. The future trend in relying more on sustainable systems determines the potential in applying wind turbines on Mars.

5.3 Looking Ahead

There is potential in using wind turbines on Mars, which means that further research is vital to further develop the concept. An important step is the structural analysis of the design, mainly intending to determine how much a possible wind turbine would weigh. Focusing on transport, payload sizing, and deployment of a design gives the needed measures for direct comparison to other energy sources.

Next to the structural analysis, further research regarding ultra-low Reynolds airfoils is valuable to optimize the aerodynamic efficiency and maximize the possible power output. This may include looking at further CFD analysis of alternative foil designs, such as polygonal or corrugated foils, along other potentially bio-inspired designs. A large value is seen in the experimental validation of airfoils in the ultra-low Reynolds regime over the full range of angles of attack. Current research is generally limited to a small range of angles of attack, and large uncertainties exist for the extrapolation of the polars. Wind tunnel experiments showing the actual response of foils can allow for insight into the accuracy of extrapolation and simulation methods.

In the 1990s, the National Science Foundation aimed at using wind turbines to power a research station at the South Pole but was struggling with the implications of the harsh environment. Meanwhile, research was conducted by NASA for possible wind farms for human settlements on Mars. Through the transfer of knowledge gained from researching Martian wind turbines, not only was a solution found to power the research station, but it also resulted in the development of the Northern Power 100, a wind turbine suitable for extreme climates and remote applications.

Innovation for space feeds progress on Earth, as having different relations to production costs or design requirements can lead to disruptive innovations. Having to design very lightweight turbines, which are extremely weather resilient and require no maintenance, can lead to innovative solutions applicable on Earth and thus give a new, tangible meaning to the research.

Bibliography

[1] S. D. Fraser, *Power System Options for Mars Surface Exploration: Past, Present and Future*. Berlin, Heidelberg: Springer Berlin Heidelberg, 2009, pp. 1–23.

[2] P. S. Anderson, "Viking remembered: Celebrating the 40th anniversary of the first search for life on mars," 2016. [Online]. Available: https://www.americaspace.com/2016/07/19/viking-remembered-celebrating-the-40th-anniversary-of-the-first-search-for-life-on-mars/

[3] B. Roston, "Nasa mars 2020 rover's name will be revealed live on march 5," 2020. [Online]. Available: https://www.slashgear.com/nasa-mars-2020-rovers-name-will-be-revealed-live-on-march-5-03612060/

[4] D. L. Shirley, "Touching mars: 1998 status of the mars robotic exploration program," *Acta Astronautica*, vol. 45, no. 4, pp. 249–265, 1999, third IAA International Conference on Low-Cost Planetary Missions. [Online]. Available: https://www.sciencedirect.com/science/article/pii/S0094576599001423

[5] Science Mission Directorate, "Final environmental impact statement for the mars 2020 mission," 2014. [Online]. Available: https://mars.nasa.gov/mars2020/files/mep/Mars2020_Final_EIS.pdf

[6] D. J. Clayton, "Nuclear risk assessment 2019 update for the mars 2020 mission environmental impact statement," 2019. [Online]. Available: https://www.osti.gov/biblio/1569349

[7] H. Haslach, Jr, "Wind energy: a resource for a human mission to mars," *Jbis-journal of The British Interplanetary Society - JBIS-J BR Interplanet SOC*, vol. 42, 1989.

[8] M. Lichter and L. Viterna, "Performance and feasibility analysis of a wind turbine power system for use on mars," 1999.

[9] A. Hemmat, C. Nguyen, B. Singh, Keir, D. Zimmerman, Advisor, and R. Kastor, "Conceptual design of a martian power generating system utilizing solar and wind energy," 1999.

[10] D. Brach, J. Dube, J. Kelly, J. Peterson, J. Bollig, L. Gohr, K. Mahoney, and D. Polidori, "Mars vertical axis wind machines. The design of a Darreus and a Giromill for use on Mars," NASA STI/Recon Technical Report N, p. 36807, 1992.

[11] G. James, P. B. R. Singh, K. Wylie, A. Hemmet, C. Nguyen, and G. Chamitoff, "Design of a wind turbine for martian power generation," *Space 2000*, 2000.

[12] V. Kumar, M. Paraschivoiu, and I. Paraschivoiu, "Low reynolds number vertical axis wind turbine for mars," *Wind Engineering*, vol. 34, no. 4, pp. 461–476, 2010. [Online]. Available: https://doi.org/10.1260/0309-524X.3.4.461

[13] D. Lockney, "Spin off," 2013. [Online]. Available: https://spinoff.nasa.gov/Spinoff2013/pdf/Spinoff2013.pdf

[14] C. Holstein-Rathlou, P. Thomas, J. Merrison, and J. Iversen, "Wind turbine power production under current martian atmospheric conditions," *Mars Workshop on Amazonian Climate*, 2018. [Online]. Available: https://www.hou.usra.edu/meetings/amazonian2018/pdf/4004.pdf

[15] B. Dorminey, "Nasa eyes wind turbines to power martian weather stations," 2020. [Online]. Available: https://www.forbes.com/sites/brucedorminey/2020/08/30/nasa-eyes-tiny-wind-turbines-to-power-martian-weather-stations/?sh=729b4eff2c0d

[16] G. James, G. Chamitoff, and D. Barker, "Design and resource requirements for successful

wind energy production on mars," *Mars Soc. Convention 1999*, 1999. [Online]. Available: http://www.marspapers.org/paper/James_1999.pdf

[17] B. Balaram, T. Canham, C. Duncan, H. Grip, W. Johnson, J. Maki, A. Quon, R. Stern, and D. Zhu, "Mars helicopter technology demonstrator," in *2018 AIAA Atmospheric Flight Mechanics Conference*, 2018.

[18] W. Johnson, S. Withrow-Maser, L. Young, C. Malpica, W. Koning, W. Kuang, M. Fehler, A. Tuano, A. Datta, C. Chi, R. Lumba, D. Escobar, J. Balaram, T. Tzanetos, and H. Grip, "Mars science helicopter conceptual design," 2020, nASA/TM–2020–220485. [Online]. Available: https://mars.nasa.gov/mars2020/files/mep/Mars2020_Final_EIS.pdf

[19] W. J. Koning, "Airfoil selection for mars rotor applications," 2019. [Online]. Available: https://ntrs.nasa.gov/api/citations/20190031929/downloads/20190031929.pdf

[20] D. Wood, *Small wind turbines: analysis, design, and application*. Springer, 2013.

[21] J. F. Manwell, J. G. McGowan, and A. L. Rogers, *Wind energy explained: Theory, Design and Application*. Wiley, 2011.

[22] F. Forget, F. Hourdin, R. Fournier, C. Hourdin, O. Talagrand, M. Collins, S. R. Lewis, P. L. Read, and J.-P. Huot, "Improved general circulation models of the Martian atmosphere from the surface to above 80 km," *jgr*, vol. 104, no. E10, pp. 24 155–24 176, 1999.

[23] E. Millour, F. Forget, A. Spiga, M. Vals, V. Zakharov, T. Navarro, L. Montabone, F. Lefevre, F. Montmessin, J.-Y. Chaufray, M. Lopez-Valverde, F. Gonzalez-Galindo, S. Lewis, P. Read, M.-C. Desjean, and MCD/GCM Development Team, "The Mars Climate Database (MCD version 5.3)," p. 12247, 2017.

[24] P. L. Read and S. R. Lewis, *The Martian climate revisited: atmosphere and environment of a desert planet*, ser. Springer Praxis Books: Geophysical Sciences. Springer, 2004, vol. 26. [Online]. Available: http://oro.open.ac.uk/4930/

[25] F. Forget, E. Millour, M. Vals, V. Zakharov, and S. Lewis, "Mars climate database v5.3 detailed design document," 2017. [Online]. Available: http://www-mars.lmd.jussieu.fr/mars/info_web/MCD5.3_ddd.pdf

[26] P. Read, S. Lewis, and D. Mulholland, "The physics of martian weather and climate: A review," *Reports on progress in physics. Physical Society (Great Britain)*, vol. 78, p. 125901, 2015.

[27] M. Szurgot, "Heat capacity of mars," *LPI Contributions*, 2012.

[28] S. Lewis and P. Barker, "Atmospheric tides in a mars general circulation model with data assimilation," *Advances in Space Research*, vol. 36, no. 11, pp. 2162–2168, 2005, planetary Atmospheres, Ionospheres, and Magnetospheres. [Online]. Available: https://www.sciencedirect.com/science/article/pii/S0273117705007842

[29] C. Leovy, "Weather and climate on mars," *Nature*, vol. 412, 2001. [Online]. Available: http://web-static-aws.seas.harvard.edu/climate/pdf/leovy-2001.pdf

[30] R. Haberle, "Solar system/sun, atmospheres, evolution of atmospheres | planetary atmospheres: Mars," in *Encyclopedia of Atmospheric Sciences (Second Edition)*, 2nd ed., G. R. North, J. Pyle, and F. Zhang, Eds. Oxford: Academic Press, 2015, pp. 168–177. [Online]. Available: https://www.sciencedirect.com/science/article/pii/B9780123822253003121

[31] Royal Meteorological Society (RMetS), "Anabatic wind." [Online]. Available: https://www.skybrary.aero/index.php/Anabatic_Wind

[32] ——, "Katabatic wind." [Online]. Available: https://www.skybrary.aero/index.php/Katabatic_Wind

[33] NASA Goddard Spaceflight Center, "Mola altimeter topographic map." [Online]. Available: https://attic.gsfc.nasa.gov/mola/index.html

[34] M. Balme and R. Greeley, "Dust devils on earth and mars," *Reviews of Geophysics*, vol. 44, no. 3, 2006. [Online]. Available: https://agupubs.onlinelibrary.wiley.com/doi/abs/10.1029/2005RG000188

[35] NASA/JPL, "Nasa mars 2020 rover's name will be revealed live on march 5," 2005. [Online]. Available: https://mars.nasa.gov/mer/gallery/press/spirit/20050527a.html

[36] E. HÉBRARD, C. Listowski, P. Coll, B. Marticorena, G. Bergametti, A. Määttänen, F. Montmessin, and F. Forget, "An aerodynamic roughness length map derived from extended martian rock abundance data," *Journal of Geophysical Research*, vol. 117, 2012.

[37] Koninklijk Nederlands Meteorologisch Instituut, "Weibull shape parameter k for different heights," 2017. [Online]. Available: https://www.dutchoffshorewindatlas.nl/atlas/image-library/image-library/weibull-shape-parameter-k

[38] W. J. Larson and J. R. Wertz, *Space mission analysis and design*, 3rd ed. Kluwer Academic Publishers, 2005.

[39] P. Lognonné, W. Banerdt, D. Giardini, W. Pike, U. Christensen, P. Laudet, s. Raucourt, P. Zweifel, S. Calcutt, M. Bierwirth, K. Hurst, F. Ijpelaan, J. Umland, R. Llorca-Cejudo, S. Larson, R. Garcia, S. Kedar, B. Knapmeyer-Endrun, and D. Mimoun, "Seis: Insight's seismic experiment for internal structure of mars," *Space Science Reviews*, vol. 215, 2019.

[40] NASA, "Moving around mars." [Online]. Available: https://mars.nasa.gov/mer/mission/timeline/surfaceops/navigation/#:~:text=While%20a%20complete%20martian%20day,to%20move%20quickly%20and%20effectively.

[41] C. Survey, *Vision And Voyages for Planetary Science in the Decade 2013–2022*, 2011.

[42] NASA Science, "Perseverance rover electrical power," 2021. [Online]. Available: https://mars.nasa.gov/mars2020/spacecraft/rover/electrical-power/

[43] C. Skocik, "Atk to provide ultraflex solar arrays for insight lander," 2014. [Online]. Available: https://www.spaceflightinsider.com/missions/atk-provide-ultraflex-solar-arrays-insight-lander/

[44] P. K. McConnaughey, M. G. Femminineo, S. J. Koelfgen, R. A. Lepsch, R. M. Ryan, and S. A. Taylor, "Draft launch propulsion systems roadmap," *DRAFT Launch Propulsion Systems Roadmap*, 2010. [Online]. Available: https://www.nasa.gov/pdf/500393main_TA01-LaunchPropulsion-DRAFT-Nov2010-A.pdf

[45] BBC, "Insight lander: Martian dust devil has hit nasa's mars rover," 2019. [Online]. Available: https://www.bbc.co.uk/newsround/48214887

[46] NASA, "In-situ exploration and sample return: Entry, descent, and landing." [Online]. Available: https://mars.nasa.gov/mer/mission/technology/edl/

[47] E. Ionescu, "Sky crane's mars landing a success," 2012. [Online]. Available: https://www.cranesy.com/sky-cranes-mars-landing-a-success/mars-landing/

[48] E. Lakdawalla, *Getting to Mars*. Cham: Springer International Publishing, 2018, pp. 57–109. [Online]. Available: https://doi.org/10.1007/978-3-319-68146-7_2

[49] R. R. Roe, "Load analyses of spacecraft and payloads nasa-std-5002a," 2019.

[50] United Launch Alliance, "Atlas v launch services user's guide," *ULA Launch*, 2010. [Online]. Available: https://www.ulalaunch.com/docs/default-source/rockets/atlasvusersguide2010.pdf

[51] P. N. Desai, J. L. Prince, E. M. Queen, M. M. Schoenenberger, J. R. Cruz, and M. R. Grover, "Entry, descent, and landing performance of the mars phoenix lander," *Journal of Spacecraft and Rockets*, vol. 48, no. 5, pp. 798–808, 2011. [Online]. Available: https://doi.org/10.2514/1.48239

[52] M. San Martin, G. Mendeck, P. Brugarolas, G. Singh, F. Serricchio, S. Lee, E. Wong, and J. Essmiller, "In-flight experience of the mars science laboratory guidance, navigation, and control system for entry, descent, and landing," *CEAS Space Journal*, vol. 7, 2015.

[53] R. Braun and R. Manning, "Mars exploration entry, descent and landing challenges," *2006 IEEE Aerospace Conference*, 2007.

[54] "Thermal control," 2020. [Online]. Available: https://www.nasa.gov/smallsat-institute/sst-soa-2020/thermal-control

[55] K. Novak, A. Paris, F. Kelly, and J. Miller, "Thermal response of the mars science laboratory spacecraft during entry, descent and landing," *46th International Conference on Environmental Systems, Vienna, Austria*, 2016. [Online]. Available: https://trs.jpl.nasa.gov/handle/2014/46104

[56] R. Sostaric, "The challenge of mars edl (entry, descent, and landing)," 2010. [Online]. Available: https://ntrs.nasa.gov/api/citations/20100017668/downloads/20100017668.pdf

[57] R. D. Braun, "The mars science laboratory entry, descent, and landing system," *Journal of Spacecraft and Rockets*, vol. 51, no. 4, pp. 993–993, 2014. [Online]. Available: https://doi.org/10.2514/1.A33068

[58] N. Barlow, *Mars: An Introduction to its Interior, Surface and Atmosphere*, ser. Cambridge Planetary Science. Cambridge University Press, 2008.

[59] NASA, "Vista from curiosity shows crossbedded martian sandstone," 2015. [Online]. Available: https://www.jpl.nasa.gov/images/vista-from-curiosity-shows-crossbedded-martian-sandstone

[60] Arizona State University, "Flood basalts." [Online]. Available: https://marsed.asu.edu/mep/volcanoes/flood_basalts

[61] S. Loff, "All along the fractures," 2015. [Online]. Available: http://www.nasa.gov/image-feature/all-along-the-fractures

[62] N. E. Putzig, M. T. Mellon, K. A. Kretke, and R. E. Arvidson, "Global thermal inertia and surface properties of mars from the mgs mapping mission," *Icarus*, vol. 173, no. 2, pp. 325–341, 2005. [Online]. Available: https://www.sciencedirect.com/science/article/pii/S0019103504002957

[63] J. Pitre and S. Huang, "Mobile wind turbine," 2014.

[64] J. Harrison, D. Turnbull, and D. King, "Deployable wind power and battery unit," 2011.

[65] L. Puig, A. Barton, and N. Rando, "A review on large deployable structures for astrophysics missions," *Acta Astronautica*, vol. 67, no. 1, pp. 12–26, 2010. [Online]. Available: https://www.sciencedirect.com/science/article/pii/S0094576510000743

[66] Y. Liu, H. Du, L. Liu, and J. Leng, "Shape memory polymers and their composites in aerospace applications: a review," *Smart Materials and Structures*, vol. 23, no. 2, p. 023001, 2014. [Online]. Available: https://doi.org/10.1088/0964-1726/23/2/023001

[67] W. Sokolowski and S. Tan, "Advanced self-deployable structures for space applications," *Journal of Spacecraft and Rockets - J Spacecraft Rocket*, vol. 44, pp. 750–754, 2007.

[68] O. Probst, J. Martinez, J. Elizondo, and O. Monroy, *Small Wind Turbine Technology*, 2011.

[69] T. Burton, D. Sharpe, N. Jenkins, and E. Bossanyi, "Wind energy handbook," *Wind Engineering*, vol. 25, no. 3, pp. 197–199, 2001. [Online]. Available: http://www.jstor.org/stable/43749820

[70] J. Winslow, H. Otsuka, B. Govindarajan, and I. Chopra, "Basic understanding of airfoil characteristics at low reynolds numbers (104–105)," *Journal of Aircraft*, vol. 55, no. 3, pp. 1050–1061, 2018. [Online]. Available: https://doi.org/10.2514/1.C034415

[71] D. Wood, *Advances in Wind Energy Conversion Technology*, M. Sathyajith and G. S. Philip, Eds. Berlin, Heidelberg: Springer Berlin Heidelberg, 2011. [Online]. Available: https://doi.org/10.1007/978-3-540-88258-9_8

[72] B. Chide, S. Maurice, D. Mimoun, N. Murdoch, R. D. Lorenz, and R. C. Wiens, "Speed of sound measurement on mars and its implications," in *51st Lunar and Planetary Science Conference)*, 2020. [Online]. Available: https://www.hou.usra.edu/meetings/lpsc2020/pdf/1366.pdf

[73] D. Marten, J. Peukert, G. Pechlivanoglou, C. Nayeri, and C. Paschereit, "Qblade: An open source tool for design and simulation of horizontal and vertical axis wind turbines," *International Journal of Emerging Technology and Advanced Engineering*, vol. 3, pp. 264–269, 2013.

[74] D. Marten and J. Peukert, "Qblade guidelines v0.6," 2013.

[75] W. Cao, Y. Xie, and Z. Tan, *Wind Turbine Generator Technologies*. Advances in Wind Power: IntechOpen, 2012. [Online]. Available: https://www.intechopen.com/books/advances-in-wind-power/wind-turbine-generator-technologies

[76] J. Pyrhönen, J. Nerg, P. Kurronen, J. Puranen, and M. Haavisto, "Permanent magnet technology in wind power generators," *19th International Conference on Electrical Machines, ICEM 2010*, 2010.

[77] A. O. Di Tommaso, R. Miceli, G. R. Galluzzo, and M. Trapanese, "Efficiency maximization of permanent magnet synchronous generators coupled coupled to wind turbines," in *2007 IEEE Power Electronics Specialists Conference*, 2007, pp. 1267–1272.

[78] F. C. Krause, J. P. Ruiz, S. C. Jones, E. J. Brandon, E. C. Darcy, C. J. Iannello, and R. V. Bugga, "Performance of commercial li-ion cells for future NASA missions and aerospace applications," *Journal of The Electrochemical Society*, vol. 168, no. 4, p. 040504, 2021. [Online]. Available: https://doi.org/10.1149/1945-7111/abf05f

[79] V. Petrović and C. Bottasso, "Wind turbine optimal control during storms," *Journal of Physics: Conference Series*, vol. 524, p. 012052, 2014.

[80] S. Reijniers, "Design and aeroelastic analysis of flexible wind turbine blades," 2015.

[81] L. Thomas and M. Ramachandra, "Advanced materials for wind turbine blade- a review," *Materials Today: Proceedings*, vol. 5, no. 1, Part 3, pp. 2635–2640, 2018, international Conference on Advanced Materials and Applications (ICAMA 2016), June 15-17, 2016, Bengaluru, Karanataka, INDIA. [Online]. Available: https://www.sciencedirect.com/science/article/pii/S221478531830049X

[82] N. Ren, "Dust effect on the performance of wind turbine airfoils," *Journal of Electromagnetic Analysis and Applications*, vol. 01, pp. 102–107, 2009.

[83] I. Tzinis, "Technology readiness level," 2018. [Online]. Available: https://www.nasa.gov/directorates/heo/scan/engineering/technology/technology_readiness_level

[84] J. Amos, "China's zhurong mars rover takes a selfie." [Online]. Available: https://www.bbc.com/news/science-environment-57441757

[85] P. J. Kunz, "Aerodynamics and design for ultra-low Reynolds number flight," Ph.D. dissertation, Stanford University, 2003.

[86] H. Shah, N. Bhattarai, S. Mathew, M. Chee, and Lim, "Low reynolds number airfoil for small horizontal axis wind turbine blades," in *Sustainable Future Energy 2012 and 10th SEE Forum*, 2012.

[87] M. Hansen, "Aerodynamics of wind turbines, second edition," *Aerodynamics of Wind Turbines, Second Edition*, pp. 1–181, 2013.

[88] O. Apata and D. Oyedokun, "An overview of control techniques for wind turbine systems," *Scientific African*, vol. 10, p. e00566, 2020. [Online]. Available: https://www.sciencedirect.com/science/article/pii/S2468227620303045

[89] J. L. Torres-Madroñero, J. Alvarez-Montoya, D. Restrepo-Montoya, J. M. Tamayo-Avendaño, C. Nieto-Londoño, and J. Sierra-Pérez, "Technological and operational aspects that limit small wind turbines performance," *Energies*, vol. 13, no. 22, 2020. [Online]. Available: https://www.mdpi.com/1996-1073/13/22/6123

[90] O. Probst, J. Martinez, J. Elizondo, and O. Monroy, *Small Wind Turbine Technology*, 2011.

[91] J. Bialasiewicz, "Furling control for small wind turbine power regulation," in *2003 IEEE International Symposium on Industrial Electronics (Cat. No.03TH8692)*, vol. 2, 2003, pp. 804–809 vol. 2.

[92] A. Petrosyan, B. Galperin, S. Larsen, S. Lewis, A. Määttänen, P. Read, N. Rennó, P. Rogberg, H. Savijarvi, T. Siili, A. Spiga, A. Toigo, and L. Vazquez, "The martian atmospheric boundary layer," *Reviews of Geophysics*, vol. 49, p. RG3005, 2011.

[93] W. Z. Shen, R. Mikkelsen, J. N. Sørensen, and C. Bak, "Tip loss corrections for wind turbine computations," *Wind Energy*, vol. 8, no. 4, pp. 457–475, 2005. [Online]. Available: https://onlinelibrary.wiley.com/doi/abs/10.1002/we.153

[94] J. Hernandez and A. Crespo, "Aerodynamic calculation of the performance of horizontal axis wind turbines and comparison with experimental results," *Wind Engineering*, vol. 11, no. 4, pp. 177–187, 1987. [Online]. Available: https://www.jstor.org/stable/pdf/43749310

[95] Y.-J. Chen, Y.-F. Tsai, C.-C. Huang, M.-H. Li, and F.-B. Hsiao, "The design and analysis of passive pitch control for horizontal axis wind turbine," *Energy Procedia*, vol. 61, pp. 683–686, 2014, international Conference on Applied Energy, ICAE2014. [Online]. Available: https://www.sciencedirect.com/science/article/pii/S1876610214027726

[96] C. van Wijk, "Design of a small wind turbine rotor and hub for wind tunnel testing," *University of Twente*, 2020.

Appendices

Appendix A - Map of Mars

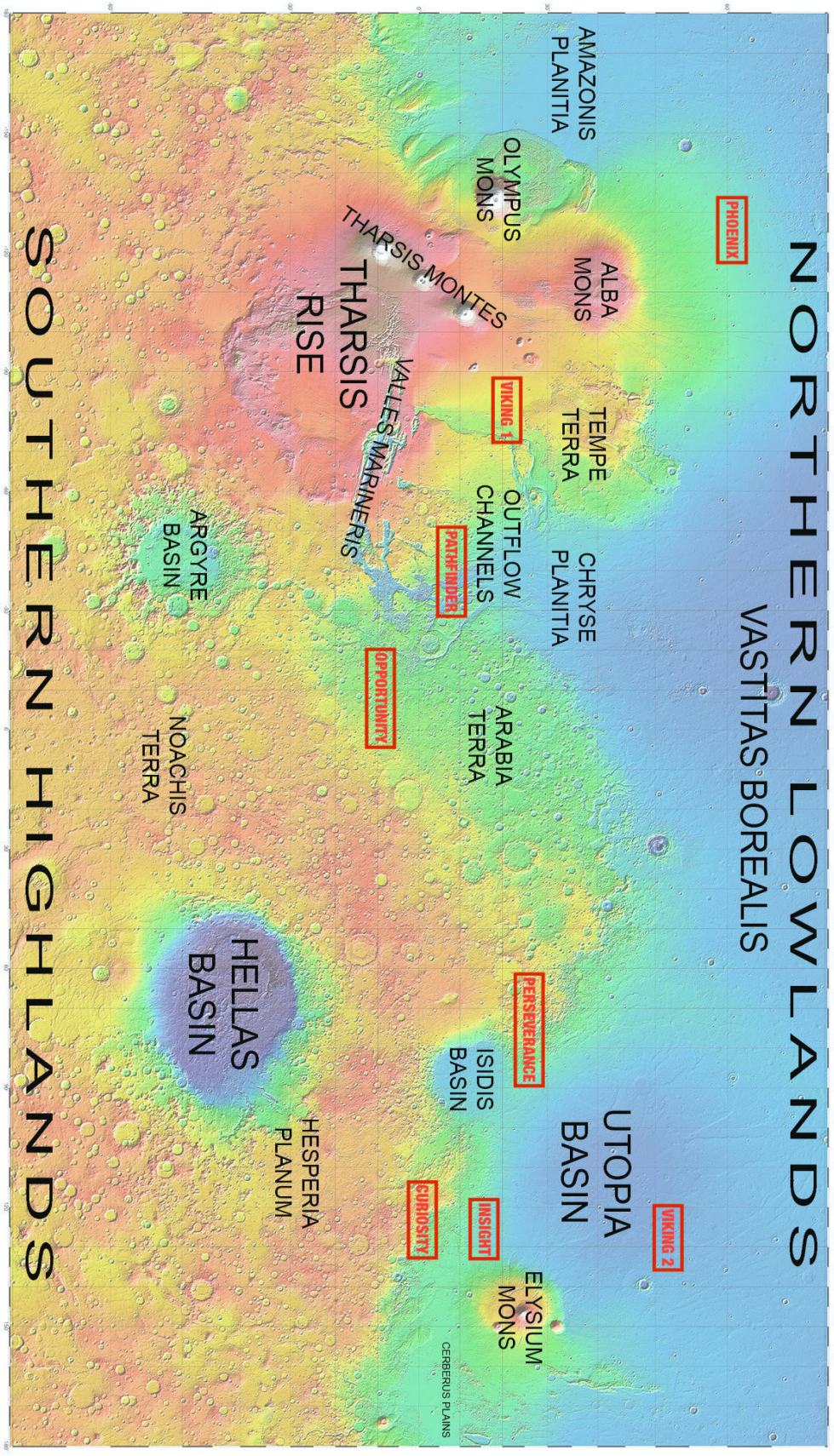

THE TOPOGRAPHY OF MARS BY THE MARS ORBITER LASER ALTIMETER (MOLA)

Appendix B - Wind Turbine Theory

Fundamental Principles

A theoretical foundation is necessary for the optimized design of wind turbines. Different types of energy can be ranked in a hierarchical structure based on their quality, displaying the ease of their conversion into another energy type. The higher the quality is, the less energy is lost in the conversion process to a lower quality energy. Wind energy is a lower quality energy compared to mechanical and electrical energy, which makes the conversion through a wind turbine more lossy.

Derivation of the Betz Power Coefficient

A fundamental efficiency limit can be found for this conversion, known as the Betz coefficient, which uses an idealized version of a wind turbine as a energy extracting disk. The derivation assumes there is no hub to house the generator and connect the blades, no drag on the system and the flow is uniform, non-compressible with constant density. The volume flow into the area swept by the 'turbine disk' is equal to the volume flow out of this area. In Chapter 2, the power contained in wind was defined as:

$$P = \frac{1}{2}\rho A v^3 \tag{B.1}$$

The pressure and velocities around the turbine can be defined as illustrated in Figure B.1. Sufficiently far upwind of the turbine, the wind has a constant speed v_∞, undisturbed by the

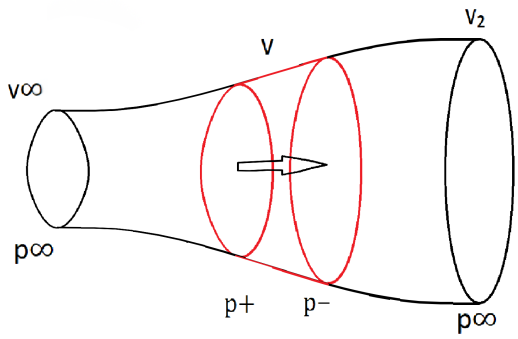

Figure B.1: Velocity and pressure for the idealized wind turbine.

influence of the turbine. At the rotor, the wind velocity drops as some energy is converted, leading to a reduced wind speed v_2 downstream of the rotor. At infinite distance from the turbine, pressure will be constant, while pressure increases to p^+ in front of the rotor and drops to p^- just after the rotor as a result of the drop in velocity. Bernoulli's equation can be applied to find the drop in pressure over the turbine, which is defined as:

$$\frac{D}{Dt}\left[\frac{p}{\rho} + \frac{1}{2}u_j u_j + g_j h\right] = 0 \tag{B.2}$$

This material derivative is only zero if the term inside is constant along streamlines. Without a gravity component and a single velocity component this results in:

$$\frac{p}{\rho} + \frac{1}{2}v^2 = \text{c.a.s.} \tag{B.3}$$

This can be applied to the region before and after the drop in energy through the turbine, resulting in:

$$\frac{p_\infty}{\rho} + \frac{1}{2}v_\infty^2 = \frac{p^+}{\rho} + \frac{1}{2}v^2 \quad \text{and} \quad \frac{p_\infty}{\rho} + \frac{1}{2}v_2^2 = \frac{p^-}{\rho} + \frac{1}{2}v^2 \tag{B.4}$$

Which can be combined to describe the pressure drop across the turbine:

$$p^+ - p^- = \frac{1}{2}\rho(v_\infty^2 - v_2^2) \tag{B.5}$$

The axial thrust T generated through this pressure drop over the swept area A is:

$$T = A(p^+ - p^-) = \frac{1}{2}\rho A(v_\infty^2 - v_2^2) \tag{B.6}$$

This thrust can also be expressed as the velocity difference times the mass flow rate:

$$T = \dot{m}(v_\infty - v_2) = \rho A v(v_\infty - v_2) \tag{B.7}$$

With both thrust expressions being valid, their calculated value has to be equal, so:

$$\frac{1}{2}\rho A(v_\infty^2 - v_2^2) = \rho A v(v_\infty - v_2) \tag{B.8}$$

Which can be rewritten to give a value for the velocity by the rotor:

$$v = \frac{1}{2}(v_\infty + v_2) \tag{B.9}$$

An expression for amount of kinetic energy that can be extracted by the turbine can be found as the difference in energy before and after the turbine, based on the volume flow:

$$E = \frac{1}{2}\rho Q v^2 = \frac{1}{2}\rho A v(v_\infty^2 - v_2^2) \tag{B.10}$$

To find the efficiency, the fraction of energy extracted over the total wind energy can be found as a power coefficient by combining Equation B.1 and B.10:

$$C_p = \frac{\frac{1}{2}\rho A v(v_\infty^2 - v_2^2)}{\frac{1}{2}\rho A v_\infty^3} = \frac{v(v_\infty^2 - v_2^2)}{v_\infty^3} \tag{B.11}$$

Plugging in Equation B.9:

$$C_p = \frac{(v_\infty + v_2)(v_\infty^2 - v_2^2)}{2v_\infty^3} \tag{B.12}$$

This is the equation that has to be maximized in order to find the highest possible energy extraction. If there is no turbine, $v_\infty = v_2$, which leads to zero power extracted. If all power would be extracted, v_2 is zero, leading to an efficiency of 0.5. Defining the axial induction factor $a = \frac{v_\infty - v_2}{v_\infty}$ leads to:

$$C_p = 4a(1-a)^2 \tag{B.13}$$

This function has one maximum:

$$C_{p,max} = \frac{16}{27} \quad (a = 1/3) \tag{B.14}$$

This is the maximum amount of energy that can be extracted from the wind, known as the Betz coefficient. An important note is that this simplified model does not approximate axial induction factors above 0.5 accurately, as complex turbulence behind the turbine requires more detailed analysis.

Derivation of the Power Coefficient for a Drag-based Turbine

The drag force by the wind on a blade can be defined as:

$$F_d = \frac{1}{2}C_D A\rho v_\infty^2 \tag{B.15}$$

Defining u_{blade} as the speed of an idealized blade, which could move with and in the direction of the wind without any resistance ($u = v_\infty$), could be a fixed obstacle ($u_{blade} = 0$), or anywhere in between, the force acting on the blade is:

$$F_d = \frac{1}{2} C_d A \rho (v_\infty - u_{blade})^2 \tag{B.16}$$

Which allows for a power extraction of:

$$E = F_d u_{blade} = \frac{1}{2} C_d A \rho (v_\infty - u_{blade})^2 u_{blade} \tag{B.17}$$

If the blade provides no resistance, no energy is extracted as $E(u_{blade} = v_\infty) = 0$, and if it resists the flow fully, also no energy is extracted as also $E(u_{blade} = 0) = 0$. Therefore, analogous to the derivation of the Betz limit, a maximum power coefficient can be found to find the efficiency limit of the system. The power coefficient is:

$$C_p = \frac{\frac{1}{2} C_D A \rho (v_\infty - u_{blade})^2 u_{blade}}{\frac{1}{2} \rho A v_\infty^3} = \frac{C_D (v_\infty - u_{blade})^2 u_{blade}}{v_\infty^3} \tag{B.18}$$

By defining a factor $b = \frac{u_{blade}}{v_\infty}$ the maximum can be found:

$$C_p = b(1 - b)^2 \tag{B.19}$$

$$C_{p,max} = \frac{4}{27} C_D \quad (b = 1/3) \tag{B.20}$$

This is the maximum amount of energy that can be extracted from the wind. With large drag coefficients being around 2, this leads to a maximum coefficient of roughly $\frac{8}{27}$. Therefore, designs that work through drag are only around half as efficient compared to aerodynamic systems, which have a 16/27 theoretical limit compared to the ≈8/27 of the push system. Therefore, a system beyond simple push have to be designed, which is possible through the application of aerodynamic foils.

Aerodynamics of Airfoils

Foils are geometric objects that take advantage of the dynamic properties of fluids to generate a lifting force that is larger than the drag of the object. Various parameters determine the shape of the foil, which in turn influences the behavior of the foil when exposed to a flow. For wind turbines, finding an optimal geometry for the desired application and environment is one of the main steps in generating as much power as possible.

The *leading edge* and the *trailing edge* are the points at the front and at the back of the foil, respectively. Connecting these points results in the *chord line* of the foil. Oftentimes, foils are designed in an asymmetrical fashion, resulting in a *camber*. The *mean camber line* is defined as the line through the center of the foil from leading to trailing edge. The distance between chord and camber line then results in camber values. Finally, the *angle of attack* (AoA) is the angle between the chord line and the relative wind that the foil is subject to.

Any object with velocity relative to a flow experiences drag. Foils, however, generate an additional force, called lift. Through the shape of the foil, a downwash is created at the trailing edge, which causes an reaction force in the upwards direction. Also, air is accelerated on the upper surface. Looking at Equation B.3, it can be seen that if the velocity increases, the pressure has to decrease to keep the term constant along streamlines, assuming incompressible flow. This creates a lower pressure on top of the foil, further contributing to the upwards lift force.

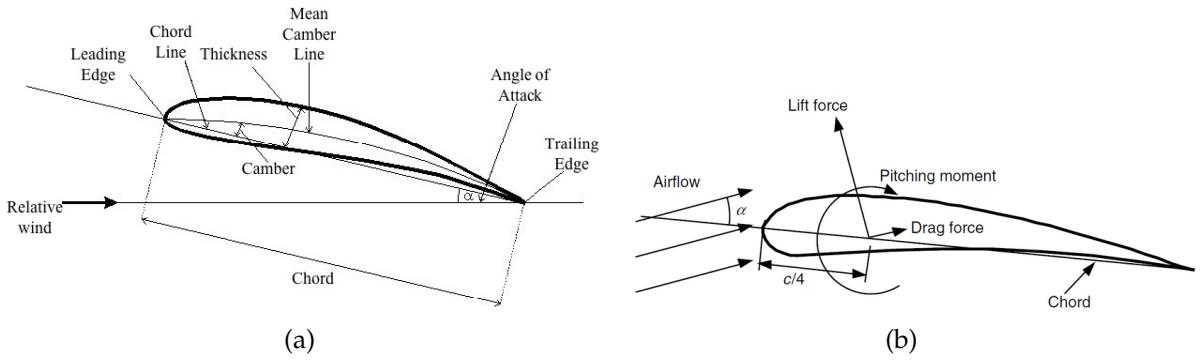

(a) (b)

Figure B.2: Schematic of an airfoil shape with (a) typical nomenclature and (b) main aerodynamic forces [21]

The effects of drag and lift can be summarized into two main forces perpendicular to each other, acting at one quarter of the chord length. This also explains the reasoning for using a camber. Without camber, in the case of zero AoA, no lift would be generated because of the perfectly symmetrical situation. The camber introduces the asymmetry required for the generation of the pressure difference. For cambered foils, an additional torque, called the pitching moment is also present. The center of pressure and aerodynamic center are offset in non-symmetrical cases, which causes this moment to be created.

A lot of different shape variations are possible which influence the way the foil behaves under different conditions. To allow for an accurate comparison, non-dimensional coefficients can be found that quantity the reaction of the foil, namely the drag, lift and pitch moment coefficient, which are defined as:

$$C_d = \frac{F_D/l}{\frac{1}{2}\rho v_\infty^2 c} \tag{B.21}$$

$$C_l = \frac{F_L/l}{\frac{1}{2}\rho v_\infty^2 c} \tag{B.22}$$

$$C_m = \frac{M_p}{\frac{1}{2}\rho v_\infty^2 A_{foil} c} \tag{B.23}$$

With F_D being the drag force, l the airfoil span, v_∞ the velocity of undisturbed flow, c the chord length, F_L the lift force, M_p the pitching moment and A_{foil} being the (projected) airfoil area. These formulas describe a 2-dimensional case, in which edge effects at the end of the span are not considered. For wind turbines these are usually used, as will be explained when discussing Blade Element Momentum (BEM) theory. Additionally, an important non-dimensional parameter for many calculations involving fluids is the Reynolds number, defined as:

$$Re = \frac{\rho v L}{\mu} \tag{B.24}$$

It characterizes flows in terms of their inertial and viscous forces. Flow at low Reynolds numbers is mainly influenced by viscous (friction) forces, and as such is more laminar. At high Reynolds numbers, inertial forces have more influence causing unstable, turbulent flows. From a design point of view, the lift coefficient should be maximized against the drag coefficient to obtain the highest power coefficient. However, both drag and lift coefficient vary depending on the AoA of the foil, as well as on the Reynolds number. Therefore, finding an optimized design requires evaluating the lift-to-drag ratio of different foils at various AoA and matching Re.

The aerodynamics of foils are crucial for the design of wind turbines, but are not sufficient for the design of the complete rotor system. In order to design the way the foils should be shaped throughout the length of each rotor blade, Blade Element Momentum Theory (BEM) can be used. In blade element theory, sections (elements) of the total blade are defined, and their characteristics are calculated independently from the previous and following elements. This is also why two-dimensional drag and lift coefficients are sufficient, each is followed by another element, so no edge effects have to be considered. This is not true for the first and last element, which is why two losses, root and tip loss, have to be accounted for in an accurate model. In momentum theory, the forces on an object are analyzed on the premise of conservation of linear and angular momentum. BEM is the combination of these two approaches.

Analogous to the way the power coefficient was found in deriving the Betz Limit, the thrust coefficient can be written as:

$$C_t = 4a(1-a) \tag{B.25}$$

Again, a maximum thrust coefficient is achieved for an axial induction factor of $1/3$, so that C_t becomes $8/9$. Power and thrust of the turbine can then be defined from Equation B.6 and B.10 as:

$$P = \frac{1}{2}\rho v_\infty^3 A C_p \tag{B.26}$$

$$T = \frac{1}{2}\rho v_\infty^2 A C_t \tag{B.27}$$

These formulas for power and thrust are valid under neglection of the wake rotation. In reality, a turbine is made from multiple blades, which rotate with an angular speed. Since angular momentum is always conserved, a rotation must also be induced on the wind, known as wake rotation. Including this effect leads to two terms, one for the axial component, i.e. the thrust and one for the radial component, i.e. the torque. Since the effect of the wake rotation depends on the radius, as blade velocity is higher at larger radii, the equations are given in differential form:

$$dT = \rho v_\infty^2 C_t \pi r dr \tag{B.28}$$

$$dQ = \rho v_\infty 4a'(1-a)\pi r^3 \omega dr \tag{B.29}$$

with a' being the angular induction factor, described as the ratio between angular velocity of the rotor and the wake rotation:

$$a' = \frac{\omega_w}{2\omega} \tag{B.30}$$

These two equations describe the momentum theory, so blade element theory is needed to get the full picture. Looking at a blade element of length dr, relations can be found for the forces and angles illustrated in Figure B.3. This leads to the following relations [21]:

$$\tan\varphi = \frac{v_\infty(1-a)}{\omega r(1+a')} = \frac{1-a}{(1+a')\lambda_r} \tag{B.31}$$

$$v_{rel} = v_\infty(1-a)/\sin\varphi \tag{B.32}$$

$$dF_L = C_l \frac{1}{2}\rho v_{rel}^2 c dr \tag{B.33}$$

$$dF_D = C_d \frac{1}{2}\rho v_{rel}^2 c dr \tag{B.34}$$

$$dF_N = dF_L \cos\varphi + dF_D \sin\varphi \tag{B.35}$$

$$dF_T = dF_L \sin\varphi + dF_D \cos\varphi \tag{B.36}$$

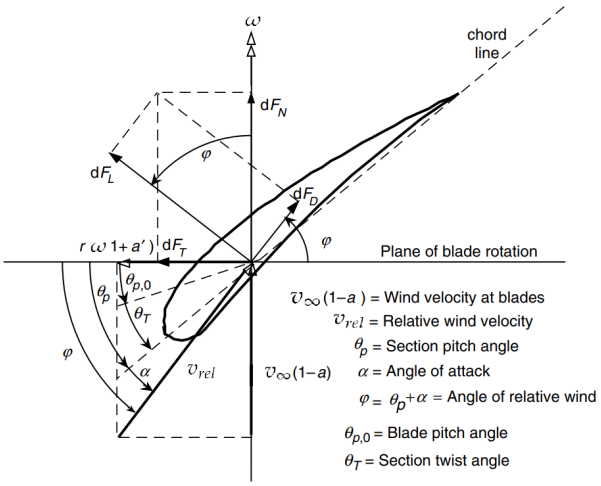

Figure B.3: Key relations and directions of forces on an airfoil, adapted from: [21]

From here, the two key equations for the element theory can be found. Plugging in B.33 and B.34 into B.35, and multiplying by the number of blades B gives the total normal force at a certain distance:

$$dF_N = B\frac{1}{2}\rho v_{rel}^2(C_l\cos\varphi + C_d\sin\varphi)cdr \tag{B.37}$$

Similarly, the total torque at a certain distance, and plugging in Equation B.36 gives:

$$dQ = BrdT = B\frac{1}{2}\rho v_{rel}^2(C_l\sin\varphi + C_d\cos\varphi)crdr \tag{B.38}$$

From both blade element theory and momentum theory, equations for the axial and radial component of the force were found. These can now be used in BEM analysis.

The main two blade design parameters that can be determined this way are the chord length and twist angle. A relatively simple approach is by using the optimal case assumed by Betz, with maximum power at an axial induction factor of 1/3. Neglecting the wake rotation means that $a' = 0$, so Equation B.31 can be written to reflect the chord twist throughout the blade:

$$\varphi_{Betz} = \arctan\left(\frac{2}{3}\lambda_r\right) \tag{B.39}$$

It can be with increasing local speed ratio, which increases towards the tip becoming the TSR, the twist increases as well. This leads to an even lift throughout the rotor, as adapting the twist from the root would cause the tip to stall, and adapting the twist from the tip would cause low lift towards the root. The Betz approximation for the change in chord length can be found next. For this, Equation B.38 is rewritten under the assumption that the drag coefficient C_d is much smaller than the lift coefficient C_l, leading to:

$$dQ = BrdT = B\frac{1}{2}\rho v_{rel}^2 C_l\sin(\varphi)crdr \tag{B.40}$$

The power that is transmitted is the torque times the angular velocity:

$$P = \omega Q \tag{B.41}$$

So that dP can be written as:

$$dP = \omega B\frac{1}{2}\rho v_{rel}^2 C_l\sin(\varphi)crdr \tag{B.42}$$

An alternative formulation of the power can be obtained through the definition of power of Equation B.26, and using the Betz coefficient from Equation B.14, giving:

$$P = \frac{16}{27}\frac{1}{2}\rho v_\infty^3 A \tag{B.43}$$

and for a ring dr:

$$dP = \frac{16}{27}\frac{1}{2}\rho v_\infty^3 2\pi r dr \tag{B.44}$$

Equations B.42 and B.44 can be combined to get an equation for the chord length:

$$c = \frac{32}{27}\frac{v_\infty^3 \pi}{\omega B v_{rel}^2 C_l \sin\varphi} \tag{B.45}$$

Using the expression for the relative velocity in Equation B.32, assuming Betz optimum efficiency at $a = \frac{1}{3}$ again, gives:

$$c = \frac{8}{3}\frac{v_\infty \pi \sin\varphi}{\omega B C_l} \tag{B.46}$$

The equation can be rewritten to show the chord length as a function of local speed ratio, defined as $\lambda_r = \frac{\omega r}{v_\infty}$, resulting in the formulation for the Betz chord length.

$$c_{Betz} = \frac{8}{3}\frac{\pi r \sin\varphi}{\lambda_r B C_l} \tag{B.47}$$

This is a first way of determining chord length and twist angle, but it is based on some strong simplifications, like the assumption that $C_l \gg C_d$. Especially in the application on Mars, where Reynolds numbers are smaller in general causing smaller lift-to.drag ratios. Effects of wake rotation are also neglected throughout the derivation, as well as tip and root losses, since the first and last element are treated no different than the middle elements. Better approximations exist, such as the Schmitz twist angle and chord length approximation, which includes the effects of wake rotation. Furthermore, correction factors for losses at the tip and root can be integrated as well. Since these relations are integrated in turbine design tools such as QBlade, they will not be derived here, but can be found in [96].

Appendix C - Final Wind Turbine Blade Design Data

Radial Position [m]	Chord Length [m]	Twist [deg]	Airfoil Name
5.00E-02	1.26E-01	7.37E+01	NACA4602
1.16E-01	2.31E-01	5.99E+01	NACA4602
1.80E-01	2.82E-01	4.88E+01	NACA4602
2.46E-01	3.00E-01	4.00E+01	NACA4602
3.11E-01	3.00E-01	3.34E+01	NACA4602
3.76E-01	2.89E-01	2.82E+01	NACA4602
4.42E-01	2.74E-01	2.41E+01	NACA4602
5.40E-01	2.49E-01	1.96E+01	NACA4602
6.38E-01	2.26E-01	1.62E+01	NACA4602
7.36E-01	2.05E-01	1.36E+01	NACA4602
8.33E-01	1.87E-01	1.16E+01	NACA4602
8.99E-01	1.76E-01	1.04E+01	NACA4602
9.64E-01	1.66E-01	9.46E+00	NACA4602
1.03E+00	1.57E-01	8.60E+00	NACA4602
1.09E+00	1.49E-01	7.83E+00	NACA4602

Table C: Optimized blade geometry for a 5-bladed turbine